Synthesis of Reactive and Stimuli-Responsive Polymer Thin Films by Initiated Chemical Vapor Deposition and Their Sensor Applications

by

Wyatt E. Tenhaeff

Honors B.S. in Chemical Engineering
Oregon State University, Corvallis, Oregon, 2004

Submitted to the Department of Chemical Engineering
in Partial Fulfillment of the Requirements for the Degree of

DOCTOR OF PHILOSOPHY IN CHEMICAL ENGINEERING

AT THE

MASSACHUSETTS INSTITUTE OF TECHNOLOGY

September 2009

Signature of Author.....
Department of Chemical Engineering
July 16, 2009

Certified by.....
Karen K. Gleason
Professor of Chemical Engineering
Thesis Supervisor

Accepted by .....
William M. Deen
Professor of Chemical Engineering
Chairman, Committee for Graduate Students

Synthesis of Reactive and Stimuli-Responsive Polymer Thin Films by Initiated Chemical Vapor Deposition and Their Sensor Applications

By

Wyatt E. Tenhaeff

Submitted to the Department of Chemical Engineering
on the July 16, 2009, in Partial Fulfillment of the
Requirements for the Degree of
Doctor of Philosophy in Chemical Engineering

Abstract

Stimuli-responsive polymer thin films provide the ability to control the interaction of a surface with its environment. Synthetic techniques with fine compositional control are required to engineer specific responses to stimuli. Initiated chemical vapor deposition (iCVD) is a novel vacuum deposition technique in which polymer films are synthesized bottom-up as monomer and initiator vapors are introduced into a vacuum coating chamber. iCVD can conformally coat nanoscale, three-dimensional geometries with a high level of compositional control. Such coating capabilities are difficult by solution-based film synthesis techniques, and compositional control is difficult by other CVD techniques. In this thesis work, the synthesis and application of stimuli-responsive and reactive polymer thin films by iCVD have been studied. First, functionally versatile alternating copolymers of poly(styrene-alt-maleic anhydride) were synthesized. This was the first demonstration of alternating copolymer synthesis by CVD. Fourier transform infrared spectroscopy, x-ray photoelectron spectroscopy, and ^{13}C NMR characterization verified that well-defined alternating structure was present, as predicted from standard solution phase polymerizations. Next, polymer crosslinking was tuned in the synthesis of pH-responsive hydrogel thin films composed of poly(maleic anhydride-co-dimethylacrylamide-co-di(ethylene glycol) divinyl ether). These films had swelling ratios, defined as the thickness in the water-swollen state over the thickness in the dry state, in excess of 11. These films were employed as ultrathin permeable, size-selective skin layers in composite membranes. The final two projects involved the synthesis of polymer thin films as chemically selective layers in microscale chemical sensors. In a sensing system based on the detection of amine compounds through their reaction with reactive polymer coatings on microcantilevers, it was shown that increased crosslinking of the polymer layer leads to greater cantilever deflection. This increased deflection enabled the design of simple, resistance-based signal readout schemes with low power requirements. New polymer compositions and sensing strategies were also developed for the detection of nitroaromatic explosives vapors. Poly(4-vinylpyridine) was shown to swell when exposed to nitroaromatics, while showing little response to common interferents. In contrast to conventional nitroaromatic-selective layers, it was shown that poly(4-vinylpyridine) does not interact with nitroaromatics through hydrogen bonding, which is important for multicomponent sensor arrays. A new microscale sensing concept utilizing this swelling was designed, fabricated, and characterized.

Thesis Supervisor: Karen K. Gleason
Title: Professor of Chemical Engineering and Associate Dean of Engineering for Research

To Christy

Acknowledgments

Writing this thesis is the culmination of five years of diligent effort, with the highs and lows of my thesis research behind me. My graduate career has been an immense educational experience, and I have matured in my research and problem-solving approaches. Reflecting on the past five years, though, I realize that I could not have accomplished this feat without the help of many people. I thank everyone who has supported me during this period of my life.

I want to thank my parents first. Thank you for encouraging me to follow this path. Dad, the example you set when you started graduate school with three young kids and 13 years of industrial experience has motivated me more than anything else to pursue this goal. It has also shaped my work ethic. Mom and dad, I am grateful to both of you for your wholehearted support of my educational and career goals. I would never have made it to MIT without all your support along the way.

One of the benefits of an MIT education is the professors. Thank you, Karen for allowing me to join your group. I appreciate the freedom you gave me to investigate research areas that I found interesting. Some of these studies weren't as fruitful as either of us would have liked, but I did learn from them. Thank you for your confidence in me and support. Through our meetings and research discussions, I have become more focused in my research, which ultimately will help me be more successful. Also, your suggestions on the less technical aspects of research, such as creating effective presentations, have been invaluable.

I appreciate the discussions with the members of my thesis committee: Professor Herb Sawin and Professor Alan Hatton. Your suggestions and ideas have prompted me to approach my projects from different angles, and I appreciate being able to draw on your broad perspectives to pursue relevant research problems and try new ideas.

I am also thankful for my friends in the Gleason group and classmates in the Chemical Engineering department. I definitely would not have developed familiarity with vacuum equipment and the ability to troubleshoot problems without the help of Kelvin Chan and Ken Lau during my first months in lab. Shannon and Tyler were also helpful in bringing me up to speed in lab, and were just a lot of fun to hang out with. Sal and Sung Gap have been great friends throughout the five years. Their approach to research is different from mine, and I have learned much from their examples. Sreeram and Rama have been fun to chat with and discuss all matters of topics. Everyone else in the Gleason group has been a lot of fun. Together, we have faced many mini-crises in lab, such as exploding waste containers, dying pumps, and numerous lab clean-ups.

Friends and classmates from the department have been great for diversions from research. In particular, Brian and Arman were great friends to live with for three years. I could always count on Brian for logical considerations of problems and questions. Also, I owe him much for his help with computer issues. Arman has been a great friend to spend time with. Arman always has a positive life philosophy, and I could always count on him to encourage me when I was disillusioned with graduate school.

Last and most importantly, profound gratitude and love goes to my wife, Christy. Thank you for the endless encouragement through this process. You never gave up on me, even when I wanted to give up on myself. It may have not been apparent to you, but your supportive words and belief in me were incredibly motivating. Also, I am indebted to you for listening to many practice interview and thesis presentations. By now, you are also an expert on iCVD.

Table of Contents

List of Figures

CHAPTER ONE

CHAPTER TWO

CHAPTER THREE

CHAPTER FOUR

Figure A-6. (a) Response of fabricated sensors to varying nitrobenzene concentrations at 40 °C. The response to water vapor is also included. For the first five minutes, no analyte was introduced into the system. A constant analyte concentration was introduced for the next 40 minutes, followed by five minutes of purging with pure N_2.128

List of Tables

List of Acronyms and Abbreviations

4NT	4-nitrotoluene
CVD	chemical vapor deposition
FTIR	Fourier transform infrared spectroscopy
GPC	gel permeation chromatography
HFCVD	hot filament chemical vapor deposition
iCVD	initiated chemical vapor deposition
MLD	molecular layer deposition
NB	nitrobenzene
NMR	nuclear magnetic resonance
P4VP	poly(4-vinylpyridine)
PECVD	plasma enhanced chemical vapor deposition
P_M/P_{sat}	ratio of a species partial pressure to its saturated partial pressure at the system temperature
PMaDD	poly[maleic anhydride-co-dimethylacrylamide-co-di(ethylene glycol) divinyl ether]
poly(Ma-D)	poly[maleic anhydride-co-di(ethylene glycol) divinyl ether]
poly(Ma-V-D)	poly[maleic anhydride-co-vinyl pyrrolidone-co-di(ethylene glycol) divinyl ether]
ppq	parts per quadrillion
ppt	parts per trillion
PSMa	poly(styrene-alt-maleic anhydride)
sccm	standard cubic centimeters per minute
TNT	2,4,6-trinitrotoluene

CHAPTER ONE

Introduction

1.1 Motivation

Polymeric thin film coatings are critical components in many practical applications. Low surface energy interfaces,[1-3] adhesive surfaces,[4-6] biocompatible surfaces,[7-9] membrane separations,[10] lithographic patterning,[11-14] microfabrication,[15-17] and sensors[18-20] are common practical applications utilizing polymer thin films. Ultimately, the chemical composition and physical properties (e.g. conformation) of a polymer will determine its suitability for specific applications. For example, the surface energy of a coating controls the interaction of a surface with fluid environments.

In practical implementations of devices or processes, the environment is not static.[21] As the environment changes, the surface adapts to accommodate these changes. Better control over the system can be achieved by precisely engineering the surface's response. For example, one might want the surface to switch from being hydrophobic to hydrophilic, conductive to non-conductive, charged to uncharged, or adhesive to repellant. Stimuli-responsive polymer films, often termed "smart" surfaces, which undergo compositional or conformational changes upon application of an external stimulus, can be designed to meet these requirements. All polymers are essentially stimuli-responsive, as polymer conformation changes with solvent quality.[22] The objective in designing stimuli-responsive polymer films, though, is enabling a response to practically and conveniently manipulated stimuli. Convenient stimuli include temperature,[23] pH,[24] light,[25] voltage or electric potentials,[26, 27] magnetism,[28] and specific physical and chemical interactions.[29, 30] Stimuli responsive polymers is a very broad field, and the response mechanisms vary depending on the application. To illustrate general principles, though, a conceptual drawing of the response of a surface-grafted polyelectrolyte brush to a pH change is provided in Figure 1-1. Here an anionic polyelectrolyte is drawn; it becomes negatively charged and its chain extends as the pH of the fluid is increased past the polymer's pK_a. Opposite behavior is observed for cationic polyelectrolytes. At low pH, the polymer is positively charged, and then becomes uncharged as the pH is increased.

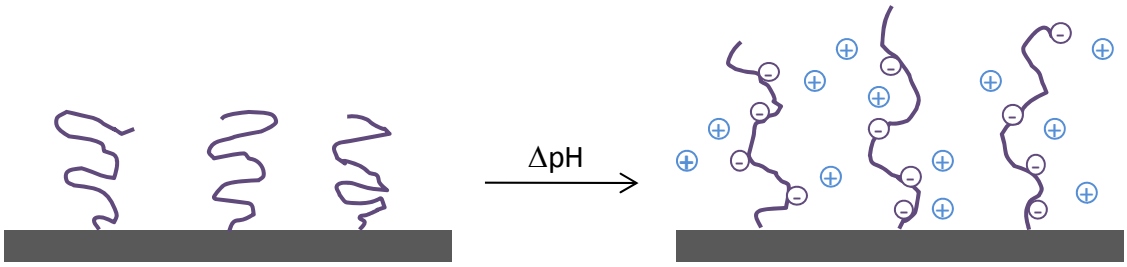

Figure 1-1. Illustration of the response of an anionic polyelectrolyte brush to a change in pH of the surrounding medium. The ionizable functional groups deprotonate to become negatively charged, and the brushes extend due to increased repulsive forces.

The polymer composition is integral to defining if and how a film responds to external stimuli.[5] To engineer films with highly specific and desired responsive behavior, the ability to finely tune the film composition through synthesis is required. Generally, there are two classes of polymer thin film synthetic techniques: bottom-up and top-down. In bottom-up fabrication, polymer precursors (i.e. monomers) are delivered to the surface, and the polymer are synthesized at the surface. In top-down, on the other hand, polymers are synthesized beforehand and then immobilized on the surface through any number of techniques. Top-down fabrication enables well-established solution polymerization techniques to be utilized in designing the compositions. Fine control over compositions in bottom-up techniques is complicated by the restrictions imposed by the surface (such as solvent properties, temperature, etc.) and the requirement of adhesion between the surface and film.

Solution-based and vapor-based techniques are capable of synthesizing polymer films from the bottom-up. Solution-based techniques generally consist of immobilizing or generating initiators on a surface, and then synthesizing polymer chains as monomers in the solution combine with activated initiator. Chemical vapor deposition (CVD) is the prominent vapor-based polymer deposition technique. In chemical vapor deposition, monomers are delivered to a coating chamber as vapors, and an energy input creates reactive species that incorporate into polymer films on the surface. Chemical vapor deposition is an invaluable technique as it avoids wetting and surface tension effects that are inevitable

in both bottom-up and top-down solution-based methods.[31] When coating three-dimensional nanoscale architectures, these effects can lead to poor conformality and non-uniformity of the polymer coatings. Also, CVD avoids the use of solvents, which is economically and environmentally advantageous.[32] Especially with spin-on deposition or solution dipping techniques, large quantities of solvent are discarded or must be recycled. Manufacturing personnel are also exposed to potentially hazardous and toxic solvents. Further benefits of CVD include fine, nanometer-level control over the coating thickness[33] and simultaneous crosslinking for mechanical stability.[34] CVD can also deposit insoluble and infusible polymers, which is exceedingly difficult by solution techniques.

1.2 Chemical Vapor Deposition of Polymers

Most chemical vapor deposition techniques occur in vacuum. Chemical vapor deposition consists of four integral processes: introduction of the precursors into the reaction chamber, generation of reactive species, transport of species to the substrate, and reaction of the species to generate the film (i.e. coating). If the precursors are liquids or solids, generally they are vaporized by heating to create sufficient vapor pressure. Bubblers can be used for precursors with lower vapor pressures. These vapors are then metered into the reaction chamber using mass flow controllers, and the pressure of the system is maintained using a pressure controller and throttle valve. The unreacted vapors are pumped through the chamber exhaust with a vacuum pump. Energy is introduced from an external source to generate the reactive species. Transport of vapor species to the substrate occurs via random thermal motion. It is also promoted by chemical potential gradients that develop as species react on the surface and the stage being at lower temperatures, which promotes adsorption of molecules onto the substrate as monolayers or multilayers. As the molecules adsorb onto the substrate, the reactive species react to create the polymeric film.

There is significant variety among polymer CVD techniques concerning the method of energy input into the system. Energy inputs from thermal, plasma, and UV light sources are the most common. Because the reactive species define the final composition of the film, energy input is a critical parameter in designing stimuli-responsive polymer thin films where film compositions need to be controlled precisely.

In thermal CVD, the entire deposition system is heated such that the vacuum chamber and vapors are at a uniform temperature. The high temperatures (as high as hundreds of degrees Celsius) lead to higher polymerization kinetics. Thermal CVD of condensation polymers, such as polyamides,[35] polyimides,[36] and polyamino acids,[37] have been demonstrated. These techniques are often termed vapor deposition polymerizations. Processes similar to atomic layer deposition, called molecular layer deposition (MLD), have been developed to conformally deposit condensation polymers with very fine thickness control.[38, 39] A common variant of thermal CVD is the deposition of poly(para-xylylenes), also called the parylene process, which was developed in 1947.[40] In the parylene process, an external furnace is used to heat the parylene monomers to greater than 600 °C to generate reactive radical species as they flow into the chamber. The vacuum chamber containing the substrate is maintained at lower temperatures (25 – 30 °C) to promote the adsorption of the reactive species.[41]

Another common polymer CVD technique is plasma enhanced chemical vapor deposition (PECVD). In PECVD, an electric discharge is generated, capacitively between parallel plate electrodes or inductively inside a spiral-wound electrode, to excite the monomer vapors.[21] Radical species are generated from the monomer species due to the excitation process, and these radical species react to create the polymer-like film.

Hot-filament CVD (HFCVD) is similar to thermal CVD in that a thermal energy source is used, but rather than heating the entire system, a filament suspended above the substrate is heated resistively –

leading to a temperature increase of the surrounding vapors. The rest of the reactor is maintained at lower temperatures, which leads to greater flux to the surface.

Other CVD techniques use UV light to activate the polymerization reaction. To use UV light, a component of the reactor feed must be UV-sensitive. As this component absorbs UV light, radical species are generated that initiate polymerization. UV CVD techniques allow for fine control over the composition as activation of the polymerization is restricted to the site of the UV-sensitive functionality.[42, 43]

Another technique that allows for very fine control over polymer compositions is initiated chemical vapor deposition (iCVD). iCVD is essentially a HFCVD technique; the difference is the vapor-phase chemistry that enables selective activation of the polymerization reactions.

1.3 Initiated Chemical Vapor Deposition (iCVD)

Initiated chemical vapor deposition is distinct from HFCVD by the inclusion of a thermally labile peroxide molecules in the precursor feed. The peroxide precursor, termed the initiator, enables the use of filament temperatures that are hundreds of degrees cooler, on the order of 200 – 300 °C. At these temperatures, the initiator molecules homolytically dissociate into radical species, while the chemical functionalities of the monomers remain intact since they are not thermally labile. The breadth of potential monomers that can be polymerized is large. Monomers that undergo free-radical polymerization or copolymerization, typically those containing vinyl bonds, are suitable precursors.[44-46] Given that solution-phase free-radical polymerization is a widely practiced commercial technique scores of vinyl monomers are commercially available.

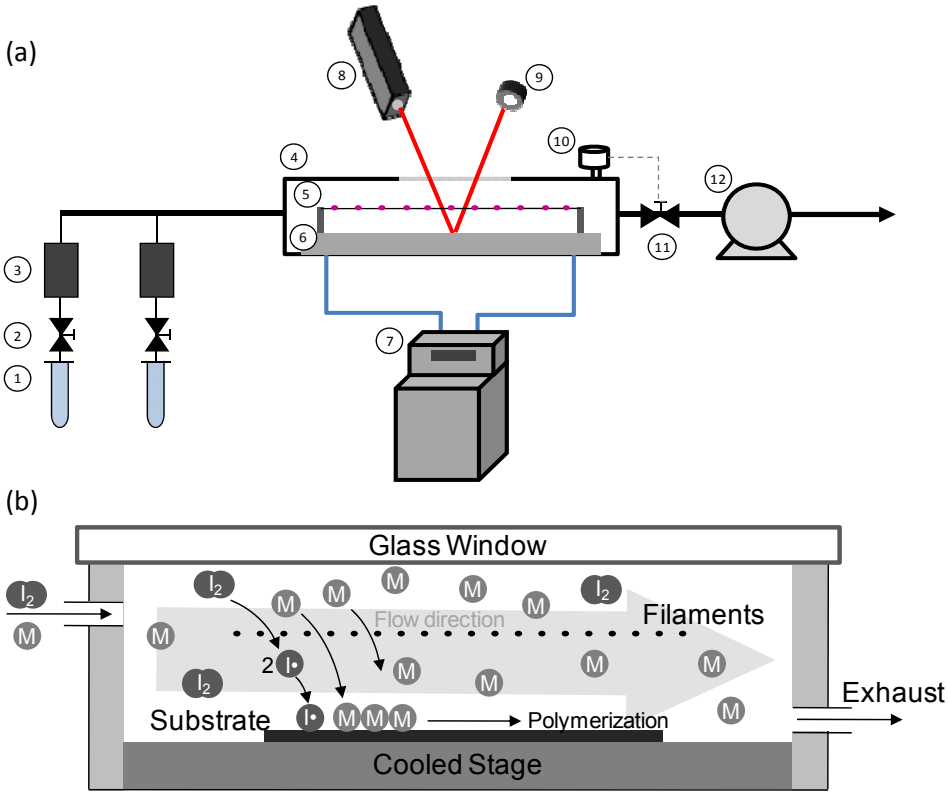

Figure 1-2. (a) Schematic of the iCVD reactor configuration. The required components are: (1) monomer source, (2) monomer isolation valve, (3) mass-flow controller, (4) vacuum chamber, (5) filament array, (6) temperature-controlled stage, (7) water recirculator (for temperature control), (8) inteferometry laser, (9) photo meter, (10) pressure gauge with feedback control loop, (11) throttling valve, and (12) vacuum pump. (b) Conceptual drawing of the cross-section of the vacuum chamber to describe the iCVD process (not drawn to scale).

The iCVD reactor configuration is provided in Figure 1-2a, and the conceptual illustration of the iCVD mechanism is shown in Figure 1-2b. The reactor schematic shows that the equipment used for iCVD and other types of CVD is essentially equivalent. The primary difference is the use of an initiator. Figure 1-2b illustrates the primary processes in iCVD. Both initiator and monomer vapors are introduced into the vacuum chamber. The substrate sits on top of a temperature controlled stage, typically maintained at 20 – 50 °C, to promote adsorption of the species onto the surface. The monomer is chemically unaffected by the filament. The extent of monomer adsorption is described through the Brunauer-Emmett-Teller equation below[44]

$$V_{ad} = \frac{V_{ml} c \left(P_M / P_{sat} \right)}{\left(1 - P_M / P_{sat} \right) \left[1 - \left(1 - c \right) \left(P_M / P_{sat} \right) \right]} \qquad \text{Eq. 1-1}$$

where V_{ad} is the volume of the adsorbed monomer (can be directly related to the surface concentration), V_{ml} is the volume of a single monolayer of monomer, c is a constant, and P_M/P_{sat} is the ratio of the monomer's partial pressure to its saturated vapor pressure defined at the substrate temperature. As P_M/P_{sat} increases, more monomer adsorbs onto the surface resulting in multilayers of adsorbed monomer.

The initiator is believed to homolytically dissociate into radicals in the gas phase surrounding the filaments. The radicals react with monomers to generate monomer radicals in the vapor phase through a collision or on the substrate. As radical species encounter the surface, they react with the adsorbed monomers to start the polymerization. The theory that polymerization occurs on the surface rather than in the gas phase is supported through analysis of the effect of molecular weight on vapor pressure and fundamental studies of iCVD kinetics and copolymerization reactivity ratios.[44, 45] Termination occurs through the same processes present in solution techniques. Given this understanding of the polymerization kinetics, the composition of polymer films synthesized by iCVD can be controlled once the solution-phase polymerization kinetics and surface concentrations are understood.

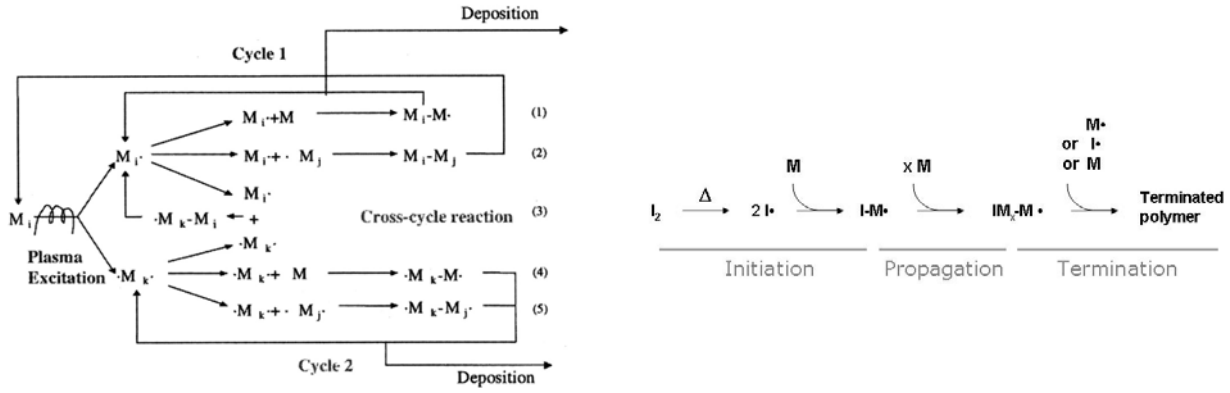

Figure 1-3. Comparison of the reaction mechanisms for (a) PECVD and (b) iCVD. The iCVD mechanism resembles free-radical polymerizations in solution. Panel (a) reproduced from [21]. Copyright 2005 Taylor & Francis Group, LLC.

The significance of this control is illustrated in Figure 1-3, where the mechanisms of PECVD and iCVD are compared. Due to the non-selective nature of plasma excitation, monoradical and diradical species are created in PECVD. Furthermore, the subscripts indicate that multiple monoradical and diradical species are created; they differ in the localization of the radical on the molecule. These radical species can react with other radical species or neutral species, and then collide with or stick to the surface or be activated again by the plasma. It is difficult to control the composition of the resulting polymer film *a priori*. Some loss of functionality and the presence of crosslinking are inevitable in PECVD, and the polymer films should not be considered equivalent to those synthesized in solution using the same precursors.[21] Pulsing the plasma to reduce the energy input leads to greater retention of chemical functionality at the expense of deposition rate (throughput), but 100% retention remains elusive. On the other hand, the mechanism of iCVD, illustrated in Figure 1-3b, is proposed to be essentially equivalent to free-radical polymerizations in solution.

1.4 Nitroaromatic Sensor Technologies

Chemical sensor fabrication is a natural application for initiated chemical vapor deposition of stimuli-responsive polymers. Sensors vary widely in terms of the underlying physical or chemical phenomena upon which they are based, but polymers are commonly employed in research and commercial systems to transduce a chemical signal into mechanical, optical, or electrical responses. The versatility in chemistry and physical properties of polymers enables the design of unique, innovative sensing strategies for many types of analytes.

Explosives are a particularly important class of analytes. Over 120 million landmines, littering 70 countries worldwide,[47] kill approximately 15 – 20,000 people each year, most of whom are civilians.[48] Furthermore, in the Second Persian Gulf War, also known as “Operation Iraqi Freedom”, 41% of United

States military casualties as of January 1, 2009, were caused by improvised explosive devices (IEDs).[49] Chemical compounds containing nitro moieties are widely used in explosive formulations; nitroaromatics compounds, such as 2,4,6-trinitrotoluene, are some of the most prevalent.

For many years, the most reliable and sensitive nitroaromatic sensing technology was the olfactory gland of canines. Canines can detect nitroaromatic concentrations in the low parts per trillion (ppt) to part per quadrillion (ppq) levels.[50] However, there are drawbacks to using canines. They have limited attention spans and can only be used uninterrupted for TNT detection for a couple of hours. Furthermore, they have short stand-off distances, requiring the dog and its human handler to be in close proximity to the bomb. They are expensive to train and operate. To overcome these limitations, the military has invested in new sensing technology. The best technology in terms of sensitivity uses amplifying fluorescent polymers. As nitroaromatics absorb into the polymer, its fluorescence intensity is attenuated[51]. These polymers have ppq sensitivity levels, and have been commercialized by iCX Technologies, Inc. in their Fido® system. This is a handheld device that can also be mounted to robots to probe for explosive devices remotely.[52] While this technology offers many advantages over canines, they are expensive (especially when the price of a robot is considered). Also, they require consumables for prolonged operation since the detector actively monitors the fluorescence of the polymer. The lifetimes of the camcorder-sized battery and sensing element are 4 and 8 hours, respectively.[52] With dismounted warfighters commonly carry loads in excess of 100 pounds of equipment, there is much emphasis on reducing the weight and volume of their equipment.[53]

Efforts to miniaturize sensors are currently ongoing. Systems based on microelectromechanical systems (MEMS) are promising.[54] Monitoring the static deflection or change in resonant frequency of microcantilevers due to their interaction with analytes is a common strategy. Figure 1-4 describes common transduction mechanisms that cause deflection. Typically, these interactions lead to deflection of the cantilever by tens of nanometers up to a micrometer. Optical, piezoresistive, piezoelectric, or

capacitive techniques are the most common schemes to measure tip deflection.[55] Optical techniques require bulky, expensive optical equipment, as does the iCX Fido® system, which is difficult to miniaturize and requires significant power. The electrical techniques also require a continuous power source. The bulk, power requirements, and expense of such systems ultimately limit the deployment of sensors, regardless of their performance.

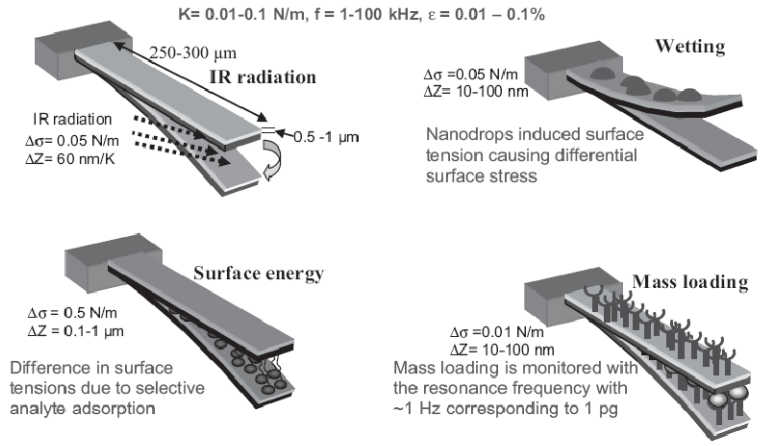

Figure 1-4. Tranduction mechanisms common to microcantilever sensors. Typical differential stresses and deflections are provided. In addition to tip deflection, the resonant frequency of the cantilever oscillations changes. Figure from Ref. [56].

The United States military is interested in stand-alone, distributed nitroaromatic sensors capable of wirelessly communicating detection events. Figure 1-5 illustrates conceptually how these sensors could be employed. Another possibility is distributing these sensors throughout neighborhoods where explosive devices are suspected to be synthesized; the sensor would transmit its location upon detecting explosives. For these schemes, the sensors will need to be microscale, selective towards explosives, and require little power. Optical readout schemes are precluded due to their size and power requirements. To mitigate power requirements of electronic circuitry, chemical switches can be designed that start in the "off" state. Initially, the switch is disconnected, preventing current from passing through the circuit. Upon the interaction of an analyte with the switch architecture, the switch closes – turning on the circuit and allowing transmission of a wireless signal. The simplicity of these

designs eliminates the need for extensive logic circuitry, ultimately allowing further miniaturization and cost reduction.

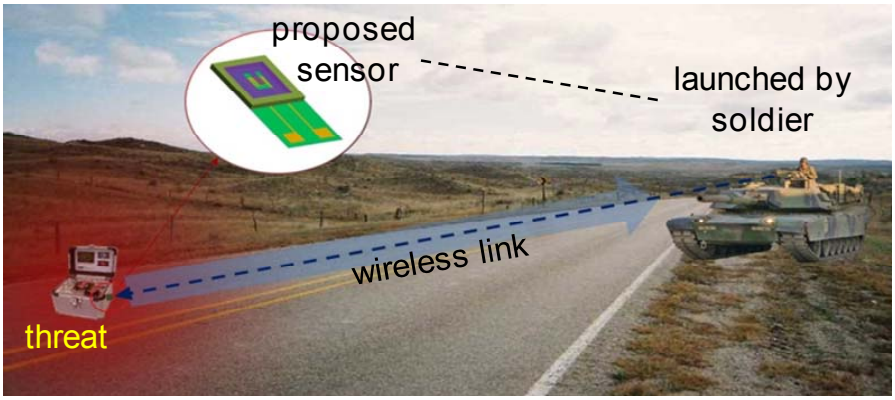

Figure 1-5. Conceptual operation of stand-alone microsensor. The switch-base sensor contains two primary components: the nitroaromatic-sensitive polymer and reporting circuitry.

In this thesis, sensor architectures with switch-like responses that are readily and cost-effectively fabricated have been designed. Experiences in finely tuning polymer thin film compositions though iCVD have been utilized to create polymers films that strongly and selectively interact with desired analytes and actuate the switches due to these interactions. The thesis research also demonstrates the unique capabilities of iCVD that enabled these new sensor designs.

1.5 Scope of Thesis

This thesis utilizes the control of iCVD over polymer film compositions to synthesize stimuli-responsive and reactive polymer thin films. Emphasis is placed on developing novel, versatile polymer chemistries and implementing the films in practical applications. Furthermore, advantages of iCVD are highlighted by reporting the synthesis of polymer chemistries or implementation of films into designs that are difficult to achieve with solution-based or other CVD techniques. Each chapter that follows introduces a new polymer chemistry, and chapters three through five describe their applications. Each chapter can be considered a separate project, yet the theme of responsive films is present throughout.

CHAPTER TWO describes the synthesis of poly(styrene-alt-maleic anhydride). This is an alternating polymer where styrene and maleic anhydride incorporate into the polymer in a one-to-one fashion to generate a structure where either monomer is neighbored by the co-monomer. This yields a well-defined reactive composition. The reactivity of maleic anhydride can be utilized in practical applications, as demonstrated in CHAPTERS THREE and FOUR. This is the first time that alternating copolymers have been synthesized by a chemical vapor deposition technique.

In CHAPTER THREE, the composition of poly(styrene-alt-maleic anhydride) is modified to create pH-responsive hydrogel materials. The ability to finely control how much crosslinker is incorporated into polymer films using iCVD has been exploited to generate highly swellable hydrogels. Maleic anhydride is responsible for creating stable adhesion of the film to the substrate, as well as the pH-responsive behavior. These films have been shown to act as permeable, size-selective skin layers in composite membranes.

CHAPTER FOUR examines another maleic anydyride-based copolymer chemistry, but for sensor applications. Herein, the volume expansion response due to the reaction of maleic anhydride with amines has been used to design selective sensors for amine compounds. Two copolymer compositions are compared, and it is shown that high crosslinking densities, which are conveniently achieved using iCVD, are necessary for efficient operation of the sensor. The reactive films are integrated onto silicon nitride microcantilevers to fabricate chemical sensors with switch-like changes in electrical resistance. The sensor design is innovative in terms of its power requirements and readout simplicity.

In CHAPTER FIVE, poly(4-vinylpyridine) (P4VP) polymer films deposited by iCVD are investigated as nitroaromatic-responsive materials. Nitroaromatics are common explosives in improvised explosives devices and landmines, and the objective of this work was to develop materials to enable microscale sensors. Upon exposure to explosive simulants nitrobenzene and nitrotoluene, the iCVD-deposited P4VP layers swell by over 30%. The importance of this finding is emphasized by considering the

requirements of multicomponent sensor arrays and comparing the performance of P4VP to conventional nitroaromatic-selective layers.

CHAPTER SIX provides conclusions concerning the synthesis of the responsive polymer films by iCVD. The intricacies of iCVD are highlighted to reveal the capabilities and limitations of the technique. Future studies an aspects of the projects deemed most valuable are also suggested. In particular, the project concerning nitroaromatic explosives sensors is emphasized as a fruitful area for continued study since minitiaturization and simplification of sensing hardware can lead to practical implementation of the technology to solve important real-world challenges.

An appendix is also included describing the development of a new sensing design that utilizes the swelling response of P4VP to nitroaromatic exposure. This new design seeks to maintain the low power requirements characteristic of the design in CHAPTER FOUR and reduce the length scale of the active component by over two orders of magnitude. The performance of this design is analyzed with respect to P4VP, and proof-of-principle detection of nitrobenzene vapors in an unoptimized design is demonstrated.

This material is based upon work supported under a National Science Foundation Graduate Research Fellowship. The research was also supported in part by the U.S. Army through the Institute for Soldier Nanotechnologies, under Contract DAAD-19-02-0002 with the U.S. Army Research Office. The work made use of MRSEC Shared Facilities supported by NSF Grant DMR-9400334.

References

[1] K. K. S. Lau, J. Bico, K. B. K. Teo, M. Chhowalla, G. A. J. Amaratunga, W. I. Milne, G. H. McKinley, K. K. Gleason, *Nano Letters* **2003**, *3*, 1701.

[2] Y. Mao, K. K. Gleason, *Macromolecules* **2006**, *39*, 3895.

[3] S. K. Murthy, K. K. Gleason, *Macromolecules* **2002**, *35*, 1967.

[4] L. Leger, E. Raphael, H. Hervet, "Surface-anchored polymer chains: Their role in adhesion and friction", in *Polymers in Confined Environments*, Springer-Verlag Berlin, Berlin, 1999, p. 185.

[5] I. Luzinov, S. Minko, V. V. Tsukruk, *Prog. Polym. Sci.* **2004**, *29*, 635.

[6] V. V. Tsukruk, *Adv. Mater.* **2001**, *13*, 95.

[7] J. Lahann, *Polym. Int.* **2006**, *55*, 1361.

[8] B. Rihova, *Adv. Drug Deliv. Rev.* **1996**, *21*, 157.

[9] E. Ruckenstein, Z. F. Li, *Adv. Colloid Interface Sci.* **2005**, *113*, 43.

[10] M. Ulbricht, *Polymer* **2006**, *47*, 2217.

[11] C. J. Hawker, T. P. Russell, *MRS Bull.* **2005**, *30*, 952.

[12] B. Michel, A. Bernard, A. Bietsch, E. Delamarche, M. Geissler, D. Juncker, H. Kind, J. P. Renault, H. Rothuizen, H. Schmid, P. Schmidt-Winkel, R. Stutz, H. Wolf, *IBM J. Res. Dev.* **2001**, *45*, 697.

[13] J. A. Moore, J. O. Choi, *Acs Symposium Series* **1991**, *475*, 156.

[14] Z. H. Nie, E. Kumacheva, *Nat. Mater.* **2008**, *7*, 277.

[15] A. Facchetti, M. H. Yoon, T. J. Marks, *Adv. Mater.* **2005**, *17*, 1705.

[16] G. Maier, *Prog. Polym. Sci.* **2001**, *26*, 3.

[17] J. Veres, S. Ogier, G. Lloyd, D. de Leeuw, *Chem. Mat.* **2004**, *16*, 4543.

[18] B. Adhikari, S. Majumdar, *Prog. Polym. Sci.* **2004**, *29*, 699.

[19] J. W. Grate, *Chem. Rev.* **2000**, *100*, 2627.

[20] S. W. Thomas, G. D. Joly, T. M. Swager, *Chem. Rev.* **2007**, *107*, 1339.

[21] H. Yasuda, "*Luminous Chemical Vapor Deposition and Interface Engineering*", Marcel Dekker, New York, 2005.

[22] L. H. Sperling, "*Introduction to Physical Polymer Science*", 4th edition, John Wiley & Sons, Hoboken, 2006.

[23] A. Kikuchi, T. Okano, *Prog. Polym. Sci.* **2002**, *27*, 1165.

[24] I. Tokarev, S. Minko, *Soft Matter* **2009**, *5*, 511.

[25] S. H. Bergman, F. Wudl, *Journal of Materials Chemistry* **2008**, *18*, 41.

[26] R. V. Kulkarni, S. Biswanath, *J. Appl. Biomater. Biomech.* **2007**, *5*, 125.

[27] S. Murdan, *J. Control. Release* **2003**, *92*, 1.

[28] Z. Lu, M. D. Prouty, Z. Guo, V. O. Golub, C. S. S. R. Kumar, Y. M. Lvov, *Langmuir* **2005**, *21*, 2042.

[29] H. Inoue, K. Sato, J.-i. Anzai, *Biomacromolecules* **2005**, *6*, 27.

[30] P. M. Mendes, *Chem. Soc. Rev.* **2008**, *37*, 2512.

[31] S. H. Baxamusa, K. K. Gleason, *Chem. Vapor Depos.* **2008**, *14*, 313.

[32] W. S. O'Shaughnessy, S. K. Murthy, D. J. Edell, K. K. Gleason, *Biomacromolecules* **2007**, *8*, 2564.

[33] M. Karaman, S. E. Kooi, K. K. Gleason, *Chem. Mat.* **2008**, *20*, 2262.

[34] W. J. Arora, W. E. Tenhaeff, K. K. Gleason, G. Barbastathis, *J. Microelectromech. Syst.* **2009**, *18*, 97.

[35] J. Sakata, M. Mochizuki, *Thin Solid Films* **1996**, *180*, 277.

[36] J. R. Salem, F. O. Sequeda, J. Duran, W. Y. Lee, R. M. Yang, *J. Vac. Sci. Technol. A-Vac. Surf. Films* **1986**, *4*, 369.

[37] N. H. Lee, C. W. Frank, *Langmuir* **2003**, *19*, 1295.

[38] N. M. Adarnczyk, A. A. Dameron, S. M. George, *Langmuir* **2008**, *24*, 2081.

[39] Y. Du, S. M. George, *J. Phys. Chem. C* **2007**, *111*, 8509.

[40] M. Szwarc, *Discussions of the Faraday Society* **1947**, *2*, 46.

[41] W. F. Gorham, *Journal of Polymer Science, Part A1* **1966**, *4*, 3027.

[42] S. H. Baxamusa, L. Montero, J. M. Dubach, H. A. Clark, S. Borros, K. K. Gleason, *Biomacromolecules* **2008**, *9*, 2857.

[43] K. Chan, K. K. Gleason, *Langmuir* **2005**, *21*, 11773.

[44] K. K. S. Lau, K. K. Gleason, *Macromolecules* **2006**, *39*, 3688.

[45] K. K. S. Lau, K. K. Gleason, *Macromolecules* **2006**, *39*, 3695.

[46] W. E. Tenhaeff, K. K. Gleason, *Adv. Funct. Mater.* **2008**, *18*, 979.

[47] V. K. Pamula, "Detection of Explosives", in *Handbook of Machine Olfaction - Electronic Nose Technology*, T.C. Pearce, S.S. Schiffman, H.T. Nagle, and J.W. Gardner, Eds., Wiley-VCH, Weinheim, 2003.

[48] Explosive Science. http://www.rsc.org/chemistryworld/restricted/2005/December/Explosive.asp (accessed March 1, 2009).

[49] Iraq Coalition Casualty Count. http://www.icasulties.org (accessed Feb. 1, 2009).

[50] J. W. Gardner, J. Yinon, "*Electronic Noses & Sensors for the Detection of Explosives*", Kluwer Academic Publishers, Boston, 2004.

[51] J.-S. Yang, T. M. Swager, *Journal of the American Chemical Society* **1998**, *120*, 5321.

[52] Fido Explosives Detector, ICx Technologies, Inc. http://www.icxt.com/products/icx-detection/explosives/fido (accessed Apr 1, 2009).

[53] National Research Council, Committee of Soldier Power/Energy Systems. *Meeting the Energy Needs of Future Warriors*; Washington, DC, 2004.

[54] L. Senesac, T. G. Thundat, *Mater. Today* **2008**, *11*, 28.

[55] N. V. Lavrik, M. J. Sepaniak, P. G. Datskos, *Rev. Sci. Instrum.* **2004**, *75*, 2229.

[56] S. Singamaneni, M. C. LeMieux, H. P. Lang, C. Gerber, Y. Lam, S. Zauscher, P. G. Datskos, N. V. Lavrik, H. Jiang, R. R. Naik, T. J. Bunning, V. V. Tsukruk, *Adv. Mater.* **2008**, *20*, 653.

CHAPTER TWO

Initiated Chemical Vapor Deposition of Alternating Copolymers of Styrene and Maleic Anhydride*

Abstract

Initiated chemical vapor deposition (iCVD) of alternating copolymer thin films has been achieved for the first time. Copolymerization is desirable for maleic anhydride (Ma) since this monomer does not homopolymerize to an appreciable extent. At conditions where the observed deposition rates for styrene (S) and Ma homopolymers were only 0 and 5.5 nm/min, respectively, combining the two monomers resulted in a much higher deposition rate of 75.4 nm/min. iCVD processes utilize low energy (<30 W) to generate peroxy radicals from initiator molecules while avoiding degradation of functional groups in the monomers. Indeed, full retention of the anhydride functionality from the Ma monomer and avoidance of undesirable side reactions was observed in iCVD of poly(styrene-alt-maleic anhydride) (PSMa) copolymer films. Fourier transform infrared spectroscopy (FTIR), x-ray photoelectron spectroscopy (XPS), and ^{13}C nuclear magnetic resonance (NMR) conclusively demonstrate that all of the copolymer films contain 50% styrene and 50% maleic anhydride (within experimental error), irrespective of gas feed ratios employed during the deposition. The ^{13}C NMR signal in the 136 – 140 ppm region from the quaternary carbon in styrene and additional distortionless enhancement polarization transfer (DEPT) experiments confirmed the copolymers are strictly alternating. Varying the gas feed ratio of maleic anhydride to styrene provided control over deposition rates and number average molecular weights. Number-average molecular weights varied from 1380 to 4680 g/mol, and deposition rates varied from 6.3 to 75.4 nm/min.

2.1 Introduction

For applications throughout many research disciplines, creating thin films of polymers with reactive pendent groups is a critical first step in device fabrication. A recent review has discussed many potential sensor and microarray applications for patterned, responsive hydrogels on surfaces[1]. Of particular interest are thin copolymer films where one comonomer is maleic anhydride. Maleic anhydride is desirable for its high reactivity; the ease in functionalizing maleic anhydride copolymers has been demonstrated in numerous studies[2-4]. Furthermore, the versatile reaction chemistry of maleic anhydride groups makes these copolymers potentially useful biomaterials; a brief survey of typical reactions relevant to biological applications has been provided by Pompe et al.[5] The high reactivity of maleic anhydride compared to other anhydrides, which allows it to react at room temperature with nucleophiles such as amines and hydroxyls, has been attributed to ring strain[6]. Drug carriers[7, 8], glycoconjugates on sufaces[9], and platforms for covalent immobilization of poly(ethylene glycol)[10], proteins[11], DNA[12], and biopolymers[13] are just a few applications taking advantage of the facile functionalization of the anhydride group in copolymers of styrene and maleic anhydride.

Chemical vapor deposition (CVD) is a convenient technique for producing thin polymer films. CVD is a one-step process that is typically performed under vacuum conditions. CVD produces conformal, pinhole-free coatings on two- or three-dimensional objects with nanometer level thickness control[14, 15]. Unlike other common film formation techniques, such as spraying, layer-by-layer assembly, dipping, or spin casting, CVD techniques do not require solvent removal after film fabrication, which is important for products that will potentially be commercialized. Processes employing solvents raise concerns over environmental pollution and potential toxicity from incomplete solvent removal[16]. For example, the importance of solvent removal is recognized by the United States Pharmacopeia, which set official limits for pharmaceuticals in 2002[17].

Plasma-enhanced CVD (PECVD) is capable of creating thin films of polymer-like biomaterials[18-20] without solvent. However, a recognized limitation of PECVD is destruction of some chemical functionality in the monomers, which can lead to non-selective crosslinking and film stoichiometries that differ from polymers prepared in conventional solution-based techniques[20]. Indeed, crosslinking and loss of anhydride functionality was observed in continuous wave PECVD of poly(maleic anhydride)[21, 22] To improve the retention of the anhydride functionality in the films, pulsed plasma depositions have been investigated. Short plasma on-times clearly improve the retention of the anhydride functionality, but in each case the carbon-to-oxygen ratio differed from the stoichiometric value[21, 22]. Spectroscopic techniques also reveal the presence of functional groups not expected for a linear, homopolymer chain from maleic anhydride[21, 23] The loss of chemical specificity makes the production of well defined copolymers by conventional PECVD exceedingly difficult.

An alternative technique to PECVD is initiated chemical vapor deposition (iCVD). In iCVD, the vapor feed consists of one or more monomers and an initiator which flow into the reactor under vacuum. All species pass over a heated filament array; where the filament temperature is maintained at a temperature sufficient to thermally dissociate the initiator but insufficient to cause thermal decomposition of the monomer species. Initiator radicals react with monomers adsorbed on the substrate to start the polymerization. The iCVD process shares many of the advantages of standard CVD techniques, but it has also been shown to produce polymers which are stoichiometrically identical to those obtained in solution[24-26]. Crosslinking and loss of pendent functionality can be completely eliminated by iCVD. In fact, detailed studies and modeling have shown that iCVD is equivalent to the solution-phase polymerizations, where the reaction kinetics are governed by surface concentrations of the monomers[27, 28]. Because iCVD is equivalent to solution phase polymerizations, free radical copolymerizations are also possible; relative surface concentrations of the comonomers govern reaction kinetics and copolymer compositions[24, 29, 30].

To produce thin films containing maleic anhydride, the strategy of this work was to copolymerize maleic anhydride with styrene via iCVD. The copolymerization approach was chosen since it is well-established that maleic anhydride does not readily homopolymerize under standard free-radical conditions, but readily copolymerizes with many monomers[31]. Styrene was chosen as the comonomer because the resulting copolymer is highly versatile and used in a wide array of applications[6], as described above. Styrene and maleic anhydride are known to yield alternating copolymers in wet chemical syntheses. Successful polymerization of alternating copolymers by an all dry method will further bolster the theory that iCVD polymerizations are analogous to solution phase polymerizations and extend the proven breadth of iCVD chemistry. Moreover, it will enable the conformal deposition of maleic anhydride functionality on three-dimensional and solvent-sensitive surfaces, which is difficult to achieve with solution-based techniques. The aim of the current work has been to characterize the copolymer films deposited through iCVD to confirm that the anhydride functionality is retained and an alternating copolymer is formed. Depositions have been performed with different ratios of styrene and maleic anhydride surface concentrations to show that deposition kinetics are indeed enhanced relative to depositions where only styrene or maleic anhydride is present. A variety of spectroscopic techniques have also been employed to characterize the composition and sequence distribution of the copolymers.

2.2 Experimental

Depositions were performed in a custom-built vacuum chamber (Sharon Vacuum) that is rectangular in shape with a 3.8-cm internal height, 40.6-cm width, and 45.7-cm length. The reactor body is stainless steel, and the lid is aluminum. A borosilicate glass plate, 15-cm in diameter and machined so its internal surface is flush with the aluminum lid, was located in the middle of the lid. The glass plate allowed convenient sample introduction and monitoring of reaction progress. Water from an

external refrigerated water recirculator (Thermo Electron) was supplied to a cold-plate (D6 Industries) in the center of the reactor in order to maintain the substrates at a constant temperature of 25 ºC through thermal contact with the plate. Chromaloy O (75% iron, 20% chromium, 5% aluminum) filaments (Goodfellow) were suspended 1.5-cm above the substrate in a custom designed filament holder. There were 14 parallel filaments, spaced 1.5-cm apart along the direction of flow. The filaments were heated to ~280 ºC, measured with a type-K thermocouple (Omega Engineering) connected directly to the filament, by supplying a constant 1.15 amps from a DC power supply (BK Precision). Vapor entered at one end of the reactor through three inlet ports, 1.27-cm in diameter, and exited through pump-out ports located underneath the reactor on the opposite side of the reactor. Vacuum was achieved by a rotary vane pump (D65, Leybold). All depositions were performed at a pressure of 1 Torr, which was measured by a capacitance monometer (Type 626A, MKS Instruments). A butterfly-type throttling valve (Type 652B, MKS Instruments) was used to maintain the pressure.

All depositions were performed on 100-mm diameter silicon (Si) wafer substrates (Wafer World). Half-wafers were used for replicate depositions. Maleic anhydride (99%), styrene (98%), and tert-butyl peroxide (97%) were purchased from Aldrich and used without further purification. Maleic anhydride (Ma) was heated to 90 ºC in a glass jar to create vapor that was then metered into the reactor at a controlled flow rate through a mass-flow controller (Model 1152C, MKS Instruments). Styrene (S) was heated to 75 ºC; its flow rate was controlled with a manual needle valve. A capacitance manometer placed upstream of the needle valve verified the flow rate remained constant throughout the deposition. Tertiary-butyl peroxide (TBPO) remained at room temperature in a glass jar; its vapor flow rate was also set with a mass flow controller (Model 1479, MKS Instruments). Depositions for nine possible combinations of three maleic anhydride and three styrene flow rates were performed. For statistical analysis, depositions were performed in triplicate. These flow rates are provided in Table 2-1. The TBPO flow rate remained constant at 4 sccm, and an argon (ultra-high purity, Airgas) patch flow was

used to maintain the total flow rate at 30 sccm. Literature values of saturation partial pressures ($P_{m,sat}$) at 25 ºC for styrene[32] and maleic anhydride[6] were used to calculate partial pressure ratios in Table 2-1. In addition to the nine depositions, two additional depositions were performed to attempt depositions of polystyrene and poly(maleic anhydride) homopolymers at the highest monomer partial pressure ratios.

Table 2-1. Experimental flow rate settings and corresponding partial pressure ratios.

Sample	Flow rates (sccm)					$P_m/P_{m,sat}$	
	Ma	S	TBPO	Ar	Total	Ma	S
Ma/S-2/5	2	5	4	19	30	0.29	0.03
Ma/S-2/10	2	10	4	14	30	0.29	0.05
Ma/S-2/20	2	20	4	4	30	0.29	0.11
Ma/S-4/5	4	5	4	17	30	0.57	0.03
Ma/S-4/10	4	10	4	12	30	0.57	0.05
Ma/S-4/20	4	20	4	2	30	0.57	0.11
Ma/S-6/5	6	5	4	15	30	0.86	0.03
Ma/S-6/10	6	10	4	10	30	0.86	0.05
Ma/S-6/20	6	20	4	0	30	0.86	0.11
Ma/S-0/20	0	20	4	6	30	0.00	0.11
Ma/S-6/0	6	0	4	20	30	0.86	0.00

The progress of the depositions was monitored *in situ* by interferometry with a 633-nm HeNe laser source (JDS Uniphase). After the depositions, more accurate measurements of film thicknesses were performed on a J.A. Woollam M-2000 spectroscopic ellipsometer. All thickness measurements were performed at a 70º incidence angle using 190 wavelengths in the range of 315 to 718 nm. For films deposited on whole wafers, 5 points were measured across the wafer; the average is reported. The Cauchy-Urbach model was used to fit data by a non-linear least square minimization algorithm. Film thickness and refractive index coefficients were obtained upon convergence of the algorithm.

Fourier transform infrared spectroscopy (FTIR) was performed on a Nicolet Nexus 870 ESP spectrometer in transmission mode. Measurements were collected from 500 to 4000 cm^{-1} with 4 cm^{-1} resolution using a DTGS KBr detector. 64 scans were integrated to improve the signal-to-noise

ratio. FTIR spectra of silicon wafers substrates, obtained after removing films with acetone, served as backgrounds, and the spectra were baseline corrected and normalized for comparison purposes. FTIR was also performed on a commercial sample of poly(styrene-co-maleic anhydride) with 50% styrene content (Scientific Polymer Products) that was spun cast onto a Si wafer from tetrahydrofuran. The number-average molecular weight of the commercial sample was 1600 g/mol (PDI was not provided). X-ray photoelectron spectroscopy (XPS) was performed on a Kratos Axis Ultra spectrometer with a monochromatized Al Kα source. Relative sensitivity factors were calibrated by measuring poly(methyl methacylate), poly(butyl methacrylate), and poly(glycidyl methacrylate) standards cast onto Si wafers from tetrahydrofuran. Deposition samples and standards were stored in a vacuum desiccator for at least 24 hours prior to analysis.

In order to obtain enough material for effective analysis via nuclear magnetic resonance (NMR), 12 ten-minute-long depositions were performed using the conditions of sample MA/S-6/20. The films were dissolved in acetone-d_6 to yield a 10 wt% solution, and hydrogen signals from acetone served as internal standards. The ^{13}C NMR spectrum was collected on a Bruker AVANCE-400 spectrometer. The experiment was performed at 75.46 MHz with ^{1}H and ^{13}C $\pi/2$ pulse times of 107.5 and 15.25 μs, respectively. CH and CH_2 subspectra were generated using the Distortionless Enhancement Polarization Transfer (DEPT) pulse sequence[33] with a J-modulation time of 3.45 ms (J = 145 Hz). Recycle time was two seconds, and 2048 scans were integrated for all spectra.

Molecular weights of all copolymer films were determined using a Waters gel permeation chromatography (GPC) system equipped with an isocratic HPLC pump (Model 1515), autosampler (Model 717plus), three styragel columns (HR1, HR3, and HR4), and a refractive index detector (Model 2414). Copolymer films were dissolved off the silicon wafers with THF and filtered through a 0.45 μm membrane; 150 μL of the solution was injected into the column. The refractive index detector, operating at a wavelength of 880 nm, was maintained at 35 ºC, and the mobile phase was THF flowing at

1 mL/min. Integrated areas of the copolymer peaks were compared to narrow polystyrene standards previously calibrated to determine number-average molecular weights and PDIs.

2.3 Results and Discussion

2.3.1 Deposition Rate

This study examined the effect of surface concentration on the deposition kinetics of poly(styrene-alt-maleic anhydride) (PSMa). Filament temperature, substrate temperature, initiator partial pressure, total system pressure, and total flow rate are constant for all depositions, as detailed in the experimental section. The effect of monomer surface concentrations is analyzed assuming the deposition process is in the reaction-limited regime. In this case, mass transfer to the surface is sufficiently fast to maintain surface concentrations at their equilibrium values, and these surface concentrations govern reaction kinetics[27, 28]. Equilibrium surface concentrations can be related to partial pressures of the vapor through the Brunauer, Emmett, and Teller (BET) isotherm[34]. The BET isotherm gives the equilibrium surface concentration as a function of the ratio $P_m/P_{m,sat}$, where P_m is the partial pressure of monomer "m" and $P_{m,sat}$ is the saturation vapor pressure of monomer "m" at the substrate temperature. To determine the effect of maleic anhydride and styrene surface concentrations on deposition rate, partial pressure ratios for both monomers were varied as shown in Table 2-1.

The measured deposition rates are provided in Figures 2-1 and 2-2. First, the homopolymerization of each monomer will be discussed (Figure 2-1). Introducing only styrene monomer into the reactor (Ma/S-0/20, Table 2-1) did not yield deposition of any homopolymer. This is not surprising since $P_S/P_{S,sat}$ was only 0.11; the corresponding low surface concentration of styrene leads to low polymerization rates. Previously, the optimal $P_m/P_{m,sat}$ range for fast iCVD of vinyl monomers was demonstrated to be 0.4 – 0.7[27]. Using only maleic anhydride monomer (Ma/S-6/0, Table 2-1) resulted

in a slow deposition rate of 5.6 nm/min. GPC and NMR data (not shown) reveal that this sample consists of short oligomers in which only a few maleic anhydride molecules are connected in a chain.

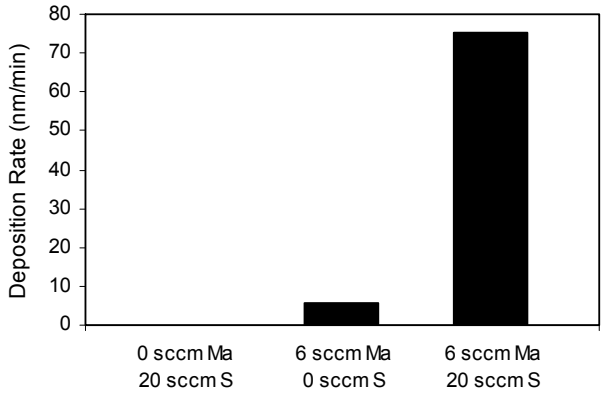

Figure 2-1. High copolymerization rate (75.4 nm/min) of electron accepting maleic anhydride with electron donating styrene is observed under the same conditions where homopolymerization is not observed for styrene and is slow for maleic anhydride.

Combining styrene and maleic anhydride monomers resulted in higher growth rates (Figure 2-2) and chains of higher molecular weight (Figure 2-3). The maximum deposition rate (sample MA/S-6/20, Table 2-1) is 75.4 nm/min – representing a 13.7-fold increase in deposition rate over maleic anhydride homopolymer. The copolymerization kinetics are dependent on surface concentrations of both styrene and maleic anhydride (Figure 2-2). As the surface concentration of either styrene or maleic anhydride increases, the deposition rate increases. This dependency is expected for radical chain copolymerizations.

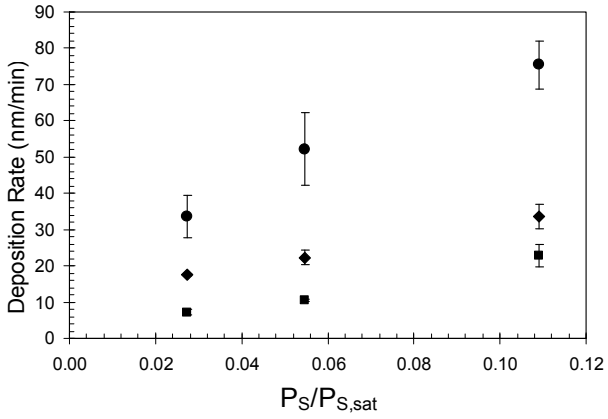

Figure 2-2. Deposition rate as a function of styrene monomer partial pressure ratio. The maleic anhydride partial pressure ratios are 0.29 (▪), 0.57 (◆), and 0.86 (●). Error bars represent standard deviations of triplicate experiments (error bars masked by data markers at three points).

Previous studies found that the complex-participation model best described experimental composition data of styrene/maleic anhydride copolymerizations in carbon tetrachloride and N,N-dimethylformamide[35]. Electronic interactions between maleic anhydride, an electron-accepting monomer, and styrene, an electron-donating monomer, lead to the formation of a complex, the concentration of which is defined by an equilibrium constant. In the complex model, the copolymerization rate is complicated by the fact that both free monomers and the complex can add to propagating radical chains[36]. Furthermore, it has been demonstrated that primary termination can play a significant role in iCVD depositions[28]. Primary termination occurs when initiator radicals combine with the propagating chain radicals; it can lead to further non-linearities in reaction kinetics and is not considered in standard kinetic models of copolymerizations, such as the complex participation model. For these reasons, conclusions concerning the order of the copolymerization rate equation with respect to either co-monomer have not been formed. It is clear, though, that partial pressure ratios provide a highly effective, controllable method to vary deposition rates.

2.3.2 Molecular Weight

Molecular weight and PDIs for polymers from each combination of three values of styrene and three values of maleic anhydride partial pressure ratios are plotted in Figure 2-3. The number-average molecular weight (M_n) increases with styrene partial pressure in each of the three series of fixed maleic anhydride partial pressures. Also, at each fixed value of styrene partial pressure, M_n increases with the partial pressure ratio of maleic anhydride. These two trends occur because copolymerization rates rise with increased concentrations of either monomer[31]. Number-average degree of polymerization is proportional to the kinetic chain length, which is defined as the rate of polymerization over the rate of termination. The effect of the rate of polymer termination on molecular weight was held constant by maintaining the same initiator flow rate and filament temperature. Comparing Figures 2-2 and 2-3 reveals that deposition rate and M_n are indeed interrelated.

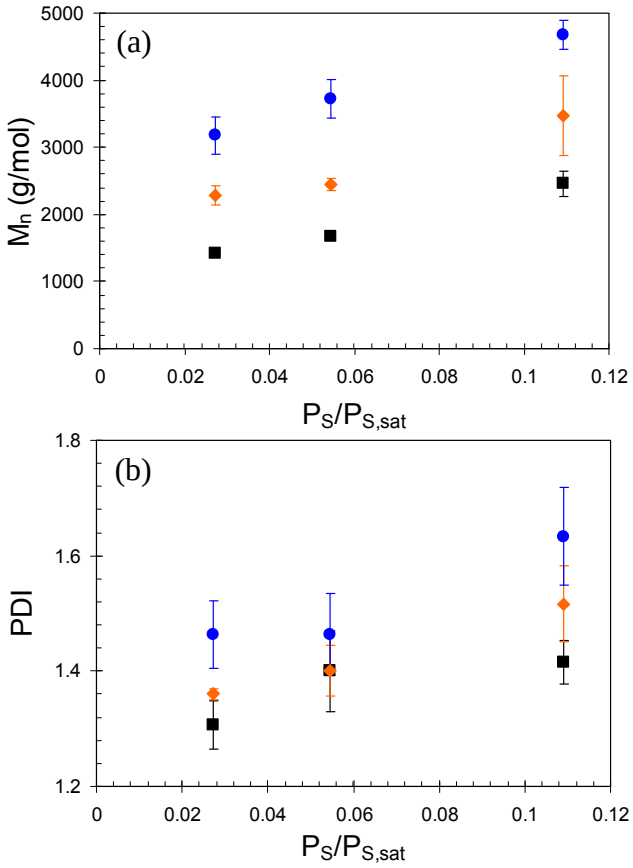

Figure 2-3. (a) Number-average molecular weight (M_n) and (b) PDI as a function of styrene partial pressure ratio. The maleic anhydride partial pressure ratios are 0.29 (▪), 0.57 (◆), and 0.86 (•). Error bars represent standard deviations of triplicate experiments.

A trend where PDI increases with monomer partial pressure ratios (or surface concentration) is also observed, which is typical of free radical polymerizations. Regardless of the mode of termination, smaller PDIs are expected for low molecular weight polymers because the rate of termination is more significant relative to the rate of propagation[31]. One reason for the relatively low molecular weights is due to the low surface concentration of styrene. Molecular weights comparable to those measured in this study were obtained in a series of acrylate polymers polymerized via iCVD when their partial pressure ratios were less than 0.2[27]. It has been argued that the probability of primary radical termination is likely at low surface concentrations[27, 28]. At low surface concentrations of styrene, the

probabilities of an initiator radical reacting with unreacted monomer or the radical end of a propagating polymer chain become comparable. Another possibility is the initiator radical adds to maleic anhydride, which has a higher surface concentration, and the maleic anhydride radical reacts with a propagating chain radical rather than itself since it does not readily homopolymerize.

2.3.3 Confirmation of Copolymerization by FTIR

FTIR spectra of each iCVD-deposited copolymer film are provided in Figure 2-4. Figure 2-4(a) shows that the chemical compositions of all nine iCVD-deposited PSMa (Table 2-1) copolymer films are identical. The spectra have absorptions unique to each co-monomer – indicating that both monomers are incorporated into the deposited film. Presence of maleic anhydride is confirmed by C=O stretching (1860 and 1780 cm^{-1}). Characteristic styrene absorptions from out-of-plane phenyl vibrations (759 and 700 cm^{-1}), in-plane phenyl C-H bending (1455 and 1495 cm^{-1}), and phenyl C-H stretching (3030 and 3060 cm^{-1}) are also apparent. The assignments are based on previous studies of anhydrides[37] and polystyrene[38]. Included in Figure 2-4(b) is the spectrum of commercial PSMa with 50% styrene content compared to iCVD sample Ma/S-6/20. Peak locations and areas of the iCVD spectrum match well with the commercial PSMa sample.

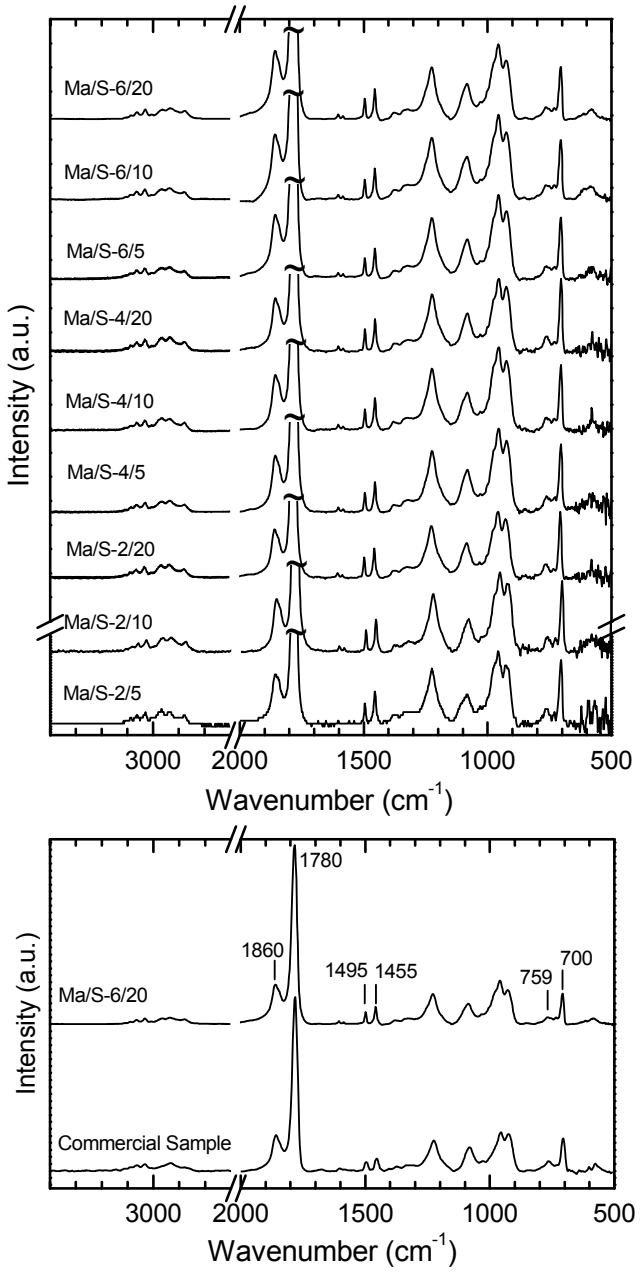

Figure 2-4. (a) The similarity of FTIR spectra for all iCVD copolymer samples. (b) Comparison of iCVD sample Ma/S-6/20 to a commercial sample of PSMa with 50% styrene content. Characteristic peaks of maleic anhydride and styrene are identified.

It is important to note that retention of the anhydride functionality is achieved in the depositions, confirmed by the presence of the double carbonyl absorption. The double absorption is due to in-phase and out-of-phase stretching of the carbonyl groups. Moreover, the higher intensity of

the band at 1780 cm^{-1} confirms the presence of five-membered rings of succinic anhydride in the polymer chains[37]. The loss of anhydride groups by ring opening reactions would lead to broad carboxylic acid O-H stretching (ca. 3000 cm^{-1}) and C=O stretching (1740 - 1660 cm^{-1}) modes. These modes are indeed absent from Figure 2-4, providing additional confirmation of the full functional group retention from the monomeric units. The spectra of iCVD films are in distinct contrast to FTIR spectra of plasma-deposited maleic anhydride, which reveal significant modification of the anhydride functionality[21, 23], where lower wavenumber shoulders on the carbonyl bands suggest the presence of carbonyls not originating from anhydride functional groups.

2.3.4 Compositional Analysis by XPS

The chemical compositions of all nine iCVD films were determined by collecting XPS survey spectra. Recognizing that styrene and maleic anhydride monomers have different carbon and oxygen compositions, the monomer compositions in the copolymer films can be calculated. Table 2-2 reports the RSF-corrected compositions measured for each iCVD film and the calculated monomer compositions. Strictly alternating copolymers, which have the repeat unit shown in Figure 2-5, are comprised of 80% carbon and 20% oxygen. Within experimental error, all of the copolymers clearly have compositions necessary for alternating sequences, and compositions are insensitive to gas feed ratios.

Table 2-2. Compositions of all iCVD-deposited polymers determined by XPS survey scans.

Sample Name	%C	%O	%Ma[a]	%S
Ma/S-2/5	80.0	20.0	50.0	50.0
Ma/S-2/10	79.6	20.4	51.0	49.0
Ma/S-2/20	79.7	20.3	50.6	49.4
Ma/S-4/5	81.2	18.8	47.2	52.8
Ma/S-4/10	81.6	18.4	46.2	53.8
Ma/S-4/20	80.3	19.7	49.4	50.6
Ma/S-6/5	80.2	19.8	49.4	50.6
Ma/S-6/10	79.9	20.1	50.1	49.9
Ma/S-6/20	80.2	19.8	49.5	50.5

[a]The standard deviation of measured maleic anhydride contents in the iCVD copolymers is 1.58%.

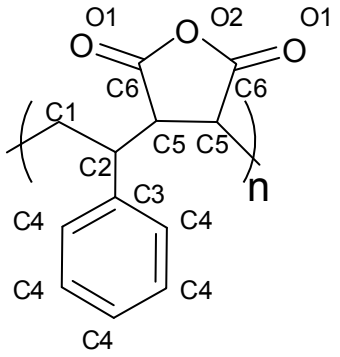

Figure 2-5. Repeat unit of strictly alternating poly(styrene-alt-maleic anhydride). Each repeat unit contains 12 carbon and 3 oxygen atoms.

Further corroboration of the copolymer composition and chemistry is provided by high resolution XPS scans in Figure 2-6. Qualitatively, the high resolution spectra appear equivalent for all iCVD films, indicating that the chemical structures of the copolymers, in addition to compositions, are equivalent.

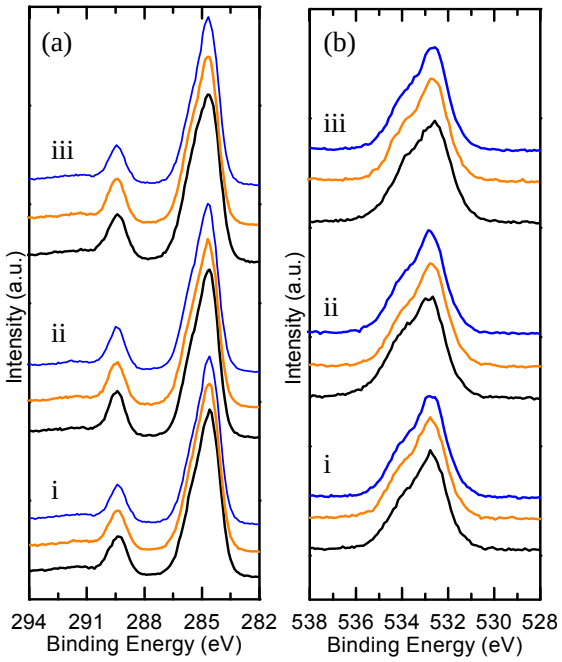

Figure 2-6. (a) Carbon C 1s and (b) oxygen O 1s high resolution XPS scans of films deposited at maleic anhydride partial pressure ratios of (i) 0.29, (ii) 0.57, and (iii) 0.86. Data for styrene partial pressure ratios of 0.03 (black), 0.05 (orange), and 0.11 (blue) are also presented.

Because the high resolution scans are invariant, synthetic component peaks were fitted and integrated for sample Ma/S-6/20 only. The component peaks are shown in Figure 2-7. In Table 2-3, integrated areas of the components are compared to a 1:1 poly(styrene-co-maleic anhydride) reference[39]. The high binding energy shoulder of the smaller peak in the carbon spectrum is due to shake-up processes and was not fitted in sample MA/S-6/20 or the reference. The entries in the "Origin" column of Table 2-3 correspond to the labels in Figure 2-5. The peak locations and integral values obtained for sample MA/S-6/20 match extremely well with the reference. Not only does this corroborate the survey scan data which show 1:1 styrene to maleic anhydride compositions, but it also shows that iCVD and conventional solution polymerizations lead to identical chemical structures.

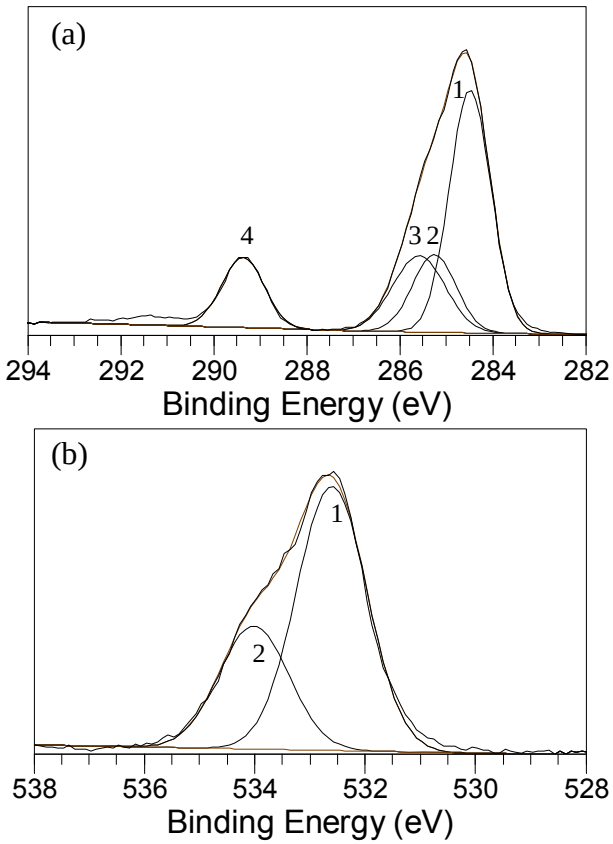

Figure 2-7. Least-square regressions of the high resolution scans of (a) C 1s and (b) O 1s core levels of sample Ma/S-6/20 using components with Gaussian lineshapes.

Table 2-3. High resolution XPS data of iCVD sample Ma/S-6/20 compared to reference polymer

Core Level	Peak	Origin[a]	Deposited Film		1:1 PSMa reference[39]	
			BE (eV)	Area (%)	BE (eV)	Area (%)
C 1s	1	C3,C4	284.5	49	284.5	51
	2	C1,C2	285.3	17	285	17
	3	C5	285.6	19	285.6	18
	4	C6	289.4	14	289.4	15
O 1s	1	O1	532.0	68	532.5	66
	2	O2	534.0	32	533.9	33

[a]Labels of the origins of carbon and oxygen peaks are shown in Figure 2-5.

2.3.5 NMR Evidence of Alternating Structure

Though FTIR and XPS data prove that all the iCVD films have equivalent compositions in which styrene and maleic anhydride occur in a 1:1 ratio, they do not reveal the sequence distributions of the copolymers. Therefore, ^{13}C NMR was used to reveal the structure of these copolymers. The ^{13}C NMR spectrum of sample Ma/S-6/20 is provided in Figure 2-8(a). The assignments are based on a previously published study[40]. All of the expected ^{13}C signals are present, further confirming the similarity of iCVD to solution-based processes. Moreover, additional signals are not present - demonstrating the absence of undesired side reactions, such as non-selective crosslinking. The quaternary C3 (Figure 5) peak is sensitive to the sequence distribution; the signal between 136 and 140 ppm, as seen in Figure 8(b), corresponds to the alternating Ma-S-Ma triad. There is no signal between 141.5 to 146 ppm and 145 to 147.5 ppm, which are assigned to semi-alternating (S-S-Ma, Ma-Ma-S) and non-alternating (S-S-S) triads, respectively[41]. Further verification of the alternating structure is provided by DEPT experiments. Figure 8(c) shows the DEPT CH_2 subspectrum for the C1 methylene carbon of styrene. Previous studies assign the 33 – 37, 37 – 42, and 42 – 47 ppm regions to alternating, semi-alternating, and non-alternating triads, respectively[33]. Only one distinct signal is observed from 32 – 37 ppm – further proof that a strictly alternating copolymer has indeed been deposited.

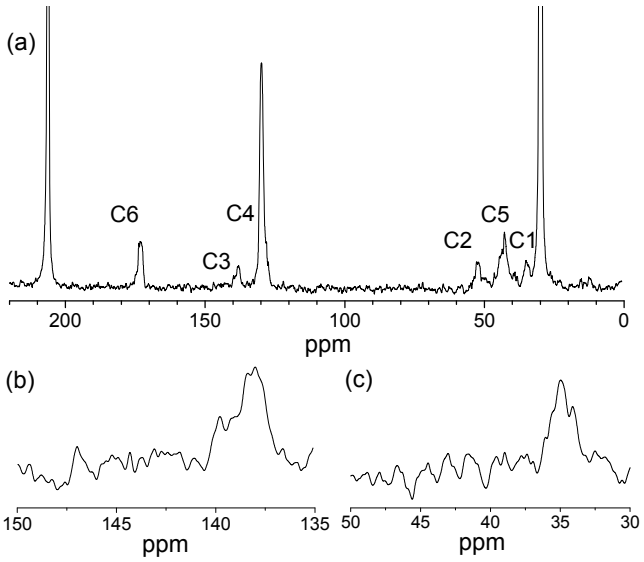

Figure 2-8. (a) ^{13}C NMR spectrum of sample Ma/S-6/20, along with (b) the expanded region of quaternary carbon C3 and (c) the DEPT CH_2 subspectrum. The large signals at 29.9 and 206.7 ppm are from acetone-d_6, used as solvent and internal standard.

2.3.6 Reactivity Ratios of iCVD Copolymers

It is important to explore the similarity between iCVD and conventional solution-phase polymerizations. An alternating copolymer forms as the result of interactions that control how monomers add to propagating polymer chains. In the absence of such interactions, both monomer concentration and reactivity affect the final copolymer composition. Copolymer reactivity ratios are a convenient way to characterize copolymerization behavior.

Monomer reactivity ratios of two other iCVD copolymer studies and this study have been compared. Monomer reactivity ratios (r_1 and r_2) were evaluated using the method of Kelen and Tudos[42]. The copolymer composition is related to the monomer concentrations through the transformed equation

$$\eta = \left(r_1 + \frac{r_2}{\alpha}\right)\xi - \frac{r_2}{\alpha}$$

where

$$\eta = \frac{\left([M_1]/[M_2]\right)(1 - m_2/m_1)}{\alpha + \left([M_1]/[M_2]\right)^2 (m_2/m_1)} \quad \text{and} \quad \xi = \frac{\left([M_1]/[M_2]\right)^2 (m_2/m_1)}{\alpha + \left([M_1]/[M_2]\right)^2 (m_2/m_1)}$$

Here, parameter $[M_i]$ is the monomer feed concentration and m_i is the fraction of the copolymer composed by monomer i. In iCVD, $[M_i]$ is set to the monomer surface concentration. The parameter α, introduced in order to symmetrically distribute data on the plot, is defined as

$$\alpha = \sqrt{\left(\left([M_1]/[M_2]\right)^2 m_2/m_1\right)_{min} \left(\left([M_1]/[M_2]\right)^2 m_2/m_1\right)_{max}}$$

Data from this study are plotted in Figure 2-9 along with two data sets from iCVD copolymerization studies of methacrylic acid (MAA) with ethyl acrylate (EA)[30] and 2,2,3,3,4,4,5,5,6,6,7,7-dodecafluoroheptyl acrylate (DFHA) with glycidyl methacrylate (GMA)[29]. Monomer feed concentrations were estimated using partial pressure ratios. In the MAA/EA study, partial pressure ratios were reported, but for DFHA/GMA, saturation pressures were estimated by fitting the Clausius-Clapeyron equation to experimental vapor pressure data tabulated in chemical databases of SciFinder Scholar 2006[43].

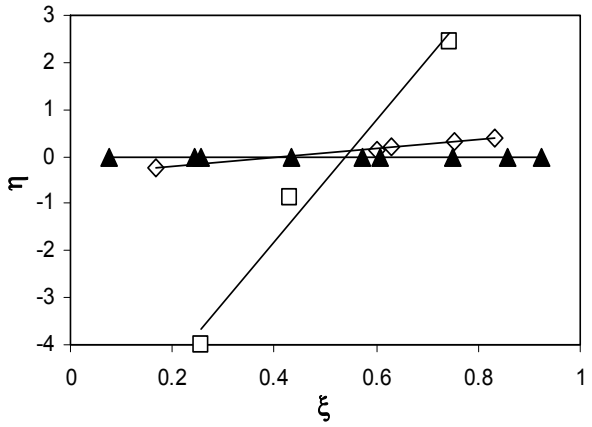

Figure 2-9. Kelen-Tudos plot for the MAA/EA (◇), DFHA/GMA (□), and Ma/S (▲) copolymer systems. Reactivity ratios are calculated from the slopes and intercepts of the regression lines.

Perfectly alternating copolymers form when reactivity ratios of both monomers are zero[31]. The fitted regression line for the PSMa iCVD films indicates that the reactivity ratios of maleic anhydride and

styrene are both zero, within experimental error. These values are expected based on the characterization of the iCVD films in this work. The plot yields reactivity ratios of 0.56 and 0.28 for MAA and EA, respectively. Because both reactivity ratios are less than one, the propagating radical of MAA tends to react with EA and vice-versa. In other words, there is tendency towards alternation, but monomer surface concentrations still affect copolymer compositions since both monomers can homopolymerize. The behavior of DFHA and GMA copolymerizations, where the reactivity ratios are determined to be 5.91 for DFHA and 0.09 for GMA, is quite different. Because DFHA's reactivity ratio is greater than unity and much greater than GMA's reactivity ratio, DFHA is preferentially added to propagating radicals, regardless if the radical is DFHA or GMA. Thus, the copolymer is rich in DFHA, which is observed experimentally[29] .

These three different copolymerization behaviors indicate relative reactivities of monomers determine the sequence behavior in iCVD copolymers in the same manner that is well-known for solution-phase processes. By recognizing the similarity of iCVD to solution-based polymerizations, tabulated reactivity ratios from solution-phase processes can guide the choice of monomer partial pressures to deposit copolymers of desired compositions. It should be noted that the reactivity ratios may not always be equivalent for iCVD and solution methods, as noted and briefly discussed in the MAA/EA copolymerization study[30], but they serve as good starting points nonetheless.

2.4 Conclusion

This work demonstrated that iCVD can be used to create thin films of alternating copolymers in a completely dry process. By supplying maleic anhydride, styrene, and TBPO to the reactor as vapors, strictly alternating poly(styrene-alt-maleic anhydride) was deposited, regardless of gas feed ratios. FTIR and XPS characterizations showed that all copolymer films had equivalent 1:1 ratios of the two monomers, while ^{13}C NMR revealed that structures were strictly alternating. Furthermore, the

anhydride functionality was retained in the films, which is critical for post-deposition functionalizations. iCVD copolymerization is clearly an effective technique for incorporating maleic anhydride, which does not homopolymerize to an appreciable extent, into polymer thin films.

This study also corroborated the idea that iCVD copolymerization has strong analogies to conventional solution-phase synthesis. Gas feed ratios, which defined surface concentrations of the monomers, influenced deposition rates (6.3 – 75.4 nm/min) and number-average molecular weights (1380 – 4680 g/mol). Analysis of copolymerizaton reactivity ratios for PSMa and two other iCVD copolymer systems[29, 30] showed that monomer reactivity ratios are critical for determining sequence distributions in iCVD copolymers, as is the case for solution-phase processes. Poly(styrene-alt-maleic anhydride) formed as a result of electronic interactions between electron-accepting maleic anhydride and electron-donating styrene. Analysis of EA/MAA and DFHA/GMA iCVD copolymers, where such interactions between monomers do not exist, showed that compositions were dependent upon monomer concentrations and reactivities. Reactivity ratios should be considered when designing experiments for iCVD copolymerizations.

References

[1] N. A. Peppas, J. Z. Hilt, A. Khademhosseini, R. Langer, *Adv. Mater.* **2006**, *18*, 1345.

[2] S. A. Evenson, J. P. S. Badyal, *J. Phys. Chem. B* **1998**, *102*, 5500.

[3] S. A. Evenson, C. A. Fail, J. P. S. Badyal, *J. Phys. Chem. B* **2000**, *104*, 10608.

[4] V. Roucoules, C. A. Fail, W. C. E. Schofield, D. O. H. Teare, J. P. S. Badyal, *Langmuir* **2005**, *21*, 1412.

[5] T. Pompe, S. Zschoche, N. Herold, K. Salchert, M. F. Gouzy, C. Sperling, C. Werner, *Biomacromolecules* **2003**, *4*, 1072.

[6] B. C. Trivedi, B. M. Culbertson, "*Maleic Anhydride*", Plenum Press, New York, 1982.

[7] S. M. Henry, M. E. H. El-Sayed, C. M. Pirie, A. S. Hoffman, P. S. Stayton, *Biomacromolecules* **2006**, *7*, 2407.

[8] H. Maeda, *Adv. Drug Deliv. Rev.* **2001**, *46*, 169.

[9] I. Donati, A. Gamini, A. Vetere, C. Campa, S. Paoletti, *Biomacromolecules* **2002**, *3*, 805.

[10] H. Derand, B. Wesslen, *J. Polym. Sci. Pol. Chem.* **1995**, *33*, 571.

[11] M. Brissova, J. Augustin, E. Staudner, *Macromol. Rapid Commun.* **1994**, *15*, 211.

[12] E. P. Ivanova, D. K. Pham, N. Brack, P. Pigram, D. V. Nicolau, *Biosens. Bioelectron.* **2004**, *19*, 1363.

[13] U. Freudenberg, S. Zschoche, F. Simon, A. Janke, K. Schmidt, S. H. Behrens, H. Auweter, C. Werner, *Biomacromolecules* **2005**, *6*, 1628.

[14] A. Greiner, *Trends in Polymer Science* **1997**, *5*, 12.

[15] H. O. Pierson, "*Handbook of Chemical Vapor Deposition - Principles, Technology, and Applications*", 2 edition, Noyes Publications, Park Ridge, NJ, 1999.

[16] F. Tewes, F. Boury, J.-P. Benoit, "Biodegradable Microspheres: Advances in Production Technology", in *Microencapsulation, Methods and Industrial Applications*, 2 edition, S. Benita, Ed., Taylor & Francis, New York, 2006, p. 8.

[17] C. B'Hymer, *Pharm. Res.* **2003**, *20*, 337.

[18] A. S. Chawla, *Biomaterials* **1981**, *2*, 83.

[19] H. G. P. Lewis, D. J. Edell, K. K. Gleason, *Chem. Mat.* **2000**, *12*, 3488.

[20] H. Yasuda, "*Luminous Chemical Vapor Deposition and Interface Engineering*", Marcel Dekker, New York, 2005.

[21] A. T. A. Jenkins, J. Hu, Y. Z. Wang, S. Schiller, R. Foerch, W. Knoll, *Langmuir* **2000**, *16*, 6381.

[22] M. E. Ryan, A. M. Hynes, J. P. S. Badyal, *Chem. Mat.* **1996**, *8*, 37.

[23] S. Schiller, J. Hu, A. T. A. Jenkins, R. B. Timmons, F. S. Sanchez-Estrada, W. Knoll, R. Forch, *Chem. Mat.* **2002**, *14*, 235.

[24] K. Chan, K. K. Gleason, *Langmuir* **2005**, *21*, 8930.

[25] K. Chan, L. E. Kostun, W. E. Tenhaeff, K. K. Gleason, *Polymer* **2006**, *47*, 6941.

[26] Y. Mao, K. K. Gleason, *Langmuir* **2004**, *20*, 2484.

[27] K. K. S. Lau, K. K. Gleason, *Macromolecules* **2006**, *39*, 3688.

[28] K. K. S. Lau, K. K. Gleason, *Macromolecules* **2006**, *39*, 3695.

[29] Y. Mao, K. K. Gleason, *Macromolecules* **2006**, *39*, 3895.

[30] K. K. S. Lau, K. K. Gleason, *Adv. Mater.* **2007**, *submitted*.

[31] G. Odian, "*Principles of Polymerization*", 4 edition, John Wiley & Sons, Hoboken, 2004.

[32] C. L. Yaws, "Chemical Properties Handbook", McGraw-Hill, New York, 1999.

[33] P. F. Barron, D. J. T. Hill, J. H. Odonnell, P. W. Osullivan, *Macromolecules* **1984**, *17*, 1967.

[34] S. Brunauer, P. H. Emmett, E. J. Teller, *Journal of the American Chemical Society* **1938**, *60*, 309.

[35] N. T. H. Ha, K. Fujimori, *Acta Polym.* **1998**, *49*, 404.

[36] D. Braun, F. C. Hu, *Prog. Polym. Sci.* **2006**, *31*, 239.

[37] D. Lin-Vien, N. B. Colthup, W. G. Fateley, J. G. Grasselli, "The Handbook of Infrared and Raman Characteristic Frequencies of Organic Molecules", Academic Press, New York, 1991.

[38] C. Y. Liang, S. Krimm, *Journal of Polymer Science* **1958**, *27*, 241.

[39] G. Beamson, D. Briggs, "*High Resolution XPS of Organic Polymers The Scientia ESCA300 Database*", John Wiley & Sons, New York, 1992.

[40] G. B. Butler, C. H. Do, M. C. Zerner, *Journal Of Macromolecular Science-Chemistry* **1989**, *A26*, 1115.

[41] N. T. H. Ha, *Polymer* **1999**, *40*, 1081.

[42] T. Kelen, F. Tudos, *Journal Of Macromolecular Science-Chemistry* **1975**, *A 9*, 1.

[43] "SciFinder Scholar 2006", Chemical Abstracts Service, American Chemical Society, Columbus OH, 2005.

CHAPTER THREE

Surface-Tethered pH-Responsive Hydrogel Thin Films as Size-Selective Layers on Nanoporous Asymmetric Membranes

Abstract

The fabrication of composite membranes consisting of permeable, size-selective hydrogel thin films on porous inorganic membrane supports is described. Smooth, pinhole-free hydrogel films with sub-100 nm thicknesses were readily synthesized using initiated chemical vapor deposition (iCVD). iCVD was a convenient technique for membrane applications as it enabled control over the coating conformality by modulating surface concentrations of the polymer precursors and film thickness through *in situ* monitoring of the deposition process. Techniques to graft films to the substrates were also developed. Membrane permeability was controlled through variation of the thickness and composition of the iCVD poly[maleic anhydride-co-dimethylacrylamide-co-di(ethylene glycol) di(vinyl ether)] (PMaDD) film. The combination of swelling and stability was achieved for a film composition of 76% N,N-dimethyl acrylamide, 14% maleic anhydride, and 10% di(ethylene glycol) divinyl ether. Swelling was shown to be pH-responsive, with a maximum swelling ratio of 11.5 at pH 8. Hydrogel nanofilms reached their swelling equilibrium in a few minutes. Diffusion and selectivity of permeants in the membrane were also modeled and characterized. The hydrogels internal pore size was calculated to be 3.2 nm at pH = 7, which readily allowed the passage of glucose while excluding bovine serum albumin (BSA). By reacting 3-aminopropyldimethylethoxysilane with silanol groups of silicon surfaces and the alumina hydroxide of alumina surfaces, covalent bonds between the substrates and anhydride functionalities in the hydrogels were formed, which was necessary for stable adhesion. Further utility of PMaDD was demonstrated by functionalizing it with 2-aminoethanethiol and poly(ethylene glycol) to modulate its interaction with proteins in solution. A simple technique to pattern the film was demonstrated, and PMaDD was functionalized with CdSe/ZnS core-shell quantum dots to reveal the hydrogel properties of the patterns.

3.1 Introduction

Membrane separations are critical to the successful, efficient operation of many commercial processes, such as kidney dialysis, pharmaceutical purification, gas separation, and water desalination.[1-5] A key motivation for using membranes is the separation selectivity. To be economically feasible, though, the permeability (throughput) of the membrane must also be high. The selectivity and permeability characteristics are paramount, but the membrane must meet many other requirements - mechanical stability, chemical stability and environmental compatibility of the surface, for example. Developing a single material to satisfy all these requirements is difficult. A common solution is the development of composite membranes consisting of a highly permeable porous bulk material that provides mechanical strength and a thin permselective skin layer on top for selectivity and proper interfacial properties.[6]

Innovative techniques have been developed to synthesize these skin layers; the Loeb-Sourirajan process, interfacial polymerization, and solution coating are the most common.[7] These skin layers must be as thin as possible to maximize permeability. In order to synthesize high quality defect-free layers with these conventional methods, thicknesses greater than 1 μm are typically required.[8] Furthermore, the layer should also be readily chemically functionalized to control undesired fouling and impart new functionality, such as enhanced selectivity or stimuli-responsiveness. Having non-fouling properties is particularly important since fouling results in reduced efficiencies. Particulate (colloidal), protein, and cellular absorption are the common culprits. Particulates are easily separated in pre-filters. A common strategy to prevent cellular absorption (and protein to a certain extent) is making the surface hydrophilic.[9] Poly(ethylene glycol) (PEG) brushes are even more effective in repelling proteins.[10-12] It is critical that these hydrophilic modification layers be firmly attached to the membrane. Indeed, poly(vinyl pyrrolidone) layers for commercial microfiltration and ultrafiltration membranes, which are

immobilized relatively weakly through physical interactions, have been shown to be washed away by shear stresses.[13]

Hydrogels, which are crosslinked polymeric networks that imbibe large volumes of water yet do not dissolve are potentially useful materials for these skin layers. The crosslinking density of the hydrogel and water absorption define a mesh size between crosslinks in the polymer[14-16], which enables separation based on hydrodynamic size. Moreover, many strategies exist to functionalize these materials with protein resistant moieties, often involving the grafting of PEG brushes[12, 17] A review was also recently published on stimuli-responsive hydrogels, which could enable further control in membrane separations.[18] It is important to note that hydrogels must be integrated in composite membranes since they lack mechanical strength in the gel state.

Hydrogels are clearly convenient materials for the skin layers in composite membranes. Commercial techniques exist to synthesize crosslinked hydrophilic materials on common membrane materials.[19, 20] Other novel techniques, such as layer-by-layer (LbL) depositions of polyelectrolytes and plasma polymerizations have also been investigated.[6, 9, 21] However, the LbL technology is generally limited to the use of polyelectrolytes of opposing charges, and modification of internal pore walls is difficult with plasma techniques because the mean free path of the plasma is larger than the pore diameter.[6] Initiated chemical vapor deposition (iCVD) is a polymer deposition technique with a broad polymerization capability – essentially equivalent to solution-phase free radical polymerizations. A broad array of polymer chemistries has been demonstrated.[22] Furthermore, membrane pores with an aspect ratio as high as 80 have been conformally coated with the technique.[23] iCVD is particularly useful for membrane applications as it enables precise, nanometer-level control over film thickness at high deposition rates through *in situ* monitoring of the deposition process using interferometry.[24] Deposition rates well above 100 nm/min have been demonstrated.[23, 25, 26] The LBL technique, on the other hand, is limited in potential practical applications by the numerous deposition and rinsing steps

required for synthesis.[27] Interfacial polymerizations also require a rinsing step. iCVD, though, is a one step process.

Furthermore, the synthesis of defect-free selective skin layers with thicknesses less than 100 nm is extremely difficult with conventional methods.[28] The synthesis of layers with thicknesses down to 50 nm is even rarer.[29] iCVD has been applied to the synthesis of sub-100 nm thick, pH-responsive hydrogel films as skin layers on porous alumina membranes. To increase the stability of the film, a strategy to covalently attach the polymer to the substrate was developed. Herein, the novel chemistry of the hydrogel film is described. Also, the network structure of the hydrogel was characterized and its utility for dialysis in a composite membrane format was characterized.

3.2 Experimental

3.2.1 Hydrogel Synthesis by iCVD

Prior to synthesizing hydrogel films, 100-mm diameter silicon (Si) wafer substrates (Wafer World, test grade) were treated with 3-aminopropyldimethylmonoethoxysilane (3-AMS) (Gelest, >95%). Using "piranha" solution (mixture of sulfuric acid and hydrogen peroxide), the surfaces of the wafers were cleaned and oxidized to create Si-OH groups at the surface, then rinsed with clean deionized water and dried. **CAUTION: Piranha solution is a strong oxidant and should be handled with extreme care.** The wafers were placed in a vacuum oven at 60 °C, and 3-AMS vapors were flowed into the vacuum chamber for one hour. The flow was then stopped, and the vacuum chamber was pumped out for a minimum of one hour to remove any physisorbed 3-AMS from the surface of the Si wafers.

iCVD was performed in a previously described iCVD reactor configuration.[30] Maleic anhydride (99%), N,N-dimethylacrylamide (99%), di(ethylene glycol) di(vinyl ether) (99%), and tert-butyl peroxide (97%) were all purchased from Sigma-Aldrich and used as received. By heating the precursors to create adequate vapor pressures, flow rates of 0.6 sccm of maleic anhydride, 5.9 sccm of N,N-

dimethylacrylamide, and 0.4 sccm of tert-butyl peroxide were maintained with MKS Instruments 1152C, 1150C, and 1479 MFCs, respectively. The di(ethylene glycol) di(vinyl ether) flow was set manually at 0.4 sccm with a needle valve. Systematic variation of the flow rate ratios was performed to yield highly swellable, yet stable films of poly[maleic anhydride-co-dimethyl acrylamide-co-di(ethylene glycol) divinyl ether] (PMaDD). An operating pressure of 400 mTorr was maintained during the deposition, and the filament temperature was set to 235 °C by passing 0.95 amps through the Chromaloy O (Goodfellow) filament, which was suspended 1.5 cm above the substrate. The stage temperature was 20 °C to promote adsorption of monomers. *In situ* interferometry with a 633-nm HeNe laser source (JDS Uniphase) was used to deposit approximately 150 nm-thick films on the Si substrates.

3.2.2 Film Characterization

FTIR measurements were performed on a Nicolet Nexus 870 ESP spectrometer in transmission mode. Measurements were collected from 500 to 4000 cm^{-1} with 4 cm^{-1} resolution using a DTGS KBr detector. 64 scans were integrated to improve the signal-to-noise ratio. Si wafers served as backgrounds, and spectra were normalized to thickness and baseline corrected. XPS survey and high resolution spectra were collected on a Kratos Axis Ultra spectrometer with a monochromatized Al Kα source. Relative sensitivity factors were calibrated by measuring poly(2-ethyl-2-oxazoline), poly(N,N-dimethylacrylamide), and poly(N-isopropylacrylamide) polymers (Scientific Polymer Products) spun-cast onto Si wafers from 2-propanol. Deposition samples and standards were stored in vacuum prior to analysis.

A J.A. Woollam M-2000 spectroscopic ellipsometer was used to measure film thicknesses. All thickness measurements were performed at a 75° incidence angle using 190 wavelengths from 315 to 718 nm. A non-linear least square minimization algorithm was used to fit ellipsometric data of dry films to the Cauchy-Urbach model. Film thickness and refractive index coefficients were obtained upon

convergence of the algorithm. To measure water-swollen films, a liquid cell accessory was used (J.A. Woollam). The cell clamped over the sample and held the solution in a liquid tight seal. The optical properties of the cell windows and solution were included in the model. Ionic strength-controlled buffer solutions of pH from 0.5 to 9 were prepared by mixing the proper ratios phosphoric acid (50% (w/v) in water), sodium dihydrogen phosphate (99%), disodium phosphate heptahydrate (99%), and sodium chloride (99%), which were all obtained from Sigma Aldrich and used as received. The ionic strength was controlled at 30 mM and the buffer strength at 10 mM. Swollen films were modeled with the effective medium approximation. One component consisted of the dry polymer (optical properties of the dry films were used), and the second component was water. The total film thickness and volume fraction of water were determined upon convergence of the non-linear least square minimization algorithm. Between each measurement the films were removed from the liquid cell, rinsed with deionized water, and then dried.

3.2.3 Membrane Integration

PMaDD film was deposited on commercially available porous alumina membranes with 20 nm pore openings (Anopore^{TM}, SPI Supplies). Hydroxyl functional groups are present on alumina surfaces and can be used for silanization.[31, 32] Silanization of the alumina with 3-AMS and deposition of PMaDD was performed using the procedure described above. High resolution images of the membrane cross sections were collected using a field emission scanning electron microscope (JEOL, 6700F).

Diffusion of glucose and bovine serum albumin (BSA) through the PMaDD membranes was measured in a standard Franz diffusion cell. The volume of the source chamber was 7 mL. The volume of the sink was 170 mL for glucose measurements and 70 mL for BSA measurements. The source and sink chambers were connected through an o-ring joint. The composite membranes were sandwiched between two o-rings. Solutions of known BSA and glucose concentrations were prepared in the pH 7

buffer described above and then loaded into the source chamber. The sink was initially pure buffer. Aliquots were collected as a function of time. Glucose concentrations were measured using a blood glucose monitor (WaveSense Presto, Agamatrix, Inc.). BSA concentrations were quantified using the Coomassie Plus Protein Assay (Pierce Protein Research Products) and measuring the UV absorption at 595 nm (Cary 600i, Varian).

3.2.4 Adhesion Characterization

PMaDD-coated membranes were submersed in pH 8 buffer (same buffer composition as used for swelling experiments). The membranes were then ultrasonicated in an ultrasonic bath for 5 minutes (VWR, Model 75D). The samples were removed from the buffer, dried, and then imaged in the SEM described above.

3.2.5 Functionalization Reaction Conditions

Cysteamine, poly(ethylene glycol), and all solvents were purchased from Sigma Aldrich and used as received. The poly(ethylene glycol) (PEG) had an average molecular weight of 400 g/mol (denoted PEG-400). For cysteamine functionalization, the PMaDD film was reacted in a 0.05 M solution of cysteamine in 2-propanol at 70 °C for 30 minutes. PMaDD was reacted with PEG-400 in a 10 %(v/v) solution of PEG-400 in butyl acetate at 110 °C for 18 hours. After the given times, the samples were removed from the reation media and rinsed in clean solvent to remove any unused reactants. The samples were then dried thoroughly in a vacuum oven to remove excess solvent.

Commercial CdSe/ZnS core-shell nanoparticles were attached to cysteamine functionalized PMaDD and imaged in a fluorescent microscope using previously described methods and equipment.[33]

3.3 Results and Discussion

3.3.1 Hydrogel Synthesis and Characterization

Poly[maleic anhydride-co-dimethylacrylamide-co-di(ethylene glycol) di(vinyl ether)] (PMaDD) films with average thicknesses of 150 nm were deposited by iCVD. The copolymer's chemical structure is shown in Figure 3-1a. The deposition rate measured on silicon was 20 nm/min on average. Prior to deposition, the silicon substrates were functionalized with 3-AMS, yielding primary amine functional groups at the surface. Maleic anhydride groups at the interface between the polymer film and substrate form covalent bonds with the substrate through the reaction between the anhydride and amine functional groups. Without silane functionalization of the silicon, hydrogel films delaminated from the surface when placed in water. In water, the maleic anhydride throughout the film's bulk hydrolyzed to maleic acid with two ionizable carboxylic acid groups. Figure 3-1b highlights the role of maleic anhydride at the film-substrate interface and throughout the bulk of the film. Ionization of the maleic anhydride increased the swelling of the film since the chemical potential of the ions on the polymer pendent group must be equal to the chemical potential of ions in solution. This introduces an ionic term in the Gibbs energy balance for hydrogel equilibrium.[16] The neutral comonomer, N,N-dimethylacrylamide, was chosen for its ability to absorb large amounts of water; its polymer is considered "super water absorbent." The di(ethylene glycol) di(vinyl ether) (DeDve) component was the crosslinker. The copolymer shown in Figure 3-1a is a three-dimensional network; di(ethylene glycol) divinyl ether groups of one polymer chain link it to multiple other chains. Through systematic variation of the ratio of monomer and crosslinker flow rates, the crosslinker content in the final copolymer composition was chosen as a compromise between the film's stability in solution and its maximum swelling ratio.

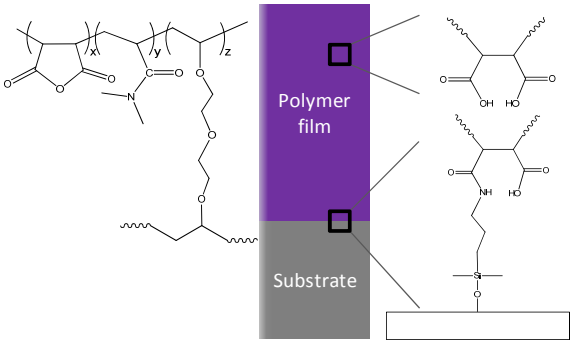

Figure 3-1. Chemical structures of (a) as-deposited PMaDD network. (b) Illustration of the roles of maleic anhydride at the substrate-film interface and throughout the film bulk.

The Fourier transform infrared spectroscopy (FTIR) spectrum of the as-deposited film (Figure 3-2) provides resolved features of the polymerized Ma and DMAA units. The double carbonyl absorption at 1778 cm^{-1} and 1849 cm^{-1} is characteristic of the carbonyl in-phase and out-of-phase stretching of maleic anhydride, while the strong absorption at 1639 cm^{-1} is assigned to the carbonyl stretch of N,N-dimethylacrylamide.[34] Characteristic absorptions of DeDve are obstructed by overlapping absorptions of dimethylacrylamide and maleic anhydride. The presence of DeDve is verified by the fact that the films did not dissolve in water or tetrahydrofuran, while films deposited without DeDve were completely dissolved. Upon placing the films in water, the characteristic FTIR double carbonyl absorption of the anhydride group disappeared. A peak at 1717 cm^{-1}, characteristic of the carbonyl in carboxylic acid groups[34], and a broad absorption circa 3500 cm^{-1}, assigned to the O-H stretch, were created (Figure 3-2a). The high resolution XPS C 1s scans in Figure 3-2c were used to quantify the composition of the film. The component peak positions were assigned as follows: 289.4 eV to C*(=O)O, 287.7 eV to NC*(=O), 286.1 eV to C*OC and NC*H_3, and 285 eV to CH_x. [35] The composition of the film was quantified by integrating the Gaussion component peaks; the composition was found to be 14% maleic anhydride, 76% N,N-dimethylacrylamide, and 10% di(ethylene glycol) divinyl ether.

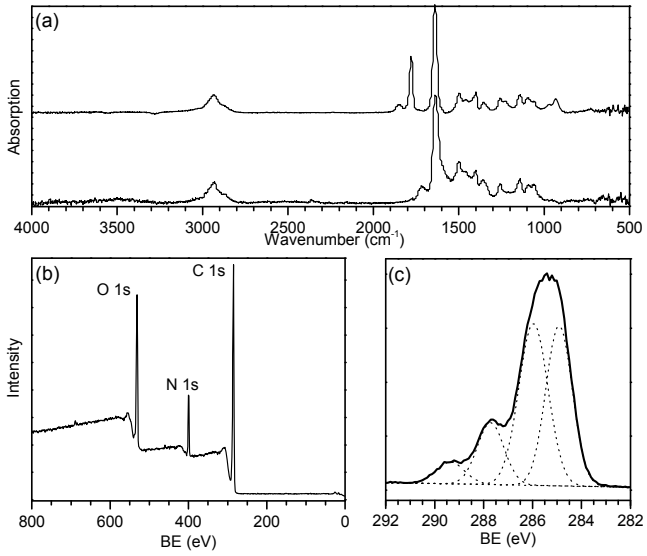

Figure 3-2. (a) FTIR spectra of as-deposited (top) and hydrolyzed PMaDD (bottom). Note the dramatic difference in intensity of the characteristic peaks of maleic anhydride (at 1778 and 1849 cm^{-1}), while there is little intensity difference in the carbonyl of dimethyacrylamide units (1632 cm^{-1}) (b) XPS survey scans of as-deposited PMaDD and (c) high resolution spectra of the C 1s region with component peaks fitted to Gaussian distributions for composition quantification.

The equilibrium swelling properties of the PMaDD films were characterized as a function of pH using spectroscopic ellipsometry. The ionic strength of the buffer solution was fixed at 30 mM and buffer strength at 10 mM. The pH dependence of the swelling ratio of PMaDD films is shown in Figure 3-3a. The degree of swelling (Q) was calculated using $Q = v_{2i}/v_{2s}$, where v_{2i} is the initial volume fraction of polymer (equal to unity for dry as-deposited films) and v_{2s} is the volume fraction of polymer in the swollen state. The error bars represent the uncertainty in the fit of the ellipsometric model. The swelling ratio clearly increased with pH due to the higher degree of ionization of the hydrogel. The two carboxylic acid groups formed upon hydrolysis of maleic anhydride have unique dissociation constants (pKa1 = 2.8, pKa2 = 6.1)[36], which accounts for the observed swelling response.[16]

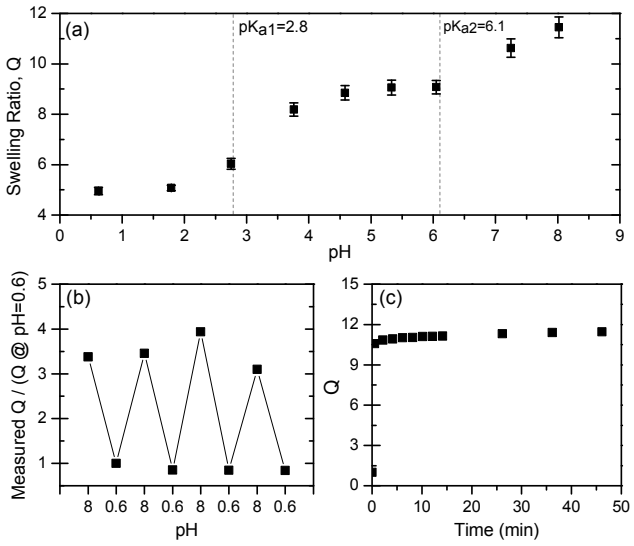

Figure 3-3. Swelling properties. (a) The pH dependence of swelling of PMaDD films at a fixed ionic strength of 30 mM. Characterization of the (b) reversibility and (c) kinetics of swelling by spectroscopic ellipsometry.

A maximum swelling ratio of 11.5 was achieved. Even though it is common for bulk ionic hydrogels to have swelling ratios greater than 100, the swelling ratios are expected to be lower for thin films due to constraints imposed by the solid substrate.[37] These swelling ratios are impressive when compared to previous results for neutral iCVD hydrogel films of poly(2-hydroxyethyl methacrylate), which have swelling ratios < 1.5.[38] Hydrogel thin films firmly attached to the substrate that are prepared through other techniques also experience restricted swelling. Four micrometer-thick films of poly(N-isopropyl acrylamide) exhibited swelling ratios of 15[39], and poly(N,N-dimethylacrylamide) films had swelling ratios of less than 10.[37] The high degree of swelling of the PMaDD material is critical for membrane applications. One of the practical limitations of utlrafiltration and nanofiltration membranes is their tendency to foul, in which the pores become blocked. Protein fouling of hydrogel materials generally decreases as water content increases[40] (greater swelling) and their surfaces become more hydrophilic.[41]

The kinetics and reversibility of swelling are also important factors. The reversibility was studied by exposing a film repeatedly to the two pH extremes. The results shown in Figure 3-3b clearly show the

swelling is reversible. Furthermore, the hydrogel swells to 95% of its equilibrium value within 2.5 minutes (Figure 3-3c). This indicates the benefit of minimizing the film thicknesses. Swelling of hydrogels is a diffusion-limited process (as is diffusion of small molecules through hydrogels). As such, the time to reach equilibrium swelling is proportional to the square of the hydrogel's smallest dimension (thickness). Thus, hydrogel nanofilms reach equilibrium swelling on the order of minutes, while bulk gels can take hours.[36]

3.3.2 Modeling of Permeant Diffusion

The internal pore size is a critical parameter in describing diffusion of solutes through hydrogels. To understand the capability of the PMaDD to serve as a size-selective separation layer, the internal pore structure of the hydrogel and its diffusivity were analyzed. To model the diffusivity of solutes in PMaDD, the Lustig-Peppas model for homogeneous hydrogels is proposed[42]

$$\frac{D_g}{D_o} = \left(1 - \frac{r_s}{\xi}\right) \exp\left(-Y \frac{v_{2s}}{1 - v_{2s}}\right) \qquad \text{Eq. 3-1}$$

where r_s is the hydrodynamic radius of the solute, ξ is the correlation length between crosslinks, and v_{2s} is the volume fraction of polymer in the gel. Intuitively, ξ can be described as the mesh size of the hydrogel. Y is a ratio between the volume required for translation movement of the solute to the molar volume of the liquid; setting it to unity is an appropriate approximation.[43] A diffusivity model for solutes in strong polyelectrolytes (also termed heterogeneous hydrogels – see Amsden's review for the distinction between homogeneous and heterogeneous hydrogels[43]) was not used since N,N-dimethylacrylamide was the primary component in PMaDD. This model (Eq. 3-1) clearly shows that the ratio of the hydrodynamic radius of the solute to the radius of the internal pores is critical. The mesh size can be calculated using Eq. 3-2:

$$\xi = \nu_{2s}^{-1/3} l \sqrt{C_n N} \qquad \text{Eq. 3-2}$$

Here *l* is the length of the C-C bond (0.154 nm), C_n is the characteristic ratio, and *N* is the number of repeat units between crosslinks. *N* can be calculated using $N=1/X$, where *X* is the crosslinking density. The crosslink density can be determined from the XPS analysis above (X=0.1), assuming that the number of physical crosslinks (from chain entanglements) is negligible. Since C_n is equal to 8.5 for poly(acrylamide)[44] and 8.4 for poly(methacrylic acid)[45], polymers with repeat units similar to those found in PMaDD, Cn was assumed to be 8.5 for PMaDD. At pH = 7 ($v_{2s}=1/Q=0.09$), the mesh size of the hydrogel is calculated to be 3.2 nm.

Inserting the calculated pore size and swelling ratio at pH = 7 into Eq. 3-2, the calculated ratios of diffusion coefficients (D_g/D_0) for glucose (r_s = 0.36 nm) and bovine serum albumin (r_s = 3.6 nm) are 0.8 and -0.1, respectively. The negative value for the BSA diffusion coefficient is unphysical, implying that the diffusion of BSA is effectively blocked by the hydrogel, which is expected since the hydrodynamic radius of BSA is greater than the hydrogel's mesh size.

3.3.3 Composite Membrane Characterization

Figure 3-4 presents an SEM of the commercial alumina membranes before and after being coated with PMaDD via iCVD. It is apparent from Figure 3-4b that PMaDD formed a blanket layer over the membrane surface. It is difficult to determine from these images the extent of pore fill-in of the PMaDD. It is likely that some of the pore was filled by the hydrogel, but from the open pores below the surface, it can be concluded that complete infill was avoided. This was achieved by depositing PMaDD under conditions where the P/P_{sat} value of dimethylacrylamide was approximately 0.56. P/P_{sat} refers to the partial pressure of the monomer over its saturated partial pressure at the temperature of the substrate. This reduced partial pressure has been shown to control coating conformality.[46] The unswelled thickness of the hydrogel layer was estimated to be 73 nm from this image and others that were analyzed but not included here.

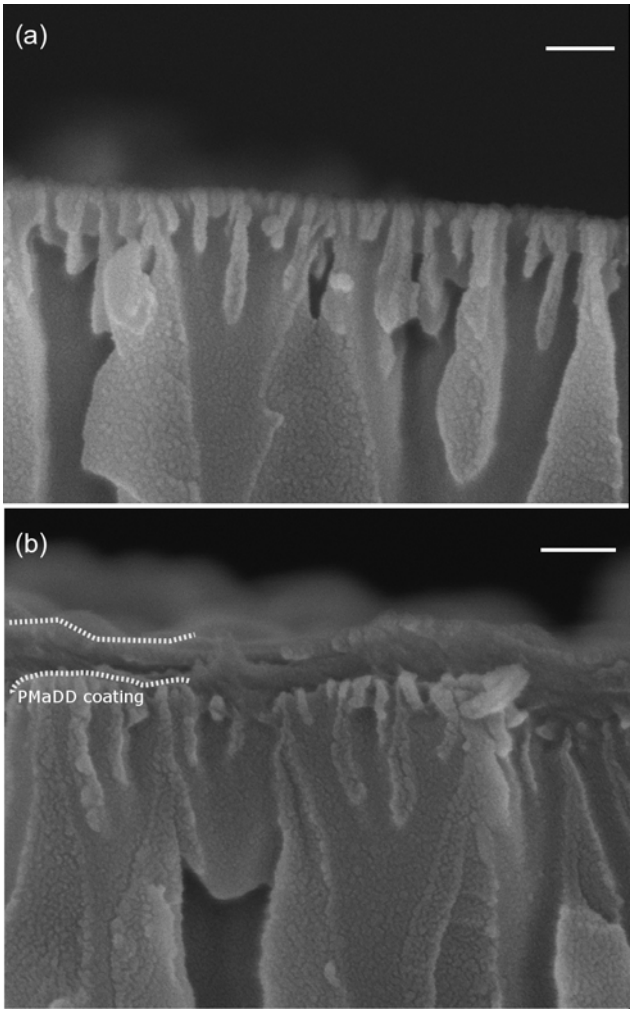

Figure 3-4. High resolution SEM images of cross-sections of porous alumina membranes (a) before and (b) after being coated with PMaDD by iCVD. Throughout most of the membrane cross-section, the pores are approximately 200 nm in diameter; they reduce to 20nm at the surface. (Scale bar = 100 nm). Top down images of the coated membranes is provided in Figure 3-6a.

Diffusion of glucose and BSA in these composite membranes was measured in a diffusion cell. The kinetics of glucose and BSA diffusion through the alumina membranes with and without the PMaDD layer are presented in Figure 3-5. Assuming that the volume of the sink is infinite compared to the source, the diffusion kinetics can be modeled using the pseudo steady state approximation in Eq. 3-3.

$$\ln\left[1-\frac{M_t}{M_1}\right]=\frac{-A\alpha D_i}{lV_1}t \qquad \text{Eq. 3-3}$$

Here M_t is the mass of permeant transferred from source to sink at time t, M_1 is the initial mass of permeant in the source, A is the area available for mass transfer, D_i is the mass transfer coefficient of component i in the composite membrane, l is the thickness of membrane, V_1 is the volume of the source. Clearly, both glucose and BSA diffused through the uncoated membranes. Using the slopes of the lines that were linearly regressed to the diffusion data for uncoated membranes in Figure 3-5, diffusion constants of $4.3\text{x}10^{-7}$ cm^2 s^{-1} and $1.8\text{x}10^{-7}$ cm^2 s^{-1} were calculated for glucose and BSA, respectively. Values of 1, 4.9 cm^2, 60 mm, and 7 mL were used for α, A, l, and V_1, respectively.

Figure 3-5b demonstrates that the PMaDD coating effectively blocks BSA diffusion, as predicted from the models above. The zero permeability confirms the lack of pinhole defects. There is a slight drop in glucose permeability in the PMaDD-coated membranes (Figure 3-5a). The overall diffusion coefficient for BSA in the PMaDD-coated membrane was calculated as $1.3\text{x}10^{-7}$ cm^2 s^{-1}. Assuming a laminated structure for the composite membrane, the composite diffusion coefficient is calculated as follows:

$$\frac{l_{composite}}{D_{composite}}=\frac{l_{alumina}}{D_{alumina}}+\frac{l_{PMaDD}}{D_{PMaDD}} \qquad \text{Eq. 3-4}$$

$D_{alumina}$ and $D_{composite}$ were determined from the slopes and reported above. Here, 0.7, 60, and 60.7 μm were used for l_{PmaDD}, $l_{alumina}$, and $l_{composite}$, respectively. Using these values in Eq. 3-4, D_{PMaDD} was calculated to be $1.8\text{x}10^{-8}$ cm^2 s^{-1}. D_g/D_o was calculated to be 0.8 using Eqs. 1 and 2 above (D_g in the terminology above is equal to D_{PMaDD} here). A diffusion coefficient of $6.4\text{x}10^{-6}$ cm^2 s^{-1} for glucose in water has been reported.[43] Therefore, modeling indicates that D_{PMaDD} should be $5.12\text{x}10^{-6}$ cm^2 s^{-1}. Because the experimentally determined diffusivity is over two orders of magnitude lower than the calculated value, it can be concluded that pore fill-in did occur. The extent of fill-in cannot be estimated.

The pore diameter confines the hydrogel, which limits swelling and leads to further reductions in diffusivity. Simple techniques can be envisioned that eliminate this problem, such as first depositing a sacrificial material to fill in the pores, followed by deposition of the desired skin layer by iCVD.

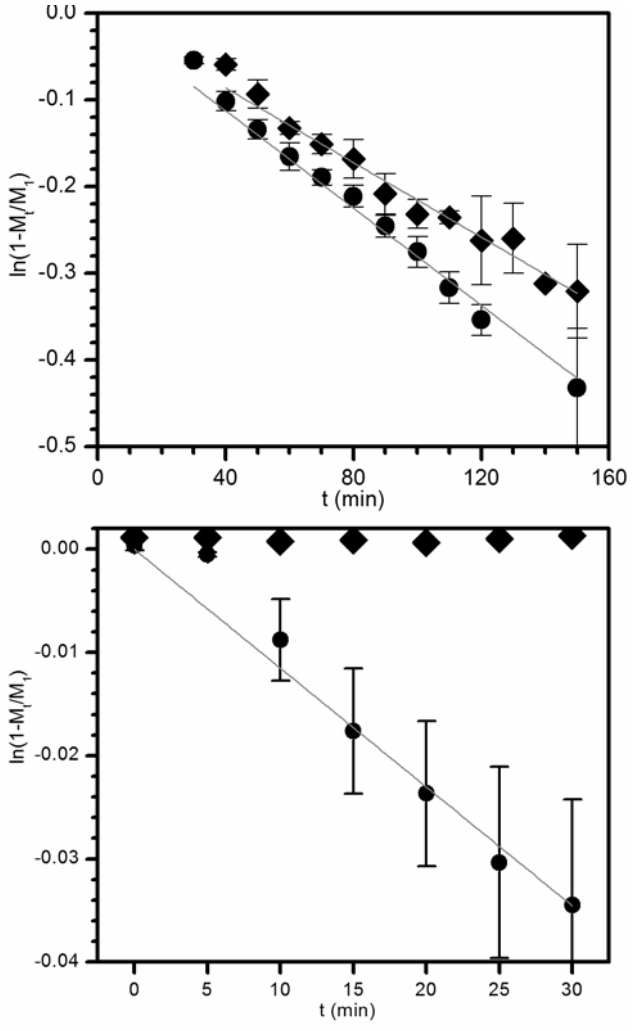

Figure 3-5. Diffusion kinetics of (a) glucose and (b) BSA through commercially available porous alumina membranes (●) and the same membranes coated with 500 nm PMaDD by iCVD (◆). The pores are 20 nm in diameter at the surface of the alumina membranes.

3.3.4 Stability of Hydrogel Thin Film

The stability of the iCVD coating is also critical. Figure 3-3a (pH-responsiveness) shows that the polymer is chemically stable in a pH range from less than one to eight. Covalent bonding of PMaDD to

the substrate through 3-AMS surface functionalities was required for adhesion stability. 3-AMS was used to covalently bond PMaDD to the alumina membrane. The observation of the successful modulation of the glucose and BSA diffusivities in the PMaDD-coated membranes is strong evidence that PMaDD remained adhered to the alumina.

In commercial or industrial operations, membrane cleaning is an important process. To show that these PMaDD films will be stable to such processes, a vigorous test of adhesion was performed by ultrasonicating the membranes in buffer solution for five minutes. SEM images of ultrasonicated PMaDD-coated membranes with and without 3-AMS exposure before the iCVD step are shown in Figure 3-6. The PMaDD coating is retained on the membrane that was treated with 3-AMS prior to iCVD, while it delaminated from the untreated membrane to expose the underlying porous surface. The cavitation forces of ultrasonication overcame the physical interaction between the hydrogel and untreated alumina but were not strong enough to break the amide bond created by the reaction of maleic anhydride with the amine of 3-AMS treated alumina.

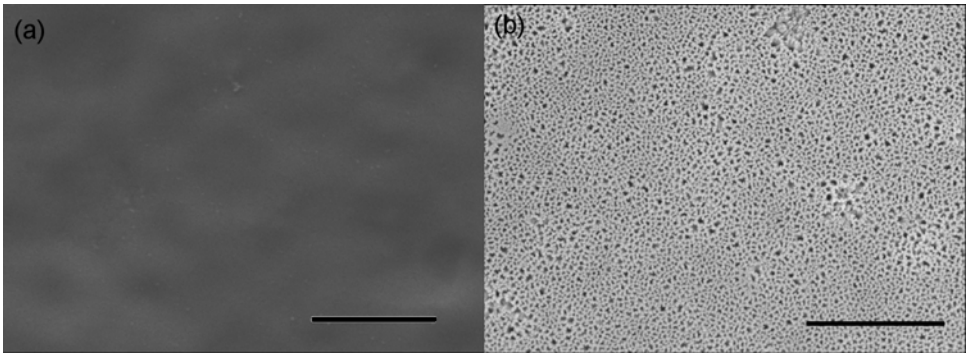

Figure 3-6. Effect of ultrasonication on PMaDD-coated alumina membranes that (a) were and (b) were not treated with 3-AMS vapors prior to iCVD of PMaDD. The 3-AMS is shown to be critical to PMaDD adhesion. (Scale bar = 1 μm)

Furthermore, the coating in Figure 3-6a, even after ultrasonication, appears to be smooth, showing no trace of the underlying pore structure. Pinholes are not readily apparent, either. By considering this image along with the zero flux of BSA through the PMaDD-coated membranes, it can be concluded that these coatings are pinhole-free.

3.3.5 Functionalization of PMaDD

The ability to control the permeability through the mesh properties of the hydrogel has been demonstrated. It is important, as well, to be able to control the interaction of the membrane surface with its environment for fouling considerations. Because the surface chemistry required to control these interactions will depend on the application, it is important to have versatile reactive functionality within the membrane. The anhydride in PMaDD is readily functionalized through nucleophilic reactions.[47] The results of functionalizing the anhydride in the PMaDD composition through simple, one-step, uncatalyzed reactions are provided in Figure 3-7a. The films were functionalized after iCVD but prior to hydrolysis in water. The reactions were chosen to demonstrate the versatility in surface chemistry that can be achieved. Surface thiols have been shown to be protein-adhesive[48], while PEG brushes are widely studied protein resistant functionalities.[12, 17] The PEG molecules had an average molecular weight of 400 g/mol and were denoted PEG-400. PEG functionalization required a longer reaction time and higher temperature because the reaction of hydroxyls with anhydrides is slower than the reaction of amines.[49] Disappearance of the carbonyl absorptions characteristic of anhydride at 1778 and 1852 cm^{-1} indicates that the reaction indeed proceeded through a nucleophilic substitution at the anhydride. In the FTIR spectrum of cysteamine functionalized PMaDD, there is a dramatic increase in the absorption at 1638 cm^{-1} and a weak but new absorption circa 2600 cm^{-1}, which are characteristic of an amide's carbonyl stretch and S–H stretch of thiols, respectively.[34] The PEG-400 functionalized PMaDD has a new absorption at 1733 cm^{-1} from the carbonyl stretching of the ester that forms upon reaction of hydroxyls with the anhydrides and increased absorptions at 1108 cm^{-1}, characteristic of the C—O—C antisymmetric stretching, and in the hydrocarbon region (2800 – 3000 cm^{-1}).[34] These spectra are consistent with the product structures drawn in Figure 3-7a.

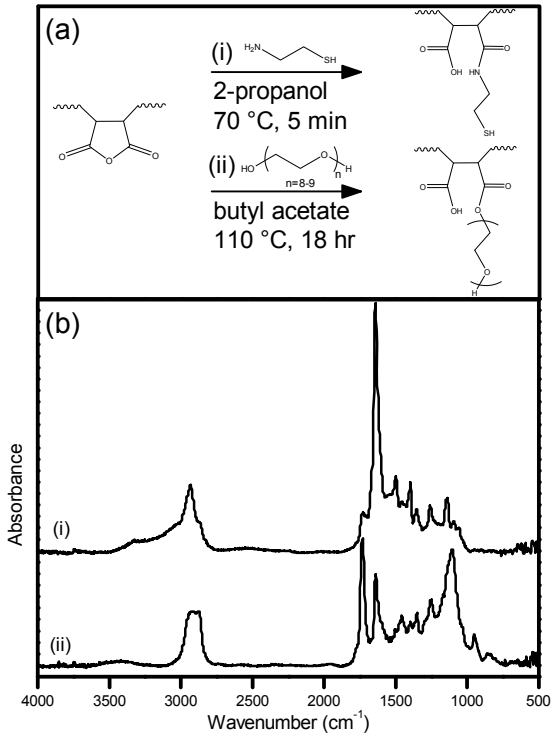

Figure 3-7. (a) Functionalization of PMaDD with (i) cysteamine and (ii) poly(ethylene glycol) through nucleophilic substitution reactions of the anhydride group. (b) The FTIR spectra of the functionalized films reveal the disappearance of the anhydride functionality and confirm the structures of the products shown in (a). Reaction conditions are provided in the Experimental section, and the original spectrum of as-deposited PMaDD is provided in Figure 3-2a. (The N,N-dimethylacrylamide and di(ethylene glycol) divinyl ether components of the PMaDD composition are not drawn in (a) due to space constraints.)

In Figure 3-8a, PMaDD thin films have been patterned using transmission electron microscope (TEM) grids. The TEM grids had 7.5x7.5 μm openings, which were used to define the hydrogel pattern. After the film had been deposited, it was reacted with cysteamine as described in Figure 3-7a. CdSe semiconductor nanoaparticles were readily attached to the thiol groups through a thiol exchange reaction to localize fluorescence to the hydrogel patterns. This allowed the use of fluorescence microscopy as a convenient method to observe hydrogel swelling. Because a carboxylic acid moiety is retained after the functionalization, which increases the swelling due to the ionic term in the Gibbs free energy balance, the hydrogel properties are retained after the functionalization. Visual confirmation of this is provided by the optical micrographs in Figure 3-8 of dry and swollen hydrogel patterns. The patterns were swollen in the pH 8 buffer described earlier. It is unclear why fluorescence diminishes in

the center of the pattern, but it is clear that swelling does occur. Figure 3-8 confirms that patterning and subsequent surface functionalization of the iCVD ionic hydrogels is possible. These capabilities may find utility in the design of novel membranes, unique surfaces for separation and sensing, or as platforms for cell growth.[50]

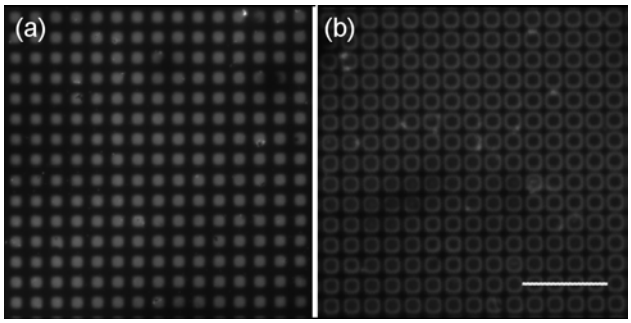

Figure 3-8. Fluorescent images of PMaDD hydrogel patterns that have been functionalized with cysteamine and linked to CdSe/ZnS nanoparticles. Initially (a) the patterns were dry and then (b) swelled upon immersion in pH 8 buffer. (Scale bar = 50 μm)

3.4 Conclusion

A highly swellable, pH-responsive ionic hydrogel thin film was synthesized using initiated chemical vapor deposition (iCVD). PMaDD has the highest swelling ratio achieved by iCVD to date, and is comparable in terms of swelling to other highly swellable thin films reported in the literature. Motivation to use the iCVD synthesis technique has been demonstrated by implementing PMaDD as a size-selective layer on asymmetric membranes. iCVD enabled the synthesis of pinhole free layers with an average thickness of 73 nm on top of porous Anopore™ alumina anisotropic membranes. Moreover, a technique was developed to covalently attach the hydrogel film to the membranes for stability in solution. It is expected that this integration technique is applicable to other membrane materials, such as polyacrylonitrile, cellulose, polysulfone, and polycarbonate, which are commonly employed in ultrafiltration and nanofiltration applications. Reactive functionalities, which are required for the reaction with organosilanes, can be introduced onto the surfaces of polymers through plasma

activation.[51] Moreover, iCVD is currently being investigated for the synthesis of high quality films with sub-50 nm thicknesses, which are difficult to achieve by other methods.

References

[1] P. Bernardo, E. Drioli, G. Golemme, *Ind. Eng. Chem. Res.* **2009**, *48*, 4638.

[2] H. Kawakami, *Journal of Artificial Organs* **2008**, *11*, 177.

[3] J. K. Oh, R. Drumright, D. J. Siegwart, K. Matyjaszewski, *Prog. Polym. Sci.* **2008**, *33*, 448.

[4] M. A. Shannon, P. W. Bohn, M. Elimelech, J. G. Georgiadis, B. J. Marinas, A. M. Mayes, *Nature* **2008**, *452*, 301.

[5] D. F. Stamatialis, B. J. Papenburg, M. Girones, S. Saiful, S. N. M. Bettahalli, S. Schmitmeier, M. Wessling, *Journal of Membrane Science* **2008**, *308*, 1.

[6] M. Ulbricht, *Polymer* **2006**, *47*, 2217.

[7] R. W. Baker, "*Membrane technology and applications*", J. Wiley, Chichester; New York, 2004.

[8] I. Pinnau, B. D. Freeman, "Formation and modification of polymeric membranes: overview", in *Membrane Formation and Modification*, I. Pinnau and B.D. Freeman, Eds., Amer Chemical Soc, Washington, 2000, p. 1.

[9] Z. G. Wang, L. S. Wan, Z. K. Xu, *Journal of Membrane Science* **2007**, *304*, 8.

[10] A. A. Brown, N. S. Khan, L. Steinbock, W. T. S. Huck, *European Polymer Journal* **2005**, *41*, 1757.

[11] P. Kingshott, H. J. Griesser, *Curr. Opin. Solid State Mat. Sci.* **1999**, *4*, 403.

[12] J. Satulovsky, M. A. Carignano, I. Szleifer, *Proceedings of the National Academy of Sciences of the United States of America* **2000**, *97*, 9037.

[13] M. Matsuda, M. Sato, H. Sakata, T. Ogawa, K. Yamamoto, T. Yakushiji, M. Fukuda, T. Miyasaka, K. Sakai, *Journal of Artificial Organs* **2008**, *11*, 148.

[14] T. Canal, N. A. Peppas, *Journal of Biomedical Materials Research* **1989**, *23*, 1183.

[15] P. J. Flory, J. J. Rehner, *The Journal of Chemical Physics* **1943**, *11*, 521.

[16] M. Sen, O. Guven, *Polymer* **1998**, *39*, 1165.

[17] T. Wazawa, Y. Ishizuka-Katsura, S. Nishikawa, A. H. Iwane, S. Aoyama, *Anal. Chem.* **2006**, *78*, 2549.

[18] I. Tokarev, S. Minko, *Soft Matter* **2009**, *5*, 511.

[19] H. Hu, Z. Cai. Hydrophilic Microporous Polyolefin Membrane. U.S. Patent 5209849, 1992.

[20] M. Steuck, N. Reading. Porous Membrane Having Hydrophilic Surface and Process. U.S. Patent 4618533, 1984.

[21] M. L. Bruening, D. M. Dotzauer, P. Jain, L. Ouyang, G. L. Baker, *Langmuir* **2008**, *24*, 7663.

[22] W. E. Tenhaeff, K. K. Gleason, *Adv. Funct. Mater.* **2008**, *18*, 979.

[23] M. Gupta, V. Kapur, N. M. Pinkerton, K. K. Gleason, *Chem. Mat.* **2008**, *20*, 1646.

[24] M. Karaman, S. E. Kooi, K. K. Gleason, *Chem. Mat.* **2008**, *20*, 2262.

[25] M. Gupta, K. K. Gleason, *Langmuir* **2006**, *22*, 10047.

[26] K. K. S. Lau, K. K. Gleason, *Macromolecules* **2006**, *39*, 3688.

[27] M. Bruening, D. Dotzauer, *Nat Mater* **2009**, *8*, 449.

[28] H. Hachisuka, T. Ohara, K. Ikeda, "A new type of asymmetric polyimide gas separation membrane having ultrathin skin layer", in *Membrane Formation and Modification*, I. Pinnau and B.D. Freeman, Eds., Amer Chemical Soc, Washington, 2000, p. 65.

[29] D. M. Sullivan, M. L. Bruening, *Chem. Mat.* **2003**, *15*, 281.

[30] W. E. Tenhaeff, K. K. Gleason, *Langmuir* **2007**, *23*, 6624.

[31] E. McCafferty, J. P. Wightman, *Surface and Interface Analysis* **1998**, *26*, 549.

[32] V. Szczepanski, I. Vlassiouk, S. Smirnov, *Journal of Membrane Science* **2006**, *281*, 587.

[33] W. E. Tenhaeff, K. K. Gleason, *Thin Solid Films* **2009**, *517*, 3543.

[34] D. Lin-Vien, N. B. Colthup, W. G. Fateley, J. G. Grasselli, "The Handbook of Infrared and Raman Characteristic Frequencies of Organic Molecules", Academic Press, New York, 1991.

[35] G. Beamson, D. Briggs, "*High Resolution XPS of Organic Polymers The Scientia ESCA300 Database*", John Wiley & Sons, New York, 1992.

[36] T. Caykara, *J. Appl. Polym. Sci.* **2004**, *92*, 763.

[37] R. Toomey, D. Freidank, J. Ruhe, *Macromolecules* **2004**, *37*, 882.

[38] K. Chan, K. K. Gleason, *Langmuir* **2005**, *21*, 8930.

[39] M. E. Harmon, D. Kuckling, C. W. Frank, *Macromolecules* **2003**, *36*, 162.

[40] H. Susanto, M. Ulbricht, *Langmuir* **2007**, *23*, 7818.

[41] H. Ju, B. D. McCloskey, A. C. Sagle, V. A. Kusuma, B. D. Freeman, *Journal of Membrane Science* **2009**, *330*, 180.

[42] S. R. Lustig, N. A. Peppas, *J. Appl. Polym. Sci.* **1988**, *36*, 735.

[43] B. Amsden, *Macromolecules* **1998**, *31*, 8382.

[44] M. Bohdanecky, V. Petrus, B. Sedlacek, *Makromolekulare Chemie-Macromolecular Chemistry and Physics* **1983**, *184*, 2061.

[45] M. T. A. Ende, N. A. Peppas, *J. Appl. Polym. Sci.* **1996**, *59*, 673.

[46] S. H. Baxamusa, K. K. Gleason, *Chem. Vapor Depos.* **2008**, *14*, 313.

[47] T. Pompe, S. Zschoche, N. Herold, K. Salchert, M. F. Gouzy, C. Sperling, C. Werner, *Biomacromolecules* **2003**, *4*, 1072.

[48] A. Bernkop-Schnurch, V. Schwarz, S. Steininger, *Pharm. Res.* **1999**, *16*, 876.

[49] B. C. Trivedi, B. M. Culbertson, "*Maleic Anhydride*", Plenum Press, New York, 1982.

[50] N. Mari-Buye, S. O'Shaughnessy, C. Colominas, C. E. Semino, K. K. Gleason, S. Borros, *Adv. Funct. Mater.* **2009**, *19*, 1276.

[51] J. M. Goddard, J. H. Hotchkiss, *Prog. Polym. Sci.* **2007**, *32*, 698.

CHAPTER FOUR

Integration of Reactive Polymeric Nanofilms into a Low Power Electro-mechanical Switch for Selective Chemical Sensing*

*Originally published as W. J. Arora, W. E. Tenhaeff, K. K. Gleason, G. Barbastathis, *J. Microelectromech. Syst.* **2009**, *18*, 97.

Abstract

This paper presents the fabrication and demonstration of an ultrathin microelectromechanical chemical sensing device. Microcantilevers are etched from 100 nm-thick silicon nitride, and a 75 nm-thick reactive copolymer film for sensing is deposited by initiated chemical vapor deposition. Crosslinking densities of the polymer films are controlled during the deposition process; it is shown that greater crosslinking densities yield greater cantilever deflections upon the polymer's reaction with the analyte. Because chemical reactions are necessary for stress formation, the sensing is selective. Cantilever deflections of greater than 3 μm are easily attained, which allow a simple switch to be designed with resistance-based outputs. When exposed to a hexylamine vapor phase concentration of 0.87 mol%, the resistance of the switch drops by over six orders of magnitude with a response time less than 90 seconds.

4.1 Introduction

Chemical sensing science is a field with many applications in industry, security, and defense. A multitude of detection mechanisms exist, but many are only applicable to very specific situations. Generally, effective chemical sensing needs to be highly selective to a target analyte and result in a large electrical response. Here we demonstrate a sensing mechanism that achieves high selectivity because it relies on covalent bond formation and achieves a large electrical resistance change due to its design as an electro-mechanical switch. The chemically selective component is a reactive polymer deposited by initiated chemical vapor deposition (iCVD[1]) onto a three-dimensional (3D) micro-switch. The polymer is engineered to produce a large stress when it reacts with the analyte, deforming the switch and causing it to short-circuit. We present a non-optimized proof-of-concept device that uses a maleic anhydride copolymer thin film to detect amines. Before reacting with hexylamine, the device is an open circuit (drawing negligible power), and after the reaction the resistance drops by over six orders of magnitude. Although this first fabricated prototype has sensitivity limits in the parts per thousand range, achievable geometric modifications will be discussed that are predicted to improve detection down into the ppb range. In addition, it is anticipated that a wide range of analytes can be detected by using the general platform method of iCVD to synthesize additional types of reactive organic nanocoatings, each offering a specific complimentary reactive functional group.[2,3]

Transducing a chemical response into an electrical response can be done most directly with a chemiresistive polymer, in which the reaction either acts to dope or undope a semiconducting polymer[2] or cause a conductivity change by swelling a partially conductive polymer.[3] However, these methods suffer from lack of analyte specificity, offer small resistance changes and draw continuous power. Instead, an intermediate transduction step, often optical or mechanical, is used. Micro-cantilevers are a common platform for transducing the chemical response into a mechanical one. One surface of the

cantilever is coated with a material (often a polymer) that the target chemical will interact with, typically through absorption (swelling) or reaction.

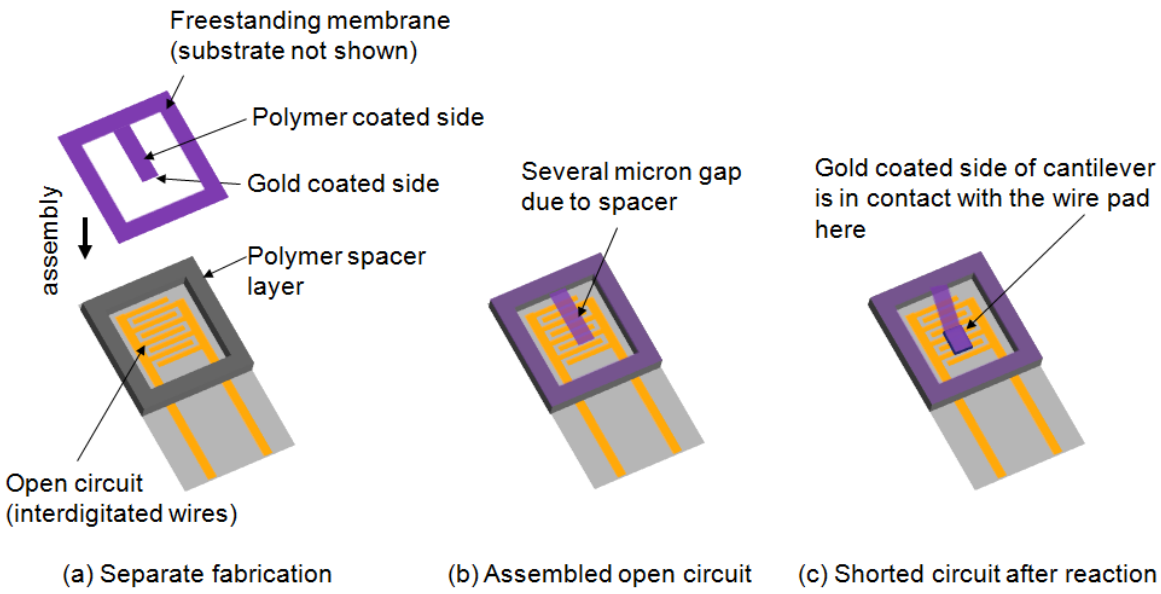

Figure 4-1. Schematic of the assembly and operation of the micro-switch. (a) A silicon nitride cantilever, still attached to a silicon handle wafer frame (not shown) is coated with 75nm of iCVD polymer on one side and evaporated gold on the other. Interleaved gold wires are patterned onto a separate silicon wafer with a silicon nitride (non-conducting) top surface. A 3µm thick spacer is formed around the gold wires using a photo-polymer. The cantilever is placed onto the spacer layer. (c) Upon reaction with the target vapor the polymer strains, forcing the cantilever to bend down and contact the interleaved gold wires. The conductive gold underside of the cantilever short-circuits these wires.

The interaction creates a stress that causes the cantilever to bend. Existing methods rely on measuring small cantilever deflections of less than a few microns[4] or measuring resonance frequency changes due to a mass increase. In order to measure these small changes, optical[5], piezoelectric[6], piezoresistive[7] or capacitive[8] schemes are employed. These measurements are susceptible to ambient interference and require additional power-consuming electronic circuitry. It has been suggested that the requirement of relatively thick sensing layers, typically on the order of several micrometers, in soft-matter-based sensors (i.e. polymers) is another major disadvantage as it limits their incorporation into nano-scale devices[9]. The best cases of "ultrathin" sensors have thicknesses greater than 300 nm.

Furthermore, such systems show only partial selectivity, which is based on the rate of different molecules diffusing into polymer layers. Herein, we report the sensing of analytes based on chemical reactions in the polymer where the polymer sensing layer is 75 nm thick.

4.2 Design

Our sensing concept produces large cantilever deflections because it uses a polymer capable of generating stresses of greater magnitude and because the cantilever is very thin (100 nm). The large deflection allows the cantilever to act as a switch. The assembly and operation of this switch is shown in Figure 4-1, and fabrication details are described in the *Experimental* section. Our work on the Nanostructured Origami^{TM} method of folding patterned membranes into three-dimensional microstructures[10-12] inspired the 3D architecture of the switch. Previously, we used the stress from a deposited metal or ion implantation to controllably fold a thin silicon nitride cantilever into a static structure. Here, the structure is dynamic because the cantilever bends as the polymer stresses. Initially, the switch is an open circuit (Figure 4-1b) separating a battery from circuitry such as an RF transmitter. Therefore, almost no power is consumed until the switch closes, and no logic circuitry is needed to determine a threshold of cantilever deflection magnitude.

In addition to an improved transduction scheme, sensing selectivity is improved by using another recently developed technique, iCVD.[1] iCVD enables designing the deposited polymer with specific functional groups that will chemically react with the target analyte. Several choices of functional monomers are available, meaning that many classes of compounds can be sensed. In this study we use maleic anhydride (Ma) because we were familiar with its properties from previous studies[13]. The reactivity of the anhydride functionality enables the detection of amines; hexylamine is used as a model analyte in this study. Detection of amines is important for industrial and environmental monitoring, food

quality control, and diagnosis of certain diseases.[14] Low concentrations of aliphatic and aromatic amines can cause toxicological responses.[15]

Maximizing the bending force and deflection magnitude of the polymer-coated cantilevers is critical to minimize the response time and contact resistance of the closed switch. For effective transmission of the stress into mechanical bending, there must be good adhesion at the polymer-cantilever interface (see *Experimental* section), and the polymer must develop a large stress from reacting with the analyte. When the analyte reacts with the polymer, it forces the polymer to expand due to the added volume. Chemical linkages in the network structure restrict expansion of crosslinked polymer films, so instead they stress compressively. With iCVD, the degree of crosslinking is accurately controlled by the ratio of cross-linker monomer to functional monomer.[16] We model the strain that forms by

$$\varepsilon_x = \varepsilon_y = \sqrt[3]{\frac{v_{ex} - v_{sf}}{v_{sf}}} = \sqrt[3]{\frac{v_{ex}}{v_{sf}}} - 1 \quad \text{Eq. 4-1}$$

where ε_x and ε_y are the in-plane strain components of the copolymer coating, v_{ex} is the actual, experimentally observed molar volume of the reacted polymer film and v_{sf} is the molar volume the polymer in a stress free state. The stress free state is a theoretical condition in which the polymer is able to freely expand without limitations imposed by the crosslinks. This equation is based on similar work by Wen et al.,[17] who were examining stress formation due to shrinkage when polymer coatings are cured. One assumption in Eq. 4-1 is the polymer volume can expand only in the direction normal to the surface, while the expansion in the lateral dimension is constrained by adhesion to the substrate. It is clear from this equation that greater strain will develop with increased coating crosslinking density since this limits volume expansion. To analyze the effect of analyte volume on stress, we make the assumption that there is a limiting value for v_{ex} due to the presence of crosslinks, while v_{sf} will increase

concomitantly with analyte size in order to maintain a constant density. Therefore, the magnitude of the strain should increase with increasing analyte size.

4.3 Experimental

4.3.1 Device Fabrication

Silicon nitride membranes windows (1 mm x 1 mm, 100 nm thick) are formed by backside TMAH etching of silicon. Photoresist is spun directly onto the membrane, exposed with cantilever shapes using a contact mask and developed. The membrane is etched with a CF_4 reactive ion etch (100 V, 200 W, 10 mTorr) until the cantilever border is completely etched. The sample is cleaned in an oxygen plasma (200 W, 400 mTorr) which removes the photoresist. The frontside is coated with electron-beam evaporated titanium (3nm, for adhesion) and gold (5 nm). To ensure good adhesion between the subsequent polymer deposition and the silicon nitride, the cantilevers are primed with a monolayer of 3-aminopropyldimethylethoxysilane in a vapor chamber at 60 °C. The sample is placed gold-side down into a reaction chamber for iCVD polymer deposition, so that the underside (non-gold side) of the cantilever is coated with polymer. Even though the membrane and free-standing cantilevers are placed directly onto the aluminum chamber stage, they do not break. One of the advantages of iCVD over traditional CVD is that the conformality of the polymer coverage can be adjusted by controlling the surface concentrations of the monomers and initiator.[18] In this case we use a low initiator flow rate and high monomer surface concentrations to make the coverage non-conformal and avoid coating the gold side. Furthermore, we have found that this principle permits us to lithographically pattern the deposited polymer using shadow-masking or lift-off both done directly on a free-standing cantilever. These negative tone patterning processes allow adjacent cantilevers on the same chip to be coated with different polymers, for multiplexed sensing.

On a separate substrate, a set of interdigitated gold wires is patterned to form an open circuit (as drawn in Figure 4-1). The space around the wires is covered with a 3µm thick polymer that is patterned by photolithography. Finally the device is assembled by placing the cantilever gold-side-down above the wires so that a ~3µm gap is maintained by the spacer polymer.

4.3.2 Polymer Film Synthesis

Poly[maleic anhydride-co-vinyl pyrrolidone-co-di(ethylene glycol) di(vinyl ether)] (poly(Ma-V-D)) is synthesized by flowing maleic anhydride, vinyl pyrrolidone, and di(ethylene glycol) di(vinyl ether) (Dedve) monomers into a previously described iCVD chamber[13] at rates of 3.6, 1.3, 0.5 sccm, respectively. Poly[maleic anhydride-alt-di(ethylene glycol) di(vinyl ether)] (poly(Ma-D)) is synthesized by feeding maleic anhydride and Dedve at 3.6 and 1.2 sccm, respectively; an alternating copolymer is formed because neither monomer will undergo free radical homopolymerization to a significant extent.[13,19] In both polymer depositions, 0.4 sccm of tert-butyl peroxide initiator and 4 sccm of Ar diluent flow are introduced. The filament temperature is 235 °C, substrate temperature is 25 °C, and the chamber pressure is 250 mTorr. X-ray photoelectron spectroscopy using a monochromatized Al Kα source (Kratos Axis Ultra) revealed that poly(Ma-V-D) is 53.4% maleic anhydride, 35.7% vinyl pyrrolidone, and 10.9% Dedve, while poly(Ma-D) is 60.5% maleic anhydride and 39.5% Dedve During the deposition, film thickness is controlled and measured by *in situ* laser interferometry on polished silicon wafer monitors.

4.3.3 Device Testing

The sensors were tested in a vapor chamber constructed from an aluminum block with a cavity for vapor introduction; the block was bolted to a temperature controlled stage on which the device was placed. The stage was maintained at 40 °C. Nitrogen flow rates into the chamber were controlled with

mass flow controllers (MKS Instruments, Model 1479). One nitrogen line (ultra-high purity, Airgas) was bubbled through the liquid analyte, where it became saturated with the analyte vapor. The second line of nitrogen was mixed with the saturated analyte stream prior to entering the chamber to control analyte concentrations. Electrical resistances were logged with a multimeter (Agilent, U1252A) attached to the sensors' electrical leads.

Before and after the reaction with hexylamine, FTIR spectra of blanket polymer films on Si were collected (Nicolet, Nexus 870). Sixty-four scans from 500 to 4000 cm^{-1} with 4 cm^{-1} resolution were collected and integrated using a DTGS KBr detector. The bare Si wafers served as backgrounds. Thicknesses were determined using spectroscopic ellipsometry, with an incident angle of 70° and 190 wavelengths between 315 and 718 nm (J.A. Woollam, M-2000).

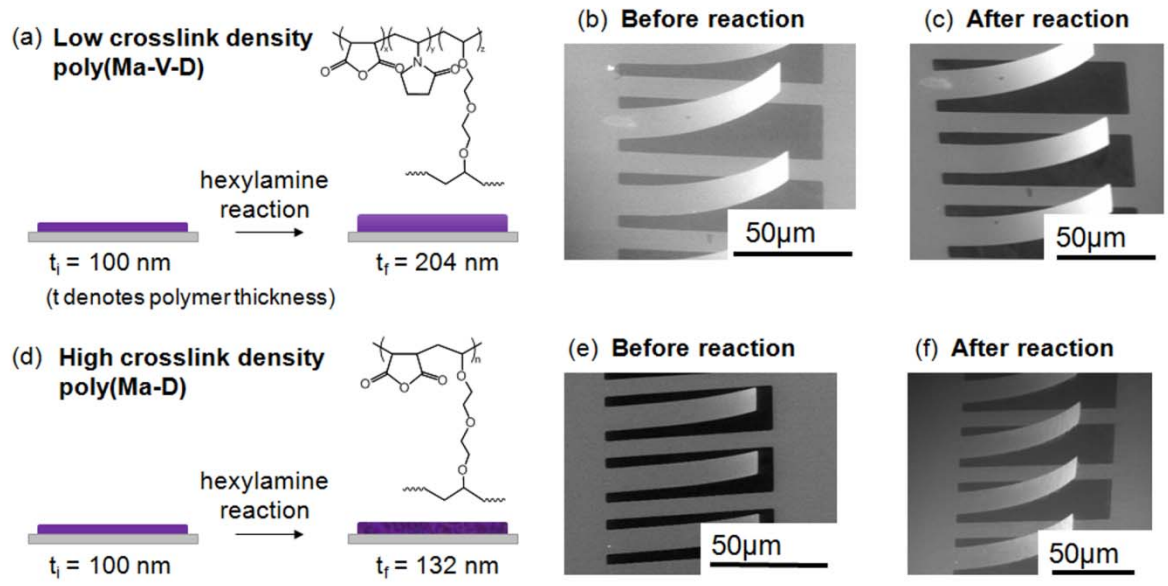

Figure 4-2. Comparison of stress formation in lightly and highly crosslinked maleic anydride polymer after reacting with hexylamine. 100 nm thick silicon nitride cantilevers are coated with iCVD polymer on their under-sides. Compressive stress within the polymer causes the cantilevers to bend upwards; the amount of stress determines the curvature. In (b) the cantilevers are initially bent due to intrinsic stress within the polymer from deposition, whereas in (e) there is very little initial stress in the polymer (desired). In both cases, the hexylamine reaction lasted for 60 min, at a concentration of 0.87% in atmosphere, at 40 ^{o}C. The poly(Ma-V-D) expanded by 102% and stressed minimally while the poly(Ma-D) expanded by 32% and stressed significantly as evidenced by the increased curvature. In addition, FTIR measurements revealed that 95% of the maleic anhydride had reacted in the poly(Ma-V-D) sample vs only 49% in the poly(Ma-D) sample, indicating how severely increased crosslinking lowers the diffusion rate.

4.4 Results and Discussion

We compare two polymers: poly(Ma-V-D) and poly(Ma-D). Figure 4-2 shows images of cantilevers coated with these two polymers before and after the reaction with hexylamine. There is little observable additional deflection of the cantilevers coated with poly(Ma-V-D) due to the hexylamine reaction, since most of the stress from the added volume of hexylamine is relieved through expansion. This degree of expansion is much more limited in the more cross-linked poly(Ma-D) film resulting in the accumulation of stress desired for deflecting the cantilever. However, the crosslinking in poly(Ma-D) also reduces the diffusion of the analyte, creating a tradeoff between stress accumulation and extent of reaction as the degree of crosslinking varies. In making the prototype device, we did not optimize the degree of crosslinking and used the poly(Ma-D) polymer comprised of 39.5% cross-linker as shown in

Figure 4-2d-f. Although there is significant initial curvature with the poly(Ma-V-D) coatings, 75nm-thick poly(Ma-D) films, which were used for device fabrication, resulted in negligible curvature before the hexylamine reaction.

Assuming that the reaction goes to completion and the polymer layer is uniformly elastically stressed, the cantilever curvature *k* can be calculated analytically[10] as

$$k = \frac{6E_1E_2t_1t_2(t_1+t_2)\cdot(\sigma/E_2)}{E_1^{\,2}t_1^{\,4}+E_2^{\,2}t_2^{\,4}+2E_1E_2t_1t_2\cdot(2t_1^{\,2}+2t_2^{\,2}+3t_1t_2)} \qquad \text{Eq. 4-2}$$

Material parameters for this experiment are: plate modulus E_1=300 GPa for silicon nitride, E_2=5 GPa (estimated) for the polymer, and silicon nitride thickness t_1=100 nm. Given a fixed amount of stress σ from the reaction, the cantilever curvature (and hence deflection) is maximized by choosing the optimal polymer layer thickness, t_2. For these parameters, a polymer thickness between 200-300 nm produces a near-maximized curvature. In our experiment we used a 75 nm thick polymer layer. Based on results shown in Figure 4-2, we deduced that the reaction was diffusion limited and that only the top region of the nanocoating reacted with the analyte in our devices.

We fabricated a prototype switch to demonstrate the concept. Images of the assembled switch, both before and after reacting with hexylamine, are shown in Figure 4-3.

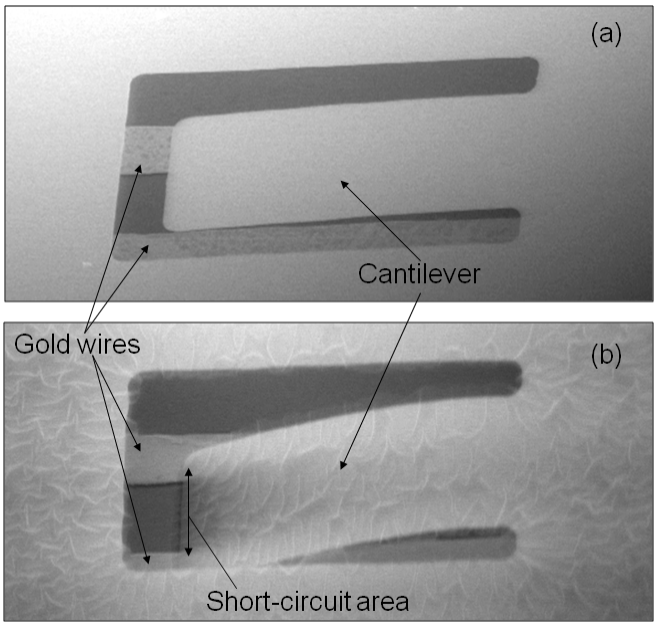

Figure 4-3. Environmental-SEM images of assembled device. Images were taken (a) before reaction (b) after reaction. Cantilever dimensions are 50x20x0.1 μm; the results in Figure 4-4 are reported for 100x20x0.1 μm cantilevers. The cantilever is made free-standing by etching the C-shape out of the silicon nitride membrane. Through this etched portion, the interdigitated gold wires on the substrate below are visible. In both (a) and (b) the visible side of the cantilever is coated with iCVD polymer, and the other side with gold. In (b), the polymer is wrinkled due to the large stress from the reaction.

Device performance was assessed by measuring the electrical resistance of the wire leads as hexylamine was introduced to a gas chamber. Resistance vs. time plots are shown in Figure 4-4 for four different hexylamine concentrations. In all cases, the electrical response exhibits a drop of several orders of magnitude as one would expect from a contact switch. The response time τ of the sensor is inversely proportional to the gas concentration and given the data in Figure 4-4 fits to a power law of $\tau = 0.004 \cdot X^{-1.3}$ where *X* is hexylamine concentration. At 9 parts per thousand of hexylamine in nitrogen, the response time is under two minutes and increases to about 700 minutes for a concentration of 90 parts per million. Devices were also tested for selectivity to hexylamine by exposure to nitrogen streams saturated with heptane, 2-propanol, and water. The resistance did not drop over each 12 hour test. Because chemical reactions are responsible for creating stress, the device is insensitive to chemicals that do not react with maleic anhydride. However, the device should be

sensitive to other amines, alcohols and nucleophiles that will react with maleic anhydride. Although 2-propanol, which was used as a control, is an alcohol, it does not react with maleic anhydride.[20] To discriminate between analytes in a given class of chemical compounds, an array of cantilevers with varying aspect ratios can be coated. Analytes with large volumes will create enough stress to deflect all of the cantilevers, while the small analytes would create only enough stress to deflect the longest cantilevers. To discriminate between classes of chemicals, multiple polymers with differing functionalities can be deposited.

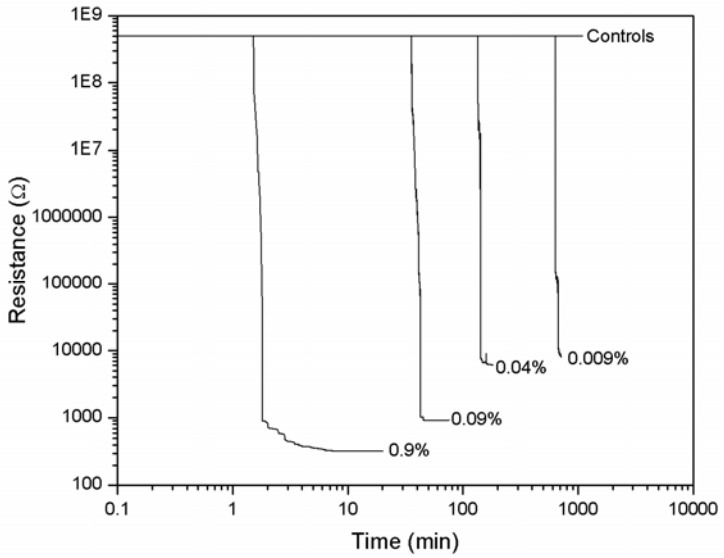

Figure 4-4. Resistance-response data of 100 µm long devices to different concentrations (mol %) of hexylamine gas. Each trace is for a separate device (because the reaction is irreversible). The initial resistance actually exceeds the shown value of 500 MΩ which is the maximum resistance our ohmmeter could measure. The tests take place in a nitrogen gas chamber, and hexylamine gas is flowed in at time = 0 at the indicated concentrations. The cantilevers start bending downwards immediately as the hexylamine is introduced, but the resistance drop does not occur until the cantilever actually touches the wire pad below. At this point the resistance drops sharply and continues to fall slightly as the reaction proceeds, creating more forceful contact. Three devices were tested for selectivity by exposure to heptane, 2-propanol, and water vapor for 700 minutes. These traces all follow the indicated horizontal line at 500 MΩ because none of them reacted sufficiently to short the circuit.

After reacting the devices with hexylamine, we exposed them to 100% nitrogen for 24 hours and observed that the resistance remained constant, indicating that the cantilevers remained stressed and bent. The tradeoff of attaining high selectivity by chemical binding is that each switch can only be used

once and must be replaced afterwards. However, in return we derive great benefit from the low manufacturing cost of each switch.

The response times in our present experiments are slow for most applications, but can be improved by optimizing the cantilever geometry to make it more compliant. Given a cantilever of length *l*, held a fixed distance *h* above the electrode wires, it is required to bend with curvature *k*, where $k=h/l^2$, in order to short circuit the electrode wires. (To arrive at this expression, we assume that $\cos(lk) \approx 1-(lk)^2$ because the curvature is small when $h<<l$). Therefore, increasing the length of the cantilever reduces the required curvature by a square law. According to Eq. 4-2, the curvature is also proportional to the stress in the film, which in turn is proportional the fraction of reacted polymer. Since less polymer mass is required to react, the response time decreases as well. A simple improvement to the current device is to elongate the cantilever by a factor of 10, which should improve the response time by about a factor of 100. In addition, Eq. 4-2 shows that the stress required to achieve a given curvature scales linearly as cantilever and polymer thicknesses are scaled linearly. Using 50 nm thick (instead of 100 nm thick) cantilevers would reduce the response time by another factor of 2. With these two improvements, the response time at 90 ppm of hexylamine should drop from 700 minutes to about 3.5 minutes.

The fundamental sensitivity limitation of this method stems from the requirement that a certain volume of polymer must react to produce enough stress to sufficiently deflect the cantilever. In our present experiments, the sensitivity is diffusion limited because the polymer is 75 nm thick. The optimal device would fully actuate upon reaction of just one monolayer of polymer on the cantilever so that it is not diffusion limited but mass transfer limited. The flux of gas molecules *F* (molecules/area/sec) to a surface is

$$F = \frac{P}{\sqrt{2\pi m k_B T}} \qquad \text{Eq. 4-3}$$

where P is the partial pressure, m is the mass of the molecule, k_B is Boltzmann's constant, and T is temperature. At hexylamine concentrations of 1 ppb, the flux is approximately 1 $nm^{-2}\,s^{-1}$. The surface density of the maleic anhydride functional group has been estimated to be 1 nm^{-2}. Assuming all of the hexylamine molecules striking the surface stick and diffuse quickly to a maleic anhydride group, one hexylamine molecule encounters an anhydride group every second and the response time should be on the order of seconds.

4.5 Conclusion

We have demonstrated a low-power, selective chemical sensor based on the formation of stress in cross-linked polymer nanofilms covalently attached to thin silicon nitride cantilevers. The value of this work is the demonstration of enhanced stress formation in highly cross-linked films, which were enabled by iCVD, and the demonstration of a sensing mechanism with simple signal interpretation. Strategies to improving sensitivities have been discussed, and additional cross-linked polymer chemistries can be synthesized by iCVD to sense other analytes.

References

[1] W. E. Tenhaeff and K. K. Gleason, "Initiated and Oxidative Chemical Vapor Deposition of Polymeric Thin Films: iCVD and oCVD," *Advanced Functional Materials,* vol. 18, pp. 979-992, Apr. 2008.

[2] J. Janata and M. Josowicz, "Conducting polymers in electronic chemical sensors," *Nature Materials,* vol. 2, pp. 19-24, Jan. 2003.

[3] D. Rivera, M. K. Alam, C. E. Davis, and C. K. Ho, "Characterization of the ability of polymeric chemiresistor arrays to quantitate trichloroethylene using partial least squares (PLS): effects of experimental design, humidity, and temperature," *Sensors and Actuators B-Chemical,* vol. 92, pp. 110-120, Jul. 2003.

[4] N. V. Lavrik, M. J. Sepaniak, and P. G. Datskos, "Cantilever transducers as a platform for chemical and biological sensors," *Review of Scientific Instruments,* vol. 75, pp. 2229-2253, Jul. 2004.

[5] F. M. Battiston, J. P. Ramseyer, H. P. Lang, M. K. Baller, C. Gerber, J. K. Gimzewski, E. Meyer, and H. J. Guntherodt, "A chemical sensor based on a microfabricated cantilever array with simultaneous resonance-frequency and bending readout," *Sensors and Actuators B-Chemical,* vol. 77, pp. 122-131, Jun. 2001.

[6] J. D. Adams, G. Parrott, C. Bauer, T. Sant, L. Manning, M. Jones, B. Rogers, D. McCorkle, and T. L. Ferrell, "Nanowatt chemical vapor detection with a self-sensing, piezoelectric microcantilever array," *Applied Physics Letters,* vol. 83, pp. 3428-3430, Oct. 2003.

[7] N. Abedinov, P. Grabiec, T. Gotszalk, T. Ivanov, J. Voigt, and I. W. Rangelow, "Micromachined piezoresistive cantilever array with integrated resistive microheater for calorimetry and mass detection," *Journal of Vacuum Science & Technology a-Vacuum Surfaces and Films,* vol. 19, pp. 2884-2888, Nov.-Dec. 2001.

[8] D. R. Baselt, B. Fruhberger, E. Klaassen, S. Cemalovic, C. L. Britton, S. V. Patel, T. E. Mlsna, D. McCorkle, and B. Warmack, "Design and performance of a microcantilever-based hydrogen sensor," *Sensors and Actuators B-Chemical,* vol. 88, pp. 120-131, Jan. 2003.

[9] S. Singamaneni, M. C. LeMieux, H. P. Lang, C. Gerber, Y. Lam, S. Zauscher, P. G. Datskos, N. V. Lavrik, H. Jiang, R. R. Naik, T. J. Bunning, and V. V. Tsukruk, "Bimaterial microcantilevers as a hybrid sensing platform," *Advanced Materials,* vol. 20, pp. 653-680, Feb. 2008.

[10] W. J. Arora, A. J. Nichol, H. I. Smith, and G. Barbastathis, "Membrane folding to achieve three-dimensional nanostructures: Nanopatterned silicon nitride folded with stressed chromium hinges," *Applied Physics Letters,* vol. 88, p. 053108, Jan. 2006.

[11] W. J. Arora, S. Sijbrandij, L. Stern, J. Notte, H. I. Smith, and G. Barbastathis, "Membrane folding by helium ion implantation for three-dimensional device fabrication," *Journal of Vacuum Science & Technology B,* vol. 25, pp. 2184-2187, Nov. 2007.

[12] A. J. Nichol, P. S. Stellman, W. J. Arora, and G. Barbastathis, "Two-step magnetic self-alignment of folded membranes for 3D nanomanufacturing," *Microelectronic Engineering,* vol. 84, p. 1168, May-Aug. 2007.

[13] W. E. Tenhaeff and K. K. Gleason, "Initiated chemical vapor deposition of alternating copolymers of styrene and maleic anhydride," *Langmuir,* vol. 23, pp. 6624-6630, Jun. 2007.

[14] T. Gao, E. S. Tillman, and N. S. Lewis, "Detection and classification of volatile organic amines and carboxylic acids using arrays of carbon black-dendrimer composite vapor detectors," *Chemistry of Materials,* vol. 17, pp. 2904-2911, May 2005.

[15] K. I. Oberg, R. Hodyss, and J. L. Beauchamp, "Simple optical sensor for amine vapors based on dyed silica microspheres," *Sensors and Actuators B-Chemical,* vol. 115, pp. 79-85, May 2006.

[16] K. Chan and K. K. Gleason, "Initiated chemical vapor deposition of linear and cross-linked poly(2-hydroxyethyl methacrylate) for use as thin-film hydrogels," *Langmuir,* vol. 21, pp. 8930-8939, Sep. 2005.

[17] M. Wen, L. E. Scriven, and A. V. McCormick, "Differential scanning calorimetry and cantilever deflection studies of polymerization kinetics and stress in ultraviolet curing of multifunctional (meth)acrylate coatings," *Macromolecules,* vol. 35, pp. 112-120, Jan. 2002.

[18] S. Baxamusa and K. K. Gleason, submitted.

[19] G. Odian, *Principles of Polymerization*, 4 ed. Hoboken: John Wiley & Sons, 2004.

[20] B. C. Trivedi and B. M. Culbertson, *Maleic Anhydride*. New York: Plenum Press, 1982.

CHAPTER FIVE

Synthesis and Characterization of Poly(4-vinylpyridine) as Nitroaromatic-Selective Layers for Microfabricated Sensor Applications

Abstract

Poly(4-vinylpyridine) (P4VP) thin films were synthesized by initiated chemical vapor deposition (iCVD) and evaluated as a nitroaromatic-selective coating for microfabricated sensor applications. Conventional nitroaromatic-selective coatings interact with hydrogen bond basic nitroaromatic compounds through hydrogen bonding. In contrast, P4VP has zero hydrogen bond acidity. Thus, P4VP is a promising material for integration into chemical sensor arrays as the chemical basis for its interaction with nitroaromatics is orthogonal to those in hydrogen bond acidic polymers. Upon exposure to explosive simulants nitrobenzene and nitrotoluene, the iCVD P4VP layers swelled by over 30%. Additionally, limited swelling was observed with potential interferents: water, ethanol, and toluene. The Flory-Huggins model was also applied to the analysis of the swelling results, which revealed the importance of the interaction parameter, χ, in controlling sensors' limits of detection.

5.1 Introduction

Explosive military ordinance (bombs, mines, etc.) and improvised explosives devices (IEDs) pose a significant security threat to both civilians and military personnel. From October 2001 to August 2007, IEDs were responsible for over 60% of American combat casualties in Iraq and over 50% of casualties in Afghanistan.[1] Additionally, over 120 million unexploded land mines are distributed across approximately 70 countries according to the International Committee for the Red Cross.[2] Organic compounds containing nitro groups are the most prevalent explosives in military ordinance.[3] Nitroaromatic compounds, 2,4,6-trinitrotoluene (TNT) perhaps being the best known example, are an important class of these explosives.

Nitroaromatic compounds are difficult to detect using vapor sensors due to their low vapor pressure. The equilibrium concentration of TNT is 6.3 ppb at 20 °C[4], yet the concentration level in proximity to a landmine or IED can be orders of magnitude lower due to encapsulation of the source or atmospheric dilution. Many recent reviews[3-6] emphasize the importance of developing sensitive and selective nitroaromatic vapor sensors. Various technologies have been applied to the problem, including surface acoustic wave detectors, microcantilevers, chemresistors, ion mobility spectroscopy, mass spectrometry, and amplifying fluorescent polymers.[7, 8]

In order to develop cost-effective, stand-alone distributed sensing systems, efforts are currently underway to reduce their size, weight, and power requirements. The development of sensors based on the deflection of chemically functionalized microcantilevers indicates progress in this area.[4, 9] To achieve selectivity in these devices, chemically selective coatings, commonly polymer thin films or self-assembled monolayers, transduce chemical interactions into mechanical responses. For example, a selective coating is applied to one side of microcantilever, which results in a differential stress leading to cantilever deflection as the analyte preferentially adsorbs onto or absorbs into the coating. The absorption of nitroaromatic vapors in hydrogen bond acidic polymers has been studied extensively.[10-14]

However, these polymers have limited selectivity towards nitroaromatics; they will also absorb interferents. To achieve greater selectivity and eliminate false positives, a common strategy is to create multi-component sensor arrays with multiple chemically selective materials.[15, 16] An unknown analyte is identified from the composite response using an analysis algorithm. To discriminate nitroaromatics from other potential hydrogen bond basic interferents, it is important to have multiple polymer layers that interact with nitroaromatics through non-hydrogen bonding mechanisms. The formation of complexes between nitroaromatics and amine bases, such as pyridine, in solution is a well-studied effect.[17-19] Two types of interactions are possible: charge transfer complexes and pi-pi stacking. To the authors' knowledge, the polymeric analog of pyridine, poly(4-vinylpyridine), has not been previously studied as a nitroaromatic-selective layer in chemical vapor sensors. Moreover, P4VP will useful in sensor arrays, as the chemical basis for its interaction with nitroaromatics, is orthogonal to those in hydrogen bond acidic polymers.

Initiated chemical vapor deposition (iCVD) has been demonstrated as a useful synthesis technique for polymer thin films in sensor applications.[20] It is a vacuum deposition technique that enables nanometer-level control of film thicknesses in planar and complex, three-dimensional geometries.[21] Fine control over the polymer composition is also possible; its ability to create crosslinked and surface-tethered films has enabled new microscale sensing designs.[20] Herein, the synthesis of poly(4-vinylpyridine) (P4VP) by iCVD is described, along with its analysis as a nitroaromatic-selective layer.

5.2 Experimental

5.2.1 Polymer Synthesis

Polymer film synthesis was performed in a previously described iCVD reactor system.[22] 4-vinylpyridine (95%) and tert-butyl peroxide (97%) were purchased from Sigma-Aldrich and used as

received. 4-vinylpyridine was heated to 50 °C to create sufficient vapor pressure to enable a flow of 8 sccm into the reactor, controlled using a heated mass flow controller (MKS Instruments, 1152C). The flow rate of tert-butyl peroxide initiator was set at 4 sccm with a mass flow controller (MKS Instruments, 1479). An operating pressure of 800 mTorr was maintained, and the filament temperature was set to 285 °C by passing 1.15 amps through a Chromaloy O (Goodfellow) filament array suspended 1.5 cm above the substrate. The stage temperature was 20 °C to promote adsorption of monomers. *In situ* interferometry with a 633-nm HeNe laser (JDS Uniphase) was used to monitor and control polymer film thicknesses.

5.2.2 Polymer and Device Characterization

Transmission Fourier transform infrared spectroscopy (FTIR) measurements (Nicolet, Nexus 870 ESP) were collected from 650 to 4000 cm^{-1} with a resolution of 4 cm^{-1} using a MCT detector. 64 scans were integrated to improve the signal-to-noise ratio. FTIR was also collected for as-received, commercial, conventionally synthesized P4VP with a weight-average molecular weight of 60,000 g/mol (Sigma-Aldrich). It was spun coat onto Si wafers from a 4% (w/v) solution in N,N-dimethylformamide (Sigma-Aldrich, 99.9%). FTIR spectra of silicon wafers substrates served as backgrounds, and the spectra were baseline corrected and normalized for comparison purposes.

Molecular weights of iCVD P4VP was determined using a Waters gel permeation chromatography (GPC) system equipped with an isocratic HPLC pump (Model 1515), autosampler (Model 717plus), three styragel columns (HR1, HR3, and HR4), and a refractive index detector (Model 2414). P4VP films were dissolved off the silicon wafers in THF and filtered through a 0.45 µm membrane. 150 µL of the solution was injected into the column; the mobile phase was THF flowing at 1 mL/min. The refractive index detector, operating at a wavelength of 880 nm, was maintained at 35 °C.

Integrated areas of the peaks were compared to narrow polystyrene standards to characterize the molecular weight distribution.

To test the swelling response of P4VP to nitroaromatics, the films were exposed to nitrogen streams with known concentrations of nitrobenzene (NB) and 4-nitrotoluene (4-NT). The films were tested in a previously described gas flow cell.[20] A metered flow rate of nitrogen (Airgas, ultra-high purity) was sparged through the liquid analyte, and the analyte's saturation vapor pressure defined its concentration in N_2. A second line of pure nitrogen was mixed with the saturated analyte prior to entering the chamber to control analyte concentrations. In a typical experiment, the first step was to set up steady-state flow of a given nitroaromatic concentration. For the first five minutes, pure N_2 was introduced into the sensor chamber. After five minutes, the nitroaromatic stream was fed into the chamber for 20 minutes. The nitroaromatic flow was then turned off, and the chamber was purged with clean N_2 for 5 minutes. The films' thickness changes due to swelling was monitored via single wavelength interferometry[23] using a 633 nm HeNe laser (JDS Uniphase).

5.3 Results and Discussion

5.3.1 Polymer Synthesis and Characterization

The thickness of poly(4-vinylpyridine) (P4VP) thin films was readily controlled to 125 nm using iCVD. The Fourier transform infrared spectroscopy (FTIR) spectrum of the as-deposited film is provided in Figure 5-1, along with the spectrum of a commercial standard. The spectra match qualitatively, suggesting that the compositions of the iCVD and standard polymers are equivalent.

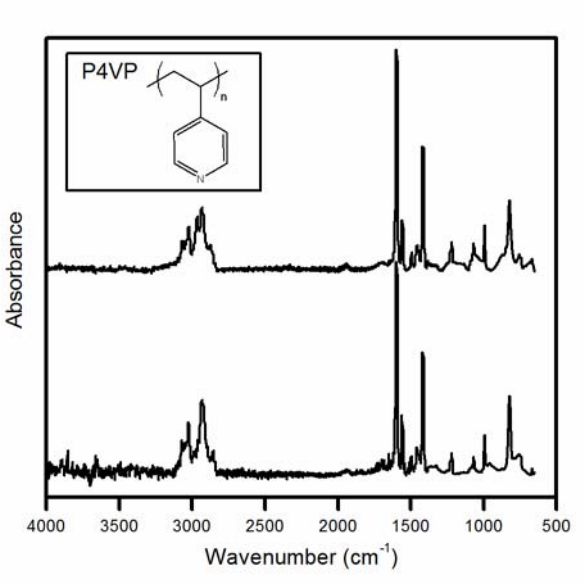

Figure 5-1. Comparison of FTIR spectra of iCVD-deposited (top) and standard solution-polymerized (bottom) P4VP . (Inset: Chemical structure of P4VP).

The molecular weight of the iCVD P4VP was determined using gel permeation chromatography. The weight average molecular weight (M_w) was 1405 g/mol relative to polystyrene standards, with a polydispersity index of 1.2. The molecular weight of 4-vinylpyridine is 105 g/mol. Therefore, the kinetic chain length was approximately 13.4, and the material can legitimately be considered an oligomer. While it is possible to increase the molecular weight using iCVD[24-26], the lower molecular weights obtained here are desirable since they result in lower Tg's[27] and, therefore, higher diffusion constants, P4VP with a M_w of 1405 g/mol was used for all subsequent characterization. Higher diffusion coefficients are desirable since diffusion rates control the sensors' response times.

5.3.2 Swelling Properties of P4VP

The objective in designing chemical sensors is detecting the smallest concentration possible (low limit of detection (LOD)), yet also be selective towards the analyte of interest in order to minimize false positives. Previous studies of nitroaromatic sensing using surface acoustic wave (SAW) devices[28] and

microcantilevers[12] have reported the importance of hydrogen bonding interactions between hydrogen bond acidic moieties in their polymeric coating and the highly electronegative (hydrogen bond basic) nitro moieties of nitroaromatic compounds. These interactions lead to higher gas-polymer partition coefficients, resulting in lower detection limits.

In common implementations, microcantilever-based sensor systems measure cantilever deflection as its polymer coating absorbs analytes. As a first approximation, the translation of swelling to an observable cantilever deflection can be modeled using Stoney's equation[29]:

$$\Delta z = \frac{3l^2(1-\nu)}{E t^2}\Delta\sigma \qquad \text{Eq. 5-1}$$

Here, Δz is the deflection at the cantilever end, l is the length of the cantilever, ν is Poisson's ratio, E is the elastic modulus of the cantilever material, and t is the thickness of the cantilever. $\Delta\sigma$ is the swelling-induced stress. Assuming that the polymer coating is elastic, the stress defined by $\Delta\sigma = -E_p\varepsilon$, where E_p is the elastic modulus of the polymer. [30] Strain, ε, develops as the polymer swells because the polymer is constrained at the cantilever-substrate interface. Assuming that swelling occurs isotropically when the polymer is not constrained by the substrate, the strain is determined as follows[30]:

$$\varepsilon = \sqrt[3]{Q} - 1 \qquad \text{Eq. 5-2}$$

Q is the swelling ratio, the volume of the polymer film in the swollen state over its volume in the dry state. The expressions for stress and strain assume elastic behavior. In reality, though, the behavior of the coating is viscoelastic, and macromolecular rearrangements occur to relieve stress.[30] Plasticization effects also occur. However, these expressions are a first order description of the importance of the polymer swelling process in sensing designs.

To evaluate iCVD-deposited P4VP as a nitroaromatic-selective layer, its interactions with simulants of nitroaromatic explosives, nitrobenzene (NB) and 4-nitrotoluene (4NT), were examined.

These simulants, rather than TNT or 2,4-dinitrotoluene, were investigated due to safety concerns. The linear swelling ratio (α) of P4VP films, which is the ratio of the film thickness in the swollen state to its initial thickness (t_s/t_i), was measured as a function of reduced partial pressures (P/P_{sat}). Due to constraints imposed by the substrate, there is negligible swelling in the plane of the substrate, and the linear swelling ratio (α) is equal to Q. P/P_{sat} is the ratio of an analyte's vapor pressure to its saturation pressure at the system temperature, and it is directly proportional to the concentration of the analyte in the vapor head space. Linear swelling was measured at 40 °C for NB and 60 °C for 4NT. Swelling by 4NT was measured at a higher temperature due to the lack of reliable vapor pressure data below its melting point of 51 °C. The results are provided in Figure 5-2.

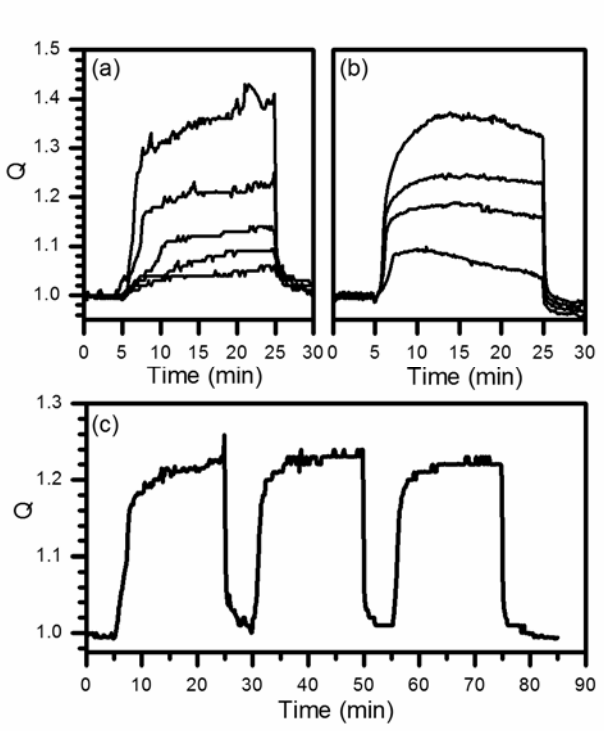

Figure 5-2. (a) Swelling of P4VP by NB at 40 °C for P/P_{sat} values of 0.25, 0.4, 0.5, 0.65, 0.85. (Larger P/P_{sat} values result in larger swelling ratios.) (b) Swelling of P4VP by 4NT at 60 °C for P/Psat values of 0.25, 0.4, 0.5, 0.75. Vertical scales in (a) and (b) are equal. (c) Reversibility of P4VP swelling upon repeated exposures to NB (P/Psat=0.65, 40 °C).

In order to generate the desired reduced partial pressures, the carrier N_2 stream saturated with analyte was fixed at a constant flow rate and mixed with an appropriate patch flow (see Experimental

section). Mass transfer calculations and experiments were performed to show that the swelling process was diffusion limited. Since the process is diffusion limited, the effect of varying N_2 flow rates on residence time did not influence the swelling kinetics or equilibrium. For the first five minutes, there was no flow into the sensor chamber in order to collect a baseline. After five minutes, the valve was opened to introduce the nitroaromatic stream, resulting in swelling of the P4VP films. Fickian kinetics do not apply since swelling naturally modifies the physical properties of the polymer, resulting in a concentration-dependent diffusion constant. Investigation of the NB swelling kinetics reveals at least two distinct stages of diffusion. There is an initial increase in film thickness due to NB sorption, followed by a second sharp increase, after which the swelling equilibrium is reached. This behavior is characteristic of Super Case II diffusion.[31, 32] After 20 minutes of nitroaromatic introduction, the sensor chamber was purged with pure nitrogen.

Figure 5-2c shows that the swelling is reversible. The nitroaromatic source was turned off after 20 minutes, and pure N_2 was introduced into the chamber. The film thickness shrank to its original thickness within five minutes. The maximum swelling ratios of the second and third cycles were qualitatively the same as the first cycle. However, the second and third cycles reached 95% of their equilibrium value within 90 seconds, as opposed to the first cycle which didn't fully reach equilibrium. By looking closely at the swelling profiles, one can also see that the second and third cycles do not display the two-stage process as in the first. Presumably, the polymer film has undergone relaxation from the first nitroaromatic absorption cycle. In the subsequent cycles, the diffusion coefficients start at higher values since the polymer is already relaxed.

In addition to measuring the linear expansion of these films, a method was developed to generalize the results for comparison to other polymer-analyte systems. The Flory-Huggins model describes the thermodynamics of mixing of polymers in small molecules (solvent).[33] The model can be

extended to polymer-vapor systems by relating the chemical potential term in the traditional formulation to the reduced partial pressure of vapor molecules[34]

$$P/P_{sat} = \left(1-\varphi_p\right)\exp\left[\left(1-1/N\right)\varphi_p + \chi\varphi_p^2\right] \quad \text{Eq. 5-3}$$

Here φ_p is the volume fraction of polymer at equilibrium (swollen state), χ is the Flory-Huggins interaction parameter for the analyte-polymer pair, and N is the degree of polymerization. Because the polymer volume fraction of the film is initially unity, the film's equilibrium swelling ratio (Q) is related to the volume fraction of polymer by $Q = 1/\varphi_p$, and Eq. 3 becomes

$$P/P_{sat} = \left(1-\frac{1}{Q}\right)\exp\left[\left(1-1/N\right)\left(\frac{1}{Q}\right)+\chi\left(\frac{1}{Q}\right)^2\right] \quad \text{Eq. 5-4}$$

Unfortunately, Eq. 5-4 cannot be solved explicitly for Q. By analyzing Eqs. 5-1, 5-2, and 5-4 together, though, it is clear that the LOD of the sensing device is lowered by reducing the required P/P_{sat} for a given Q. Therefore, Eq. 5-4 indicates that the best sensitivities are achieved by syntheszing polymers with small or negative χ values for nitroaromatics.

The equilibrium swelling ratios are plotted as function of P/P_{sat} in Figure 5-3. Eq. 5-4 was fitted to the data in Figure 5-3 to obtain χ values of 0.71 for NB at 40 °C and 0.25 for 4NT at 60 °C. A χ value of 0.5 is indicative of an ideal solution, where the heat of mixing is zero.[35] χ is less than 0.5 for both 4NT, indicating that favorable intermolecular forces develop between it and P4VP. Further studies to understand the difference in χ values for 4NT and NB and investigate the interaction of heavier nitroaromatics with P4VP are warranted. The Flory-Huggins equation is a convenient analyze selectivity and sensitivity and predicted results between systems as χ parameters are tabulated for many solvent-polymer pairs.[36]

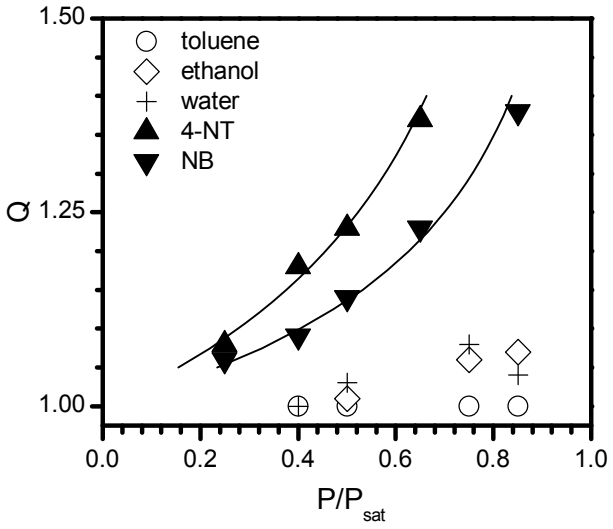

Figure 5-3. Equilibrium volumetric swelling ratios of P4VP with nitroaromatics and potential interferents. The lines describe the Flory-Huggins model (Eq. 5-4) fitted to the swelling data using a non-linear least square minimization algorithm.

The selectivity of P4VP for nitroaromatics is also important. When deployed in the field, a sensor will be exposed to a complex vapor composition that will vary with time and environmental conditions. For field success and operator confidence, the sensor must be selective towards nitroaromatics and not respond to other environmental interferents. The swelling responses of P4VP to water, which is omnipresent as humidity, ethanol, which is a product of biological processes, and toluene, which mimics hydrocarbon fuel, were tested at 60 °C. The results are provided in Figure 5-3 with a comparison to the swelling by nitroaromatics. A χ value of 1.9 was calculated for the P4VP-water and P4VP-ethanol systems at 60 °C. This quantitatively shows that these interactions are weaker than the P4VP-nitroaromatic interactions. Unfortunately, χ could not be determined for the P4VP-toluene system since the experimental technique did not have the precision to measure the swelling ratio, which was not significantly greater than one. Eq. 5-4 breaks down when Q=1 for $P/P_{sat}>0$.

Figure 5-3 clearly demonstrates that the swelling ratio at a given reduced partial pressure is greatest for the nitroaromatics. Relatively little swelling is observed for the interferents tested. It is possible other interferents exist (not tested here) that will significantly swell P4VP. The importance of

this particular polymer composition becomes apparent by comparing it to sorbent polymers currently employed in nitroaromatic sensors. Previous studies, particularly those concerning surface acoustic wave sensors, use partition coefficients, rather than χ, to analyze the suitability of polymers for different analytes.[28, 37] The partition coefficient is calculated by dividing the equilibrium concentration of analyte absorbed in the polymer by the concentration of analyte in the vapor phase. An important metric for comparing polymers for sensor applications is the selectivity (S), which is the ratio of sorbed analyte to the ratio of sorbed interferent:

$$S = \frac{K_{Pa} c_a}{K_{Pi} c_i} \qquad \text{Eq. 5-3}$$

Here, K_{Pa} is partition coefficient for the analyte of interest, c_a is the concentration of the analyte vapor, K_{Pi} is the partition coefficient of potential interferents, and c_i is the concentration of interferent vapor. Partition coefficients can be determined experimentally or estimated using the linear solvation energy relationship (LSER).[37] The LSER framework allows one to determine the relative importance of various types of intermolecular forces in the solvation process.

Nitroaromatic compounds are hydrogen bond basic and do not contain any hydrogen bond acidity.[38] A common strategy in designing nitroaromatic-selective polymers is to synthesize polymers with high hydrogen bond acidity.[14] Poly(4-(hexafluoroisopropanol)-styrene) (P4V) and poly(methyl(3,5-bis(hexafluoroisopropanol)phenyl)siloxane) (SXPHFA) are some of the best performing polymers, but the hydrogen bond acidity of carbowax polymers[10, 11] and self-assembled monolayers of 4-mercaptobenzoic acid[12] have also been used successfully. It is important to consider the selectivity of these polymers for nitroaromatics relative to water. Water contains both hydrogen bond acidity and basicity, so hydrogen bond interactions can form between water and hydrogen bond acidic polymers. Using previously reported data from McGill et al.[38] in the LSER equation, the selectivity of P4V for nitrobenzene relative to water at 25 °C was calculated to be 332(c_a/c_i).

P4VP and nitroaromatics, on the other hand, interact though pi-pi stacking and charge transfer complexes in solution. Based on the LSER parameters for pyridine, P4VP does not contain hydrogen bond acidity. It does contain hydrogen bond basic groups and can interact through hydrogen bonds with water, which likely contributed to the swelling reported in Figure 5-3. LSER parameters of P4VP were not determined using chromatographic techniques. Instead, the partition coefficients of P4VP for nitrobenzene and water were determined experimentally by estimating the analyte concentrations from the swelling data. Vapor concentrations were calculated using the P/P_{sat} values. The experimentally determined selectivity of P4VP was 58(c_a/c_i).

The selectivity of P4V for NB is 5.7 times greater than P4VP's selectivity. However, P4V's selectivity is 100 times greater than other hydrogen bonding polymers.[28] The selectivity of SXPHFA is not reported, but is likely on the same order of magnitude as P4V's. While highly selective, P4V is semi-crystalline, which is not ideal for gas diffusion purposes. Regardless of its performance relative to hydrogen bonding polymers, P4VP will be usesful in sensor arrays since its interaction with nitroaromatics is orthogonal to hydrogen bonding interactions.

5.4 Conclusion

Thin films of P4VP have been synthesized by iCVD and shown to swell upon exposure to nitroaromatics. The use of iCVD is important as it provides many advantages over other coating processes[21], some of which have been demonstrated in previous sensor studies.[20] While the interaction of amine bases with TNT have been studied in solution, the implementation of P4VP for sensor applications has not been exploited. The Flory-Huggins theory has been applied to the analysis of the swelling results, and the importance of χ in determining sensitivities for microcantilever-based systems has been demonstrated. The use of the Flory-Huggins equation should be extended to further analysis of sensor designs since χ values have been tabulated for many polymer-solvent pairs.[36] While

the selectivity of P4VP for nitrobenzene over water is 5.7 times lower than P4V's selectivity, the swelling of P4VP with nitroaromatics is nonetheless an important result as it provides a complimentary interaction for multicomponent sensors.

References

[1] C. Wilson, "Improvised Explosive Devices (IEDs) in Iraq and Afghanistan: Effects and Countermeasures", C.R. Service, Ed., Library of Congress, Washington, D.C., 2007.

[2] A. M. Rouhi, *Chemical & Engineering News* **1997**, *75*, 14.

[3] S. Singh, *Journal of Hazardous Materials* **2007**, *144*, 15.

[4] L. Senesac, T. G. Thundat, *Mater. Today* **2008**, *11*, 28.

[5] S. J. Toal, W. C. Trogler, *J. Mater. Chem.* **2006**, *16*, 2871.

[6] J. Yinon, *Anal. Chem.* **2003**, *75*, 99A.

[7] V. L. Pamula, "Detection of Explosives", in *Handbook of Machine Olfaction, Electronic Nose Technology*, T.C. Pearce, S.S. Schiffman, H.T. Nagle, and J.W. Gardner, Eds., Wiley-VCH, Weinheim, 2003, p. 547.

[8] R. L. Woodfin, "*Trace Chemical Sensing of Explosives*", John Wiley & Sons, Hoboken, 2007.

[9] P. G. Datskos, N. V. Lavrik, M. J. Sepaniak, *Sens. Lett.* **2003**, *1*, 25.

[10] G. K. Kannan, J. C. Kappor, *Sens. Actuator B-Chem.* **2005**, *110*, 312.

[11] G. K. Kannan, A. T. Nimal, U. Mittal, R. D. S. Yadava, J. C. Kapoor, *Sens. Actuator B-Chem.* **2004**, *101*, 328.

[12] L. A. Pinnaduwage, V. Boiadjiev, J. E. Hawk, T. Thundat, *Appl. Phys. Lett.* **2003**, *83*, 1471.

[13] A. W. Snow, L. G. Sprague, R. L. Soulen, J. W. Grate, H. Wohltjen, *Journal of Applied Polymer Science* **1991**, *43*, 1659.

[14] J. W. Grate, *Chem. Rev.* **2008**, *108*, 726.

[15] K. J. Albert, N. S. Lewis, C. L. Schauer, G. A. Sotzing, S. E. Stitzel, T. P. Vaid, D. R. Walt, *Chem. Rev.* **2000**, *100*, 2595.

[16] R. Archibald, P. Datskos, G. Devault, V. Lamberti, N. Lavrik, D. Noid, M. Sepaniak, P. Dutta, *Anal. Chim. Acta* **2007**, *584*, 101.

[17] R. E. Miller, W. F. K. Wynne-Jones, *Journal of the Chemical Society* **1959**, 2375.

[18] R. E. Miller, W. F. K. Wynne-Jones, *Journal of the Chemical Society* **1961**, 4886.

[19] W. Waclawek, F. Tuznik, *Bulletin de L'Academie Polonaise Des Sciences, Serie des sciences chemiques* **1972**, *XX*, 987.

[20] W. J. Arora, W. E. Tenhaeff, K. K. Gleason, G. Barbastathis, *J. Microelectromech. Syst.* **2009**, *18*, 97.

[21] W. E. Tenhaeff, K. K. Gleason, *Adv. Funct. Mater.* **2008**, *18*, 979.

[22] W. E. Tenhaeff, K. K. Gleason, *Langmuir* **2007**, *23*, 6624.

[23] N. Vourdas, G. Karadimos, D. Goustouridis, E. Gogolides, A. G. Boudouvis, J. H. Tortai, K. Beltsios, I. Raptis, *Journal of Applied Polymer Science* **2006**, *102*, 4764.

[24] K. Chan, K. K. Gleason, *Macromolecules* **2006**, *39*, 3890.

[25] K. K. S. Lau, K. K. Gleason, *Macromolecules* **2006**, *39*, 3688.

[26] K. K. S. Lau, K. K. Gleason, *Macromolecules* **2006**, *39*, 3695.

[27] R. J. Andrews, E. A. Grulke, "Glass Transition Temperatures of Polymers", in *Polymer Handbook*, 4 edition, J. Brandrup, E.H. Immergut, and E.A. Grulke, Eds., John Wiley & Sons, New York, 2005, p. 197.

[28] E. J. Houser, T. E. Mlsna, V. K. Nguyen, R. Chung, R. L. Mowery, R. A. McGill, *Talanta* **2001**, *54*, 469.

[29] N. V. Lavrik, M. J. Sepaniak, P. G. Datskos, *Rev. Sci. Instrum.* **2004**, *75*, 2229.

[30] M. J. Wenzel, F. Josse, S. M. Heinrich, E. Yaz, P. G. Datskos, *Journal of Applied Physics* **2008**, *103*, 064913.

[31] A. Sfirakis, C. A. Rogers, *Polymer Engineering and Science* **1981**, *21*, 542.

[32] A. H. Windle, "Case II Sorption", in *Polymer Permeability*, J. Comyn, Ed., Elsevier Applied Science Publishers, New York, 1985.

[33] P. J. Flory, "*Principles of Polymer Chemistry*", Cornell University Press, Ithaca, 1953.

[34] H. Elbs, G. Krausch, *Polymer* **2004**, *45*, 7935.

[35] I. W. Hamley, "*Introduction to Soft Matter*", John Wiley & Sons, New York, 2000.

[36] N. Schuld, B. A. Wolf, "Polymer-solvent interaction parameters", in *Polymer Handbook*, 4th edition, J. Brandrup, E.H. Immergut, and E.A. Grulke, Eds., John Wiley & Sons, New York, 2003, p. 247.

[37] R. A. McGill, M. H. Abraham, J. W. Grate, *Chemtech* **1994**, *24*, 27.

[38] R. A. McGill, T. E. Mlsna, R. Chung, V. K. Nguyen, J. Stepnowski, *Sensors and Actuators B: Chemical* **2000**, *65*, 5.

CHAPTER SIX

Conclusions

Initiated chemical vapor deposition has been shown to be a highly enabling technique. iCVD offers capabilities that many other CVD or solution-phase techniques cannot. This thesis has demonstrated the utility of iCVD in synthesizing stimuli-responsive and reactive polymer thin films, which require fine control over film composition for practical applications. For example, the synthesis of poly(styrene-alt-maleic anhydride) described in CHAPTER TWO was the first demonstration of an alternating copolymer with a strictly defined composition deposited by CVD. Unwanted side reactions that introduce new chemical functionalities (e.g. crosslinking), which is inevitable in plasma enhanced chemical vapor deposition, was avoided. In CHAPTER THREE, the crosslinking density of poly(maleic anhydride-co-dimethylacrylamide-co-di(ethylene glycol) divinyl ether) was optimized to yield a highly swellable yet stable surface-attached hydrogel thin film. In this formulation, the composition was critical as the crosslinking content significantly affected the swelling properties. The maleic anhydride groups had many roles: covalent bonding to the substrate surface, ionization in solution to create pH-responsive swelling, and reactivity for functionalization. CHAPTER FOUR introduced yet another polymer chemistry where crosslinking of reactive polymer films on microcantilever substrates was used to generate stress to transduce chemical signals into an electrical measurement. It was shown that a high crosslinking density led to the formation of more stress, leading to greater permanent cantilever deflection. In CHAPTER FIVE, iCVD-deposited poly(4-vinylpyridine) (P4VP) was shown to be a nitroaromatic sensitive material. Though the interaction of pyridine and TNT in solution has been elucidated previously, this was the first time that interaction of nitroaromatic vapors with P4VP has been studied. It was shown that P4VP absorbs TNT vapors, leading to polymer swelling. This swelling response was used to design a new sensing concept, as described in Appendix A. Fabrication and proof-of-principle operation of sensors based on this design were performed. In all of these projects, the compositions of the polymer films were tuned by adjusting partial pressure ratios of the monomer

precursors to control their surface concentrations. The monomers' surface concentrations and their reactivities controlled the final composition of the film.

Solution-based polymer thin film fabrication techniques also offer fine control over film compositions, especially top-down techniques where decades of polymer synthetic protocols can be utilized. A distinguishing aspect of iCVD that was essential to completing these projects was the control over the conformality of polymeric coatings on nano- and microscale features. For the composite membrane application of CHAPTER THREE, it was desired to fabricate a continuous polymer film over nanoscale pores. On the other hand, the interior of trenches needed to be coated with polymer for the nitroaromatic sensor design utilizing microfabricated trenches (see APPENDIX A). iCVD enabled the synthesis of the films in both cases by controlling the conformality though the partial pressure ratios of monomers.

From this thesis work, at least two interesting polymer compositions have been identified that can be utilized in future applications. The first is poly(maleic anhydride-co-dimethylacrylamide-co-di(ethylene glycol) divinyl ether). It was developed as a size-selection separation layer in composite membranes. It could be easily adapted for many other applications. For instance, in the composite membrane application, the polymer was applied as a blanket layer on the top surface of porous membranes. However, the deposition conditions could easily be modified to coat the interior walls of the pores, which would enable new separation mechanisms. pH-responsive separations is one possibility. Furthermore, this formulation could be interesting for biomedical applications due to the presence of reactive maleic anhydride moieties at the surface. The surfaces of these polymer films are readily functionalized with biomarkers, peptides, or other functional compounds, while the bulk composition remains unchanged. Therefore, this material could serve as a multifunctional coating: interacting specifically with components in solution while maintaining its responsive hydrogel properties. One potential application is membrane chromatography.

The discovery of P4VP thin films as nitroaromatic-sensitive materials is particularly intriguing. An important remaining study is to determine the strength of the interaction between P4VP and heavier nitroaromatics (TNT and 2,4-dinitrotoluene). Dinitrotoluene and TNT are active ingredients in explosive formulations. For safety reasons, 4-nitrotoluene and nitrobenzene, which are not explosive, were used as proxies for heavier nitroaromatics in this thesis work. In order to better predict the sensitivities of sensor designs to real explosives, heavier nitroaromatics should be tested. This will likely require collaboration with a lab with the proper safety measures in place.

Moreover, the exact nature of the P4VP-nitroaromatic interaction has not been characterized. By analogy to solution-phase behavior, it has been suggested that it occurs through pi-pi stacking or charge transfer complexes. Efforts should be taken to fully elucidate the physical nature of the interaction. This approach to designing sorption-based nitroaromatic-sensitive polymers differs from the traditional technique of creating polymers capable of forming hydrogen bonds with nitroaromatics. However, hydrogen bond-acidic polymers also form hydrogen bonds with water, resulting in interference by humidity and reduced selectivities. P4VP also shows sensitivity to water. Improved sensitivities and selectivities can likely be achieved through copolymerization. Analysis of the binding pockets of enzymes that reduce nitroaromatics reveals the presence of histidine and tryptophan amino acids. 1-vinylimidazole is a vinyl monomer structurally similar the side chains of these amino acids, and it can readily copolymerize with 4-vinylpyridine. Poly(1-vinylimidazole) homopolymer alone would likely not be a suitable nitroaromatic-selective layer since it does not contain an aromatic ring for pi-pi stacking interactions.

Using P4VP and its copolymers, new designs of nitroaromatic vapor sensors should be designed and evaluated. Key considerations in the design of sensor are sensitivity and selectivity, but the fabrication cost is also important. New sensing concepts have been designed with collaborators in order to miniaturize the active layer and simplify the fabrication. Fewer microfabrication steps will lead to

cheaper devices. The mass limit of detection is a convenient metric to use for comparing sensitivities. As sensing components are miniaturized and the amount of P4VP active layer is reduced, the mass limit of detection will also decrease. Ultimately, the goal should be commercialization for real-world applications to combat the worldwide scourge of landmines and improvised explosive devices.

APPENDIX A

Analysis and Demonstration of Microfabricated Trench-Based Sensors

A.1 Introduction

Utilization of the swelling response of poly(4-vinylpyridine) (P4VP) thin films to nitroaromatic vapors for microfabricated sensing designs was detailed in CHAPTER FIVE. Transduction of the polymer's response to mechanical deflection of microcantilevers was analyzed. These microcantilevers have typical dimensions of hundreds of micrometers (length) by tens of micrometers (width) by one micrometer (thickness).[1] The influence of these dimensions on a sensor's performance, the length and thickness in particular, is apparent from Eq. 5-1. The requirements for micrometer-scale dimensions limit further miniaturization of the sensing component. Miniaturization is an important objective in order to fabricate covert sensing devices indiscernible to the naked eye.

Moreover, it was shown that crosslinking is required to create permanent deflections of the cantilever end on the order of a few micrometers.[2] It is believed that the response time of the sensors is controlled by diffusion of the analyte into the polymer layer. Crosslinking creates glassy polymers, and the resulting diffusion coefficient is orders of magnitude lower than uncrosslinked or rubbery polymers.[3] Theory describes the influence of crosslinking on the glass transition temperature of a polymer, which defines the temperature at which the transition from a rubbery to glassy state occurs.[4] To maximize the diffusion coefficient, the operating temperature of the sensor should be as high as possible above the glass transition temperature.

A new sensing architecture has been designed to overcome these limitations. The sensing concept is shown in Figure A-1. Here, polymer does not need to create stress in the substrate for signal transduction. Rather, physical contact between two swelling polymer layers is used to bring together two electrically conductive layers. To maximize the extent of polymer swelling and minimize response time, crosslinking can be eliminated. Moreover, the critical length scale of this design (the trench width) is over at least two orders of magnitude smaller than conventional microcantilever lengths (>100 μm).

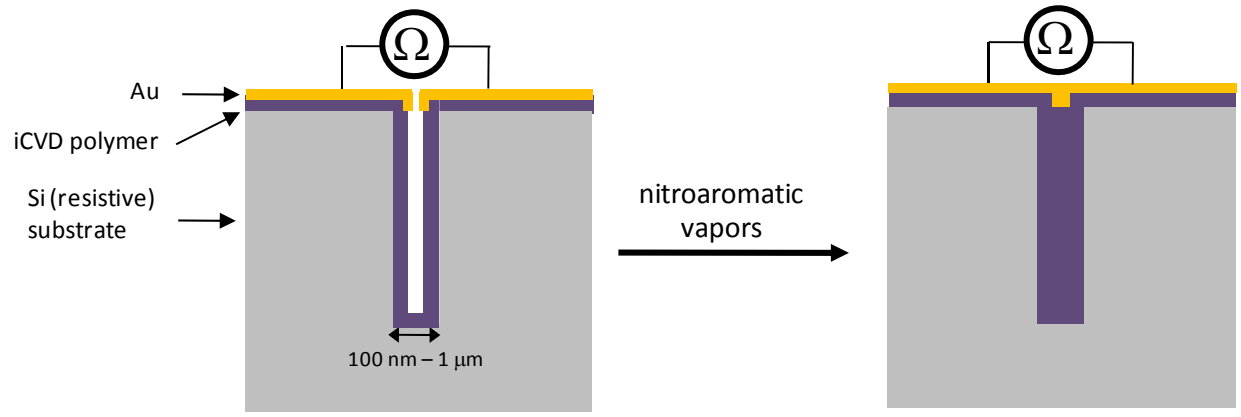

Figure A-1. Conceptual design of the trench sensors, showing the utilization polymer swelling to transduce a chemical interaction into an electrical measurement. The polymer swelling results in contact being made between Au layers that are initially separated.

Herein, this design is quantitatively analyzed for the detection of nitroaromatics using the P4VP properties determined in CHAPTER FIVE. Successful device fabrication and its ability to detect nitroaromatics is described. Non-optimal performance is reported, but the study proves that the sensing concept does work. Techniques to improve the performance are dicussed.

A.2. Design

A 400 nm-wide trench that is 1.2 μm deep has been analyzed as an illustrative example, using parameters of P4VP determined in CHAPTER FIVE. Optimization of the design will lead to improved performance. By depositing a 185 nm-thick P4VP film in the interior of the trench as shown in Figure A-2, the P4VP layers must swell by 8.1% upon exposure to nitroaromatics to create contact between the gold surfaces and decrease the electrical resistance measured across the trench. Because swelling occurs normal to the surface only, Q=1.081. The χ values of 2,4-dinitrotoluene (DNT) and (TNT) with P4VP are unknown, but they are roughly estimated to be equal to χ for the 4NT-P4VP system at 60 °C, which was measured in CHAPTER FIVE (χ=0.25). Using these Q and χ values, P/P_{sat} must be equal to 0.23 for trench closure (calculated using Eq. 5-4). The saturated partial pressures of DNT and TNT are

204 and 8.6 μTorr, respectively. Therefore, this design can achieve sensing LODs of 62.2 and 2.64 ppb for DNT and TNT, respectively.

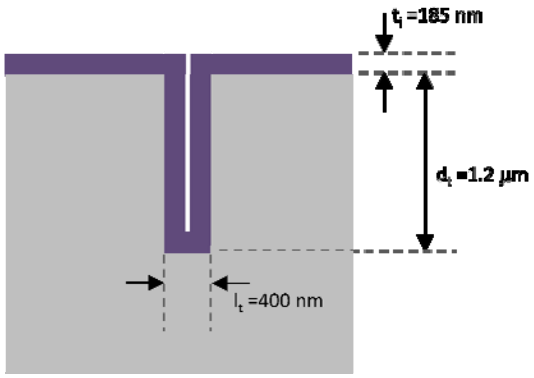

Figure A-2. Key measurements for analyzing the sensitivities of trench sensors.

In addition to the concentration LOD, the LOD on a mass basis is important. The concentration LOD describes the lowest concentration that can be detected, but it does not determine the kinetics or the required sampling volume to create a response. The required sampling volume is important because it too will determine response times. For example, it is possible that a polymer composition can respond to extremely low concentrations, but if the volume of the polymer is large when implemented as the active layer in a sensor, the sensor may fail to create a response due to the limited amount of analyte molecules in the vapor sample. Therefore, the mass LOD is an important metric. A lower mass LOD translates to better kinetics and smaller sampling volumes. To reduce the mass LOD using the trench concept, the volume of the polymer coating should be minimized. A top down image of a patterned sensor is given in Figure A-3; it does not show large conductive pads on the ends of the gold lines, which are required to make electrical measurements but do not affect the mass LOD. The pattern dimensions were chosen somewhat arbitrarily, but they can be readily fabricated with conventional microfabrication techniques. The linewidth of the pattern is critical as the top Au layer is impermeable, requiring analytes to diffuse into the underlying P4VP from the side.

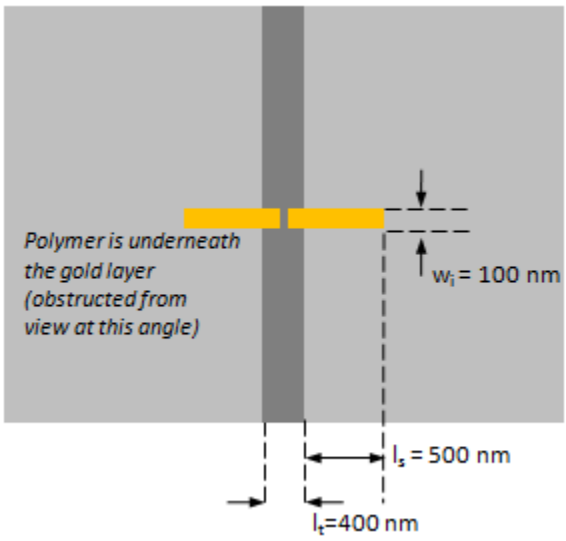

Figure A-3. Illustration of patterning the responsive and conductive layers to minimize the mass limit of detection of swelling-based trench sensors.

A first approximation of the required mass for switch closure is calculated from the following equation, which assumes volume additivity as the analyte absorbs in to the polymer.

$$m_{LOD} = \rho V_i (Q - 1) \qquad \text{Eq. A-1}$$

m_{LOD} is the mass limit of detection, ρ is the density of the absorbed analyte, V_i is the initial volume of the polymer, and Q is the swelling ratio. The initial volume is calculated by $V_i = t_i w_i (2l_s + 2d_t + l_t)$; the variables are defined in the figures above. Using the dimensions shown in Figures A-2 and A-3, along with an assumed density of 1.6 g/cm3 for absorbed nitroaromatic, the mass LOD is 9.1 fg.

Currently, this design is a “yes-no” switch; it only activates once the vapor concentration of analyte exceeds the concentration LOD. It does not discern concentration levels. For practical application in explosives sensors, this is sufficient. The operator only needs to know whether or not explosives are present. In other applications, discriminating between concentration levels is desired. This sensing design can be modified by creating multiple trenches of varying widths, and simultaneously

monitoring resistance across all of them. An array of three trenches with widths of 400, 450, and 500 nm, coated with 185 nm of P4VP has been analyzed. Figure A-4 presents a plot of the Flory-Huggins equation for χ=0.25 along with the horizontal lines representing the required swelling ratios to create contact between the three trenches. The intersections of the horizontal lines with the Flory-Huggins model show how the required P/P_{sat} (or equivalently vapor phase concentration) is affected. For further complexity, multiple polymers with varying χ values can be deposited to create multicomponent responses for analyte identification.

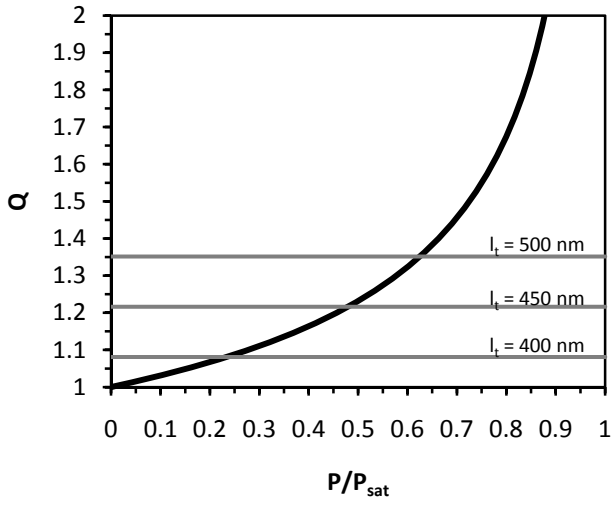

Figure A-4. Demonstration of the use of multiple trench widths to quantify analyte concentration levels. P/P_{sat} is directly proportional to the vapor concentration.

A.3 Experimental

A.3.1 Polymer Deposition and Device Fabrication

Silicon wafers substrates with pre-patterned trenches (nominally 615 nm wide at the top of the trench by 5 μm deep) were generously supplied by Ed Gleason of Analog Devices. The trench width varies throughout the trench depth. Approximately 250 nm of a silicon dioxide hard mask remained on top of the wafer. A multimeter, whose leads contacted the surface of the wafer, measured an electrical

resistance greater than 500 MΩ across the trench. Poly(4-vinylpyridine) was deposited on the trench substrates as described in CHAPTER FIVE. Five nanometers of an Au/Pd alloy were deposited on top of the P4VP film using a sputter coater (Quorom Technologies, SC7640). The leads of electrical wires were bonded to both sides of the trench using conductive silver epoxy.

A.3.2 Device Characterization

The response of the device to nitrobenzene was measured using a previously described vapor flow cell.[2] A metered flow rate of nitrogen (Airgas, ultra-high purity) was sparged through liquid nitrobenzene, and the saturation vapor pressure of nitrobenzene defined its concentration in N_2. A second line of pure nitrogen was mixed with the saturated analyte prior to entering the chamber to control analyte concentrations. In a typical experiment, the first step was to set up steady-state flow of a given nitrobenzene concentration. For the first five minutes, pure N_2 was introduced into the sensor chamber. After those five minutes, the nitrobenzene stream flowed into the chamber for 40 minutes. The nitrobenzene flow was then turned off, and the chamber was purged with clean N_2 for five minutes. Pure nitrogen flowed during the last five minutes of all resistance logging experiments. The wire leads were fed through the chamber's seals in order to log electrical resistance as a function of time with a standard multimeter (Agilent, U1252A). Images of the trench cross-sections were collected before and after nitrobenzene exposure with a scanning electron microscope (JEOL, 6700F).

A.4 Results and Discussion

A.4.1 Design

The two primary findings from analyzing the trench sensor design are the mass and concentration LODs using P4VP to detect nitroaromatics. They are estimated to be 9.1 fg and 2.6 ppb, respectively, for TNT. Amplifying fluorescent polymers that are utilized in the iCX Fido® system are

generally considered to be the most promising commercialized technology.[6] The Fido® design has mass and concentration LODs on the order of femtograms and parts per quadrillion, respectively.[7] Clearly, the Fido® system outperforms this design in terms of the concentration LOD (6 orders of magnitude better). In terms of mass, the performances are about the same. However, trench sensors have the advantage in terms of size and power requirements. In the Fido® design, the fluorescence of the amplifying fluorescent polymer is continuously monitored as it is exposed to collimated UV laser light.[6] This requires constant power. Because low power requirements are required in many sensing concepts (discussed in CHAPTER ONE), trench sensors are promising for these designs. Moreover, a pre-concentrator, which is a common component of practical implementations of sensors,[7] can be used to increase the concentration of nitroaromatics that is exposed to the trench sensors in order to address their poor concentration LOD.

A.4.2 Performance of P4VP for Nitrobenzene Detection

SEM images of the P4VP films in the trenches are provided in Figure A-5a. Prior to nitrobenzene exposure, the P4VP film thickness was approximately 450 nm on the substrate surface and 280 nm in the trench interior, measured normal to the trench sidewall directly below the trench lip (the slight protrusion near the top). The surfaces of the polymer films were separated by 140 nm. Figure A-5a shows that the thickness of the coating decreases down the depth of the trench, and the polymer coatings at the bottom of the trench will not contact after swelling. However, only the polymer films at the top of the trench need to be brought together to change the resistance. After exposure to nitrobenzene, the volume expansion clearly resulted in contact between the two sides, as seen in Figure A-5b. Given that swelling was shown to be reversible in CHAPTER FIVE, direct observation of the contact between the two sides after purging with clean nitrogen was unexpected. Moreover, the high vacuum of the SEM chamber should enhance desorption of the nitrobenzene. The reason for the permanent

contact is unknown. One possibility is that the nitrobenzene plasticizes the polymer coating, and strong adhesive forces are created upon contact. In other words, the polymer layers are "sticky." Because the contact is permanent, the switch can be used once. Applications where one-time use sensors are sufficient are described in CHAPTER ONE.

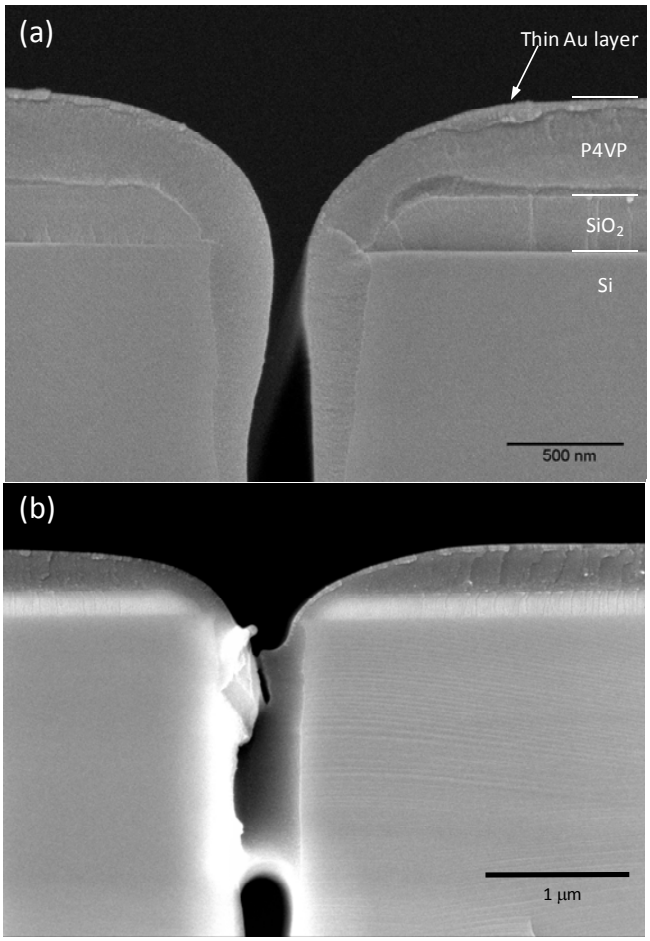

Figure A-5. SEM images of P4VP-coated trench substrates (a) before and (b) after exposure to nitrobenzene at P/P_{sat} = 0.75 and 40 °C. The image in (b) shows that the contact between the polymer sidewalls in the trench interior is permanent. (Note: different substrates were used for these images, which explains slight discrepancies between the two images.)

The electrical resistance measurements of the sensors' responses to nitrobenzene vapors at a system temperature of 40 °C are provided in Figure A-6. These sensors clearly behaved as switches. For varying nitrobenzene concentrations, the measured electrical resistance dropped on average by a factor of five to a final resistance of approximately 100 MΩ. The electrical resistance changes of the

microcantilever-based systems described in CHAPTER FOUR were much greater, showing changes as high as six orders of magnitude. It should be noted that the initial resistance across the trench is much greater than the measured 500 MΩ. 500 MΩ is the maximum resistance that the multimeter could measure. Based on a bulk resistivity of 10^{14} Ω·m for SiO_2[8] and not accounting for the resistance of the P4VP layer, the initial resistance should be at least 10^{13} Ω across the trench. Therefore, the change in resistance is much greater than what was recorded with the multimeter. As predicted from the swelling experiments with interferents described CHAPTER FIVE, the sensor did not respond to water at a P/P_{sat} value of 0.5 at 40 °C.

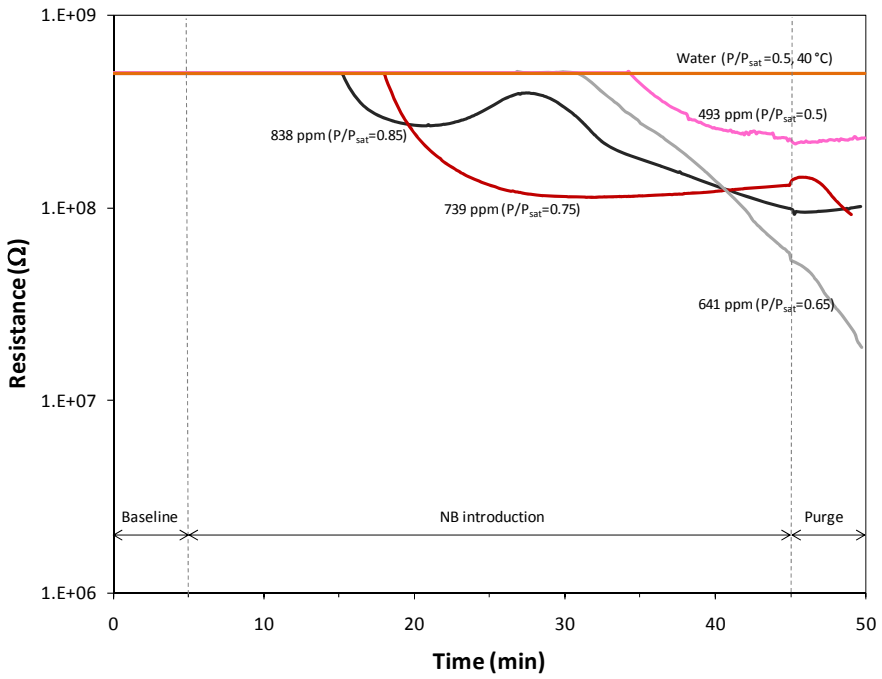

Figure A-6. (a) Response of fabricated sensors to varying nitrobenzene concentrations at 40 °C. The response to water vapor is also included. For the first five minutes, no analyte was introduced into the system. A constant analyte concentration was introduced for the next 40 minutes, followed by five minutes of purging with pure N_2.

The thinness of the Au/Pd layer on top of the P4VP gold layer is the primary reason for the relatively high resistance after trench closure. An ultrathin layer of Au/Pd was used in order to minimize the barrier to nitroaromatic diffusion into the polymer coatings. Experiments (unpublished data)

showed that a sputter coating of Au/Pd on a blanket film of P4VP completely blocked the absorption of nitrobenzene. Therefore, an ultrathin layer of Au/Pd layer was used with the P4VP-coated trench substrates. Ultrathin metal layers often have granular, semi-continuous morphologies, which potentially allow diffusion of nitrobenzene through noncontinuous regions or defects in the layer. Also, the depth of the Au coating in the trench interior is also minimized, allowing nitrobenzene to diffuse into the P4VP through uncoated regions of the polymer sidewalls. Due to the non-continuous nature of the Au/Pd layer, its resistance is compromised. Furthermore, due to the way that the polymer layers contact each other inside the trench, the interfacial contact area of Au is likely quite small. (The exact depth of Au is unknown, precluding quantitative estimates.)

The variation of the response times, measured when the resistances first begin to drop, as a function of nitrobenzene concentration is also an important aspect of the resistance data. The shortest response time is 10 minutes (15 minutes with 5 minutes subtracted for the baseline), and the longest is 30 minutes. In CHAPTER FIVE, it was shown that the P4VP layers swelled to 90% of their equilibrium value within the first five minutes of nitrobenzene exposure. For the swelling experiments of CHAPTER FIVE, the films were 120 nm thick. In these trenches, the polymer side walls were 240 nm thick. For diffusion based processes, the time constant, τ, for diffusion of species over length ℓ can be estimated through $\tau = \ell^2 / D$, where D is the diffusion constant. For the trenches used in this study, one would expect the response times to be at least four times longer than those reported in CHAPTER FIVE, neglecting all other effects. However, the Au/Pd also obstructs diffusion into the polymer, in effect increasing the overall D for the composite coating. If nitrobenzene must diffuse into the polymer coating through uncoated regions in the trench interior, the diffusion length of nitrobenzene is even greater. The diffusion process has not been modeled since the depth of the Au/Pd coating is unknown, but it clearly negatively affects the response time.

Patterning the P4VP and Au/Pd layers as shown in Figure A-3 will lead to significant improvements in the performance of these sensors. Equation A-1 describes the effect of patterning on minimizing the mass LOD (V_i will be reduced). Also, the patterning will allow diffusion of nitroaromatics into the P4VP from all exposed sides of the pattern. Since the time constant for diffusion scales with the length squared, the linewidths of the pattern should be made as narrow as possible. The 100 nm shown in Figure A-3 is an appropriate goal. Because the analytes can diffuse through the sides of the pattern and the Au/Pd layer does not impede absorption, the thickness of the Au/Pd layer can be increased. This should lead to a higher cross-sectional area for charge conduction and possibly lower contact resistance, which will result in lower resistances upon switch closure.

In addition to patterning the layer, decreasing the trench widths will improve response times and lower the mass LOD since the required initial polymer thickness is lower. In this study, the trench widths could not be controlled; the substrates were standard surplus materials supplied by an outside company. For future work, the trenches should be custom fabricated to decrease the trench width. The required thickness of the polymer coating in the trench interior scales proportionally with trench width. Again, because the process is diffusion controlled, the response time will decrease with the thickness of the polymer squared.

A.5 Conclusion

The design of a resistance-based microscale chemical sensing concept has been described. The performance of P4VP for the detection of nitroaromatics using this design was analyzed. Analysis showed that the sensitivity in terms of the mass limit of detection should be comparable to sensors using amplifying fluorescent polymers. However, the system enables the reduction of sensor size and power requirements. A quantitative comparison of the power requirements was not made, but the chemical switch design offers obvious advantages in terms of power. Moreover, a prototype device was

fabricated and tested as a proof of principle. Switch-like behavior in electrical resistance was observed. Due to limitations in fabrication capabilities, optimal performance of these devices was not reported. Fabrication techniques to improve key performance metrics were identified. Utilizing these techniques will be crucial when the trench sensors are tested with higher nitroaromatics, such as TNT and DNT, which have lower vapor phase concentrations than nitrobenzene.

References

[1] N. V. Lavrik, M. J. Sepaniak, P. G. Datskos, *Rev. Sci. Instrum.* **2004**, *75*, 2229.

[2] W. J. Arora, W. E. Tenhaeff, K. K. Gleason, G. Barbastathis, *J. Microelectromech. Syst.* **2009**, *18*, 97.

[3] W. J. Koros, W. C. Madden, "Transport Properties", in *Encyclopedia of Polymer Science and Technology*, 3rd edition, J. Korschwitz and H.F. Mark, Eds., Wiley-Interscience, Hoboken, 2002.

[4] J. Bicerano, "Glass Transition", in *Encyclopedia of Polymer Science and Technology*, 3rd edition, J. Korschwitz and H.F. Mark, Eds., Wiley-Interscience, Hoboken, 2002.

[5] W. E. Tenhaeff, K. K. Gleason, *Langmuir* **2007**, *23*, 6624.

[6] V. L. Pamula, "Detection of Explosives", in *Handbook of Machine Olfaction, Electronic Nose Technology*, T.C. Pearce, S.S. Schiffman, H.T. Nagle, and J.W. Gardner, Eds., Wiley-VCH, Weinheim, 2003, p. 547.

[7] R. L. Woodfin, *Trace Chemical Sensing of Explosives*, John Wiley & Sons, Hoboken, 2007.

[8] R.A. Serway, R.J. Beichner, *Physics for Scientists and Engineers*, Saunders College Publishing, Fort Worth, 2000.